

POLITECNICO DI TORINO

**Corso di Laurea Magistrale
in Ingegneria Energetica e Nucleare**

Tesi di Laurea Magistrale

Development of lithium nickel cobalt oxide- graphite battery model and its application in a railway regenerative braking system



Relatore

prof. Massimo Santarelli

Candidato

Laura Scandura

Co-relatore

Ing. Arpit Maheshwari

Tutor aziendale

Ing. Andrea Tosetto

A.A.2017/2018

TABLE OF CONTENTS

1	Introduction	2
1.1	Hybrid vehicles	3
1.1.1	How hybrid vehicle works	7
1.2	Diesel hybrid vehicle	9
1.2.1	Locomotive application	10
1.2.1.1	Regenerative Braking system	12
2	Batteries	14
2.1	Chemistry and kinetics	16
2.2	Polarization curve.....	19
2.3	Reactions	22
2.4	Li-ion battery	23
2.4.1	Battery configurations.....	29
3	Thermal modeling	31
3.1	Thermal issues in Li-ion battery	31
3.1.1	High temperature and low temperature performance degradations	31
3.1.2	Thermal runaway	34
3.1.3	Temperature gradient.....	35
3.2	Heat generation rate	35
3.3	Battery thermal management system (BTMS).....	37
3.4	Predicted models	44
3.4.1	Mathematical models	44
3.4.2	Equivalent circuit models.....	44
3.4.3	Electrochemical models	48
3.4.3.1	Single particle model.....	48
3.4.3.2	Ohmic porous-electrode models.....	49
3.4.3.3	Pseudo-two- dimensional models.....	49
3.4.3.4	Electrochemical-thermal coupled models	50
4	Model development.....	52
4.1.1	Electrochemical model.....	53
4.1.2	Thermal model	59
4.2	Model validation	64
4.2.1	Steps.....	64
4.2.2	Results and discussion.....	66
4.3	Case study: battery pack to regenerative braking system.....	74
4.3.1	Results and discussion.....	76
5	Conclusion and future developments	92

APPENDIX	93
REFERENCES	105

FIGURES INDEX

Fig 1- World transportation sector delivered energy consumption (quadrillion Btu).	2
Fig 2- a) Lohner-Porsche (1901); b) Toyota Prius first generation (1997).....	3
Fig 3-Market share percentage [3].....	3
Fig 4-series HEV scheme.....	8
Fig 5- Parallel HEV scheme.	9
Fig 6- Chicago METRA electro-diesel locomotive by EMD (Electro-Motive Diesel).	10
Fig 7- Axle control configuration.	11
Fig 8-How Regenerative Braking works [8].	13
Fig 9- Schematic symbol for a cell and a battery.	14
Fig 10-Schematic battery diagram.	15
Fig 11- Activation energy.....	19
Fig 12-Polarization curve.....	20
Fig 13-Comparison types of batteries: energy density, size and weight [11].	24
Fig 14-Lithium-ion electrochemical cell: discharge and charge configuration.	26
Fig 15-Li-ion discharge process.	27
Fig 16-Li-ion charge process.....	27
Fig 17- SEI scheme.....	28
Fig 18- Schematic and pictures of different battery configuration: cylindrical and prismatic [14].	29
Fig 19- Effect of temperature on battery capacity. T1 to T4 increasing temperatures [15].....	31
Fig 20-Effect of discharge load on battery capacity at various temperatures. T1 to T6 increasing temperature, T4 normal room temperature [15].	32
Fig 21- Normalize discharge capacity with cycle number at 25°C, 37°C and 55°C [16].	33
Fig 22-Accidents related with lithium ion battery failure and correlated abuse conditions [19].....	34
Fig 23- Scheme of BMS key functions [23]......	38
Fig 24- The three parts of the battery.....	38
Fig 25- Battery Thermal Management system (BTMs) [25].	40
Fig 26- a) Passive air cooling scheme; b) passive air cooling/heating scheme; c) active air cooling/heating scheme [26].	41
Fig 27- Thermal management using liquid: a)Passing liquid cooling; b) active moderate cooling/heating; c) active cooling(high temperature) /heating (cold temperature) [27].....	42
Fig 28- Battery cooling layout with additional PCM elements [28]	43
Fig 29- Heat pipes cooling system [29].	43
Fig 30- Impedance spectra at various direct currents I_{dc} [30]	45
Fig 31-Schematic diagram of the Rint model.....	46
Fig 32-Schematic diagram of the RC model.	46
Fig 33- Schematic diagram of Thevenin model.....	47
Fig 34- Schematic diagram of PNGV model.	47
Fig 35- Electrochemical models scheme as function of CPU time and predictability [33].	48
Fig 36- Schematic diagram that represents two single particles for each electrode [35].	49
Fig 37-Schematic diagram of pseudo-two-dimensional model [33].	50
Fig 38- Schematic diagram of coupling between pseudo-two-dimensional model and 3D model [37].	51
Fig 39- One dimensional geometry scheme.....	54
Fig 40-1D geometry COMSOL Multiphysics	55
Fig 41- Equilibrium potential plot of NMC.	55
Fig 42-Equilibrium potential plot of graphite.....	55
Fig 43-2D battery geometry.	59

Fig 44-Battery components [41].	60
Fig 45-Heat transfer problem scheme.	63
Fig 46- Mesh used for FEM analysis.	67
Fig 47- Electrochemical validation 0.05C, 0.1C, 0.2C, 0.5C.	68
Fig 48- Electrochemical validation 1C, 1.5C and 2C.	68
Fig 49- 0.05C pre-optimization study.	70
Fig 50-0.05C optimization study.	70
Fig 51-Thermal model validation 1C, 1.5C and 2C	71
Fig 52- 2C pre-optimization study.	73
Fig 53-2C optimization study.	73
Fig 54- Pouch cell geometry.	76
Fig 55- Cell vertical section.	77
Fig 56-Mesh used for FEM analysis.	78
Fig 57- 1C-rate discharge process.	78
Fig 58- Single cell temperature evolution during discharge and charge cycle @1C-rate.	79
Fig 59-Temperature distribution @t=1000s.	80
Fig 60-Temperature distribution @t=2000s.	80
Fig 61-Temperature distribution @t=3550s.	80
Fig 62-Heat generation @1C-rate.	81
Fig 63- Discharge and charge cycle curve.	82
Fig 64-Single cell temperature evolution during discharge and charge cycle.	82
Fig 65-2C-rate discharge process.	83
Fig 66- Single cell temperature evolution during discharge and charge cycle @2C-rate.	83
Fig 67- Heat generation during discharge process @2C-rate.	84
Fig 68- Discharge and charge cycle curve @2C.	84
Fig 69-Single cell temperature evolution during discharge and charge cycle @2C.	85
Fig 70-Heat generation during charge and discharge cycle.	85
Fig 71- Simplified module geometry.	86
Fig 72- Module domains in detail.	86
Fig 73- Mesh used in heat transfer calculation.	87
Fig 74-Average temperature evolution during discharge and charge cycle.	87
Fig 75- Discharge and charge cycle temperature evolution for the battery module section.	88
Fig 76-Battery module section domain.	89
Fig 77-Battery module section detail.	89
Fig 78- Cells domain temperature distribution @t=500s.	90
Fig 79- Cells domain temperature distribution @t=1500s.	90
Fig 80- Cells domain temperature distribution @t=3500s.	91
Fig 81- Pre-optimization and optimization study @0.05C.	93
Fig 82-Pre-optimization and optimization study @0.1C.	94
Fig 83-Pre-optimization and optimization study @0.2C.	96
Fig 84-Pre-optimization and optimization study @0.5C.	97
Fig 85-Temperature evolution comparison for different k_{pos} @1C.	98
Fig 86- Voltage comparison for different k_{pos} @1C.	98
Fig 87- Temperature evolution comparison for different Bruggman coefficient @1C.	99
Fig 88- Voltage comparison for different Bruggman coefficient @1C.	99
Fig 89- Temperature evolution comparison for different k_{pos} @2C.	100
Fig 90- Voltage comparison for different Bruggman coefficient @2C.	101
Fig 91-Temperature evolution pre-optimization and optimization study @2C.	102
Fig 92-Voltage pre-optimization and optimization @2C.	103

TABLE INDEX

Table 1- Environmental impact associated with vehicle production [4]	5
Table 2- Fuel utilization stage and overall GHG and air pollution emissions (per 100 km of vehicle travel) for different vehicle types [4]	6
Table 3- Comparison economic characteristics vehicles	7
Table 4-Comparison between types of batteries [10].	23
Table 5-Comparison of Li-ion battery cathode and anode materials [12]	25
Table 6-Geometrical parameters.	54
Table 7- Electrochemical parameters.	58
Table 8- 2D Battery dimensions.	59
Table 9-Temperature variable.....	62
Table 10-Heat source variable.	62
Table 11-Thermal parameters.....	63
Table 12-The estimated electrochemical parameters.	64
Table 13- Thermal and characteristic material estimated unknown parameters.	65
Table 14- Electrochemical parameter values for the validation.	69
Table 15-Optimization study parameters.	71
Table 16- Thermal model validation parameters.....	72
Table 17-Optimization parameter values.	74
Table 18-data to sizing battery pack [9].....	75
Table 19- NMC-graphite battery Characteristics	75
Table 20- Pouch cell geometric parameters.	77
Table 21- Boundary conditions.	89
Table 22- Varyied quantities for Oprimization study.....	93
Table 23- Fixed quantities for optimization study.	94
Table 24- Varyied quantities for Oprimization study.....	95
Table 25- Fixed quantities for optimization study.	95
Table 26- Varied quantities for Optimization study.....	96
Table 27- Fixed quantities for optimization study.	96
Table 28- Varied quantities for Optimization study.....	97
Table 29- Fixed quantities for optimization study	97
Table 30-Electrochemical parameters values.	99
Table 31-Materials parameters values.....	100
Table 32-Electrochemical parameters values.	101
Table 33- Materials parameters values.....	102
Table 34- Varied quantities for Optimization study.....	103
Table 35- Fixed electrochemical parameters for optimization study.	103
Table 36- Fixed thermal parameters for optimization study.	104

ABSTRACT

The objectives of this project thesis are focus on the thermal characterization of Li-ion battery, in particular of a battery installed on Regenerative Braking system in a diesel-electric locomotive.

Thermal behavior is one of the most important analysis in order to establish and optimize performances and aging from single cell to entire battery pack.

Thermal model is developed to calculate the heat generated during discharge battery processes and how this influences main parameters of the battery.

Defining the thermal model, the principles of regenerative braking system and the battery device work will be explained.

Thanks to experimental data, it is possible validate thermal model by comparing the simulation results with the experimental ones.

Thermal modelling validation is made to 18650 Li-ion cylindrical battery.

Thermal modelling consists of three steps:

First step is the development of thermally coupled electrochemical model of a single cell implemented in COMSOL Multiphysics® with “Batteries and Fuel cells” module. Approach utilized is “Pseudo-2D” model that simulates electrochemical behavior and “heat transfer” in 3D with which thermal behavior is obtained. Discharge cycles are developed with varying C-rate: 0.05C, 0.1C, 0.2C, 0.5C, 1C, 1.5C, 2C.

After thermal model validation, it is applied to the battery module of diesel-electric locomotive RBS.

The thermal model is defined starting with the sizing of battery pack needed to drag for short-haul a DMU existing model, thermal model will be defined for discharge and charge cycles.

The sizing has been described in the thesis of my colleague Giuseppe Boccardo and DMU model characteristics and parameters are provided from *Blue Engineering S.r.l.* company, with which collaboration this project thesis is developed.

1 Introduction

The problem of global warming and the need of reduction of greenhouse gases are main themes of international polices. From 2005 with Kyoto protocol¹ to 2016 with Paris agreement² countries of all the world have the goal of "stabilization of greenhouse gas concentrations in the atmosphere at a level that would stop dangerous anthropogenic interference with the climate system"³ and "strengthen the global response to the threat of climate change by keeping a global temperature rise this century well below 2 degrees Celsius above pre-industrial levels and to pursue efforts to limit the temperature increase even further to 1.5 degrees Celsius" [1].

Gasoline and diesel transportation vehicles are major contributors of urban air pollution (producing global CO₂ emissions with a range of 22%⁴) and global warming growth. Burning fossil fuels are the primary source of GHG emissions.

Global delivered energy consumption in the transportation sector increases at an annual average rate of 1.4%, although the share of total transportation energy declines somewhat over the projection period, from 96% in 2012 to 88% in 2040 [2].

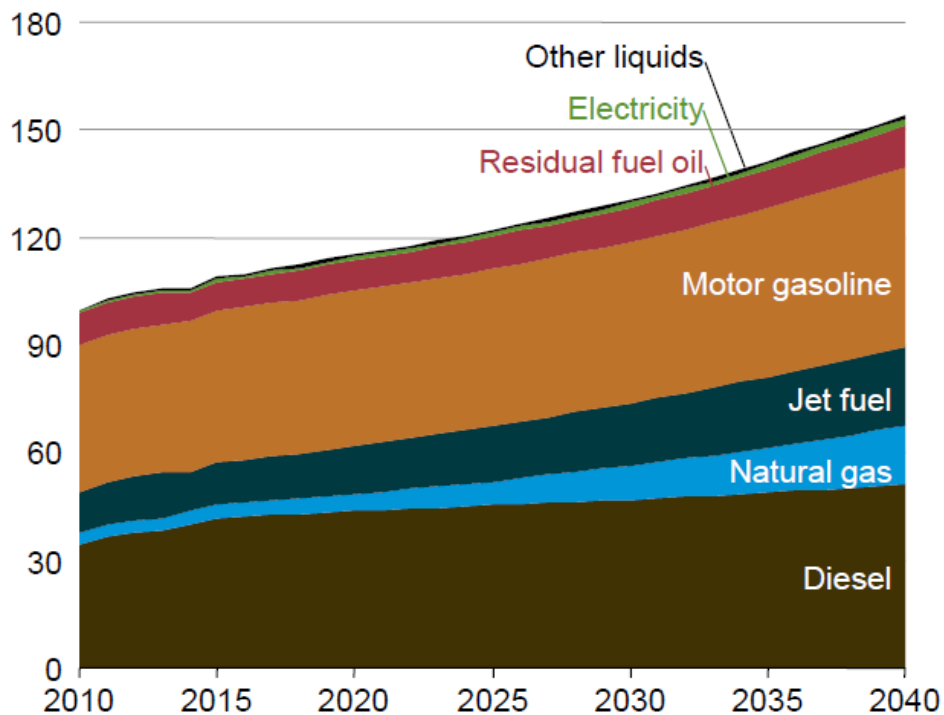


Fig 1- World transportation sector delivered energy consumption (quadrillion Btu).

¹ Kyoto protocol signed on 1997 and effective on 2005 includes 191 states.

² Paris agreement signed on 2015.

³ Kyoto protocol Article 2.

⁴ International Energy Agency (IEA), 2012.CO2 Emissions from Fuel Combustion Highlights. France.

1.1 Hybrid vehicles

The challenge of technologic development towards decrease fossil fuel consumption is at the center of interest of the major companies of the world: vehicles driven by electricity is one of the most important.

The world's first HEV, Lohner-Porsche, is built in 1901 from Ferdinand Porsche in Germany, but Toyota Prius car built in 1997 in Japan can be considered as the modern hybrid electric vehicle.

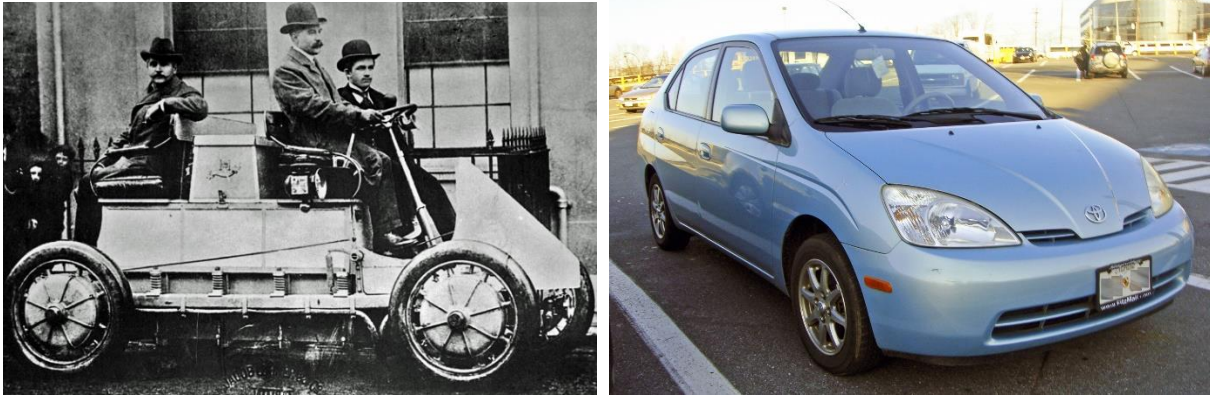


Fig 2- a) Lohner-Porsche (1901); b) Toyota Prius first generation (1997).

Today share of electric and hybrid vehicles is increasing more and more.

Market share percentage for electrified vehicles compared to all vehicles in 2013 is shown below Fig 3-Market share percentage Fig 3:

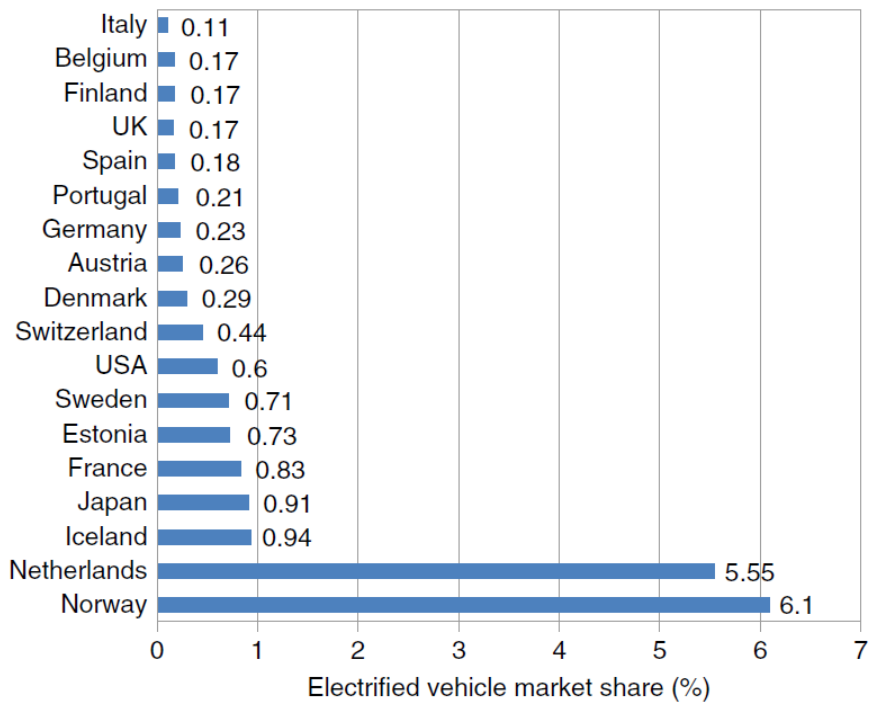


Fig 3-Market share percentage [3].

One of the component of sustainability requires the design of environmentally benign in vehicles characterized by no or little atmospheric pollution during operation.

The design of such vehicles requires, among other developments, improvements in powertrain systems, fuel processing, and power conversion technologies.

There are many types of fuel for vehicle propulsion. They can be grouped in four main classes:

- ✓ Gasoline or diesel that feeds Internal combustion engine (ICE), this type is called conventional vehicle;
- ✓ Gasoline or diesel to ICE and electricity from energy storage devices, this type is called hybrid vehicle;
- ✓ Electricity from energy storage device, this type called pure electric vehicle;
- ✓ Hydrogen from fuel cell that feeds a particular type of internal combustion engine, this type is called hydrogen fuel cell vehicle.

Environmental impact is take into account studying two main emission typologies:

Air pollution (AP) and greenhouse gas (GHG).

It is calculated the environmental impact for the vehicle production stage. It is assumed that GHG and AP emissions are proportional to the vehicle mass.

In particular, for conventional vehicle AP and GHG emissions are calculated as (1.1) e (1.3):

$$AP = m_{car} * AP_m \quad (1.1)$$

Where:

- AP_m is the emission per unit vehicle curb mass (1.2):

$$AP_m = \sum m_i * w_i \quad (1.2)$$

“i” is the index denoting air pollutant (which can be CO, NOx...) and “mi” is the mass of air pollutant and “wi” is the weighting coefficient of the air pollutant.

$$GHG = m_{car} * GHG_m \quad (1.3)$$

For hybrid and electric vehicles, the AP and GHG emissions are evaluated as (1.4) e (1.5):

$$AP = (m_{car} - m_{battery}) * AP_m + m_{battery} * AP_{battery} \quad (1.4)$$

$$GHG = (m_{car} - m_{battery}) * GHG_m + m_{battery} * GHG_{battery} \quad (1.5)$$

Finally, the environmental impact for fuel cell vehicles (1.6) e (1.7):

$$AP = (m_{car} - m_{fc}) * AP_m + m_{fc} * AP_{fc} \quad (1.6)$$

$$GHG = (m_{car} - m_{fc}) * GHG_m + m_{fc} * GHG_{fc} \quad (1.7)$$

Where:

- m_{car} , $m_{battery}$, m_{fc} are the masses of the car, battery and fuel cell respectively;
- AP_m , $AP_{battery}$, AP_{fc} are the AP emissions per kilogram of conventional vehicle, batteries and fuel cells.
- GHG_m , $GHG_{battery}$, GHG_{fc} are the GHG emissions per kilogram of conventional vehicle, batteries and fuel cells.

The amount of AP and GHG produced by diverse types of vehicles are compared in Table 1:

Table 1- Environmental impact associated with vehicle production⁵ [4]

Type of vehicle	Curb mass [kg]	GHG emissions (kg)	AP emissions(kg)	GHG emissions per 100km of vehicles travel (kg per 100km)	AP emissions per 100 km of vehicle travel (kg per 100km)
Conventional	1134	3595.8	8.74	1.490	0.00362
Hybrid	1311	4156.7	10.10	1.722	0.00419
Electric	1588	4758.3	15.09	1.972	0.00625
Fuel cell	1678	9832.4	42.86	4.074	0.0178

⁵ During vehicle lifetime (10 years), an average car drives 241,350 km.

Additional sources of GHG and AP emissions are associated with the fuel production and utilization stages. About electricity production for the electric car case, three scenarios are considered:

1. Electricity is produced from renewable energy sources and nuclear energy;
2. 50% of the electricity is produced from renewable energy source and 50% from natural gas at an efficiency of 40%;
3. Electricity is produced from natural gas at an efficiency of 40%.

Considering these electricity production cases, the environmental impact of the fuel utilization stage, as well as the overall environmental impact (including the fuel utilization, vehicle production and disposal stages) are summarized in Table 2:

Table 2- Fuel utilization stage and overall GHG and air pollution emissions (per 100 km of vehicle travel) for different vehicle types [4]

Vehicle type	Fuel utilization stage		Overall life cycle⁶	
	<i>GHG emissions (kg/100 km)</i>	<i>AP emissions (kg/100 km)</i>	<i>GHG emissions (kg/100 km)</i>	<i>AP emissions (kg/100 km)</i>
Conventional	19.9	0.0564	21.4	0.0600
Hybrid	11.6	0.0328	13.3	0.0370
Electric				
Scenario1	0.343	0.00131	2.31	0.00756
Scenario2	5.21	0.0199	7.18	0.0262
Scenario3	10.1	0.0385	12.0	0.0448
Fuel cell				
Scenario1	10.2	0.0129	14.2	0.0306
Scenario2	10.6	0.0147	14.7	0.0324
Scenario3	11.1	0.0165	15.2	0.0342

After showing competitiveness of these different technologies in term of environmental impact, the second step is represented by economic aspect.

⁶ During vehicle lifetime (10 years) an average car drives 241350 km.

Economic characteristics for four vehicle technologies are shown below in Table 3 [5]:

Table 3- Comparison economic characteristics vehicles ⁷.

Type of vehicle	Fuel	Price (thousands of US\$)	Fuel consumption (MJ per 100km)	Fuel price (US\$ per 100km)	Price of battery changes during life cycle of vehicle (thousands US\$)
Conventional	Gasoline	15.3	238.8	2.94	1X0.1
Hybrid	Gasoline	20.0	137.6	1.71	1X1.02
Electric	electricity	42.0	67.2	0.901	2X15.4
Fuel cell	hydrogen	100.0	129-5	1.69	1X0.1

The interest of main vehicle industries is to determine the best tradeoff to reduce environmental impact and reduce cost of production and cost of fuel.

One of the most competitive vehicle technologies that reach this tradeoff is the hybrid vehicle.

For this reason, today, hybrid technologies, with electric one, are studied and improved further.

1.1.1 How hybrid vehicle works

A hybrid electric vehicle (HEV) is a type of vehicle that uses an electric propulsion system and a conventional internal combustion engine (ICE). Both electrical and ICE motor can transmit the torque to the wheels through a parallel and/or mixed series system. This combination made HEV system more efficient than conventional vehicles.

A hybrid vehicle uses two or more different power sources to get started. HEV combines a conventional drive system with a system which stocks recoverable energy to obtain a better yield, a lower fuel consumption and a lower emissions level.

The hybrid drive system has the following main elements:

- electric batteries;
- electric motor;
- internal combustion engine;
- electric current generator;

⁷ Four particular vehicles, with release years ranging from 2002 to 2004, are taken as representative of each vehicle category: Toyota Corolla (conventional), Toyota Prius (hybrid), RAV4 EV (electric) and Honda FCX (hydrogen fuel cell).

- coupling elements to connect the mechanical system with the electric system;
- management system for the two drive systems.

There are two main ways to connect ICE and electric motor: series and parallel.

When the ICE and motor are connected in series, only electric motor provides mechanical power to the wheels.

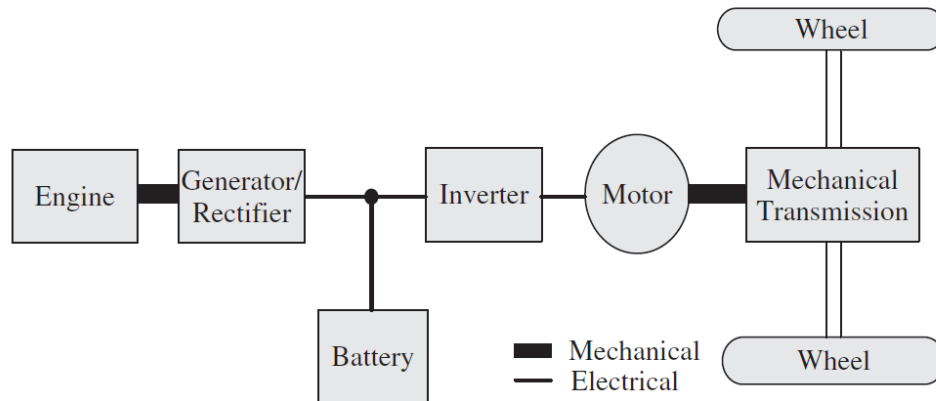


Fig 4-series HEV scheme.

Series drivetrains are the simplest hybrid configuration. The mechanical output of the ICE is converted to electricity using generator. The electric traction motor moves the final drive using electric energy directly produced from engine or from the battery where it is stored. Since ICE is not directly connected to the wheels, the engine speed can be controlled independently of vehicle speed. This permits to engine to work achieving the best fuel economy.

The different combinations with which series HEV can operate are [6]:

- Battery alone: when the battery has sufficient energy, and the vehicle power demand is low, the I/G set (the ICE and generator set) is turned off and the vehicle is powered by the battery only;
- Combined power: at high power demands, the I/G set is turned on and the battery also supplies power to the electric motor;
- Engine alone: During highway cruising and at moderately high-power demands, the I/G set is turned on. The battery is neither charged nor discharged. This is mostly due to the fact that the battery's state of charge (SOC) is already at high level but the power demand of the vehicles prevents the engine from turning, or it may not be efficient to turn the engine off.
- Power split: when the I/G s turned on, the vehicle power is below the I/G optimum power, and the battery SOC is low, then a portion of I/G power is used to charge the battery.

- Stationary charging: the battery is charged from I/G power without the vehicle being driven;
- Regenerative braking: the electric motor is operated as a generator to convert the vehicle's kinetic energy into electric energy and charge the battery. This operational way will be discussed in "1.2.1.1 Regenerative Braking system" paragraph.

When the ICE and electric motor are connected in parallel, both electric motor and ICE can deliver mechanical power to the wheels.

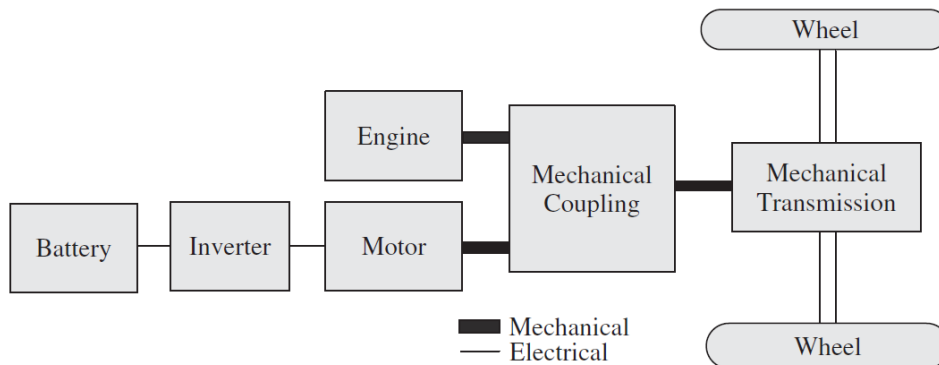


Fig 5- Parallel HEV scheme.

The ICE and electric traction motor can deliver power to the final drive in combined mode or separately.

When power demands are low, the electric motor can be utilized as a generator to recover kinetic energy during braking or absorbing a portion of power from the engine. In a parallel HEV, a second electric motor is added that serves primarily as a generator. This configuration improves the fuel efficiency increasing degree of freedom.

When these configurations are combined, the new architecture is called series-parallel HEV that incorporates the features of both series and parallel HEVs.

In comparison to a series HEV, the series-parallel HEV adds a mechanical link between the engine and the final drive, so the engine can drive the wheels directly.

1.2 Diesel hybrid vehicle

HEVs can also be built around diesel vehicles. All typologies explained, such as series, parallel, series-parallel, are also applicable to diesel hybrid. Since diesel vehicles can generally achieve higher fuel economy, when hybridized, these vehicles can provide significant fuel savings.

1.2.1 Locomotive application

Nowadays, thanks to its flexibility, hybrid technology is also utilized in other vehicular areas such as aircraft, ship and locomotive. Diesel locomotives are a special type of hybrid. A diesel locomotive uses a diesel engine and generator set to generate electricity. It uses electric motors to drive the train. Even though a diesel locomotive can be referred to as a series hybrid, in some architectures there is no battery for the main drive system to buffer energy between the ICE and the electric motor. This special configuration is sometimes referred to as simple hybrid. In other architectures, batteries are used and can help reduce the size of the generator and can also be used for regenerative energy capture. The batteries, in this case, can also be utilized for short-term high current due to torque needs, without resorting to a larger generator [6].



Fig 6- Chicago METRA electro-diesel locomotive by EMD (Electro-Motive Diesel).

There are many advantages why a diesel-electric locomotive system is utilized.

In a purely mechanical transmission a system with gearbox is needed to create the torque in the wheels, this has as consequence the decrease of efficiency due to mechanical loss.

During speed fluctuations diesel engine operates at different speed rather than the most optimum speed at which the efficiency is highest. With an electric-diesel system, the engine can always work at the optimal speed and a generator can run to produce electricity and drives the wheels.

Another improvement with respect to a pure diesel system is the best fuel economy as highlighted before.

With the advent of power electronics this system is rather easy to realize, using reliable and efficient traction motors.

Traction motor can be mounted in different configurations:

- Truck or bogie control: a single motor drives all the wheels on the truck or bogie, typically four wheels per motor;
- Axle control: the motor drives both wheels on a single axle. This is the most common configuration;
- Wheel control: each wheel is driven by its own motor. This allows the maximum degree of control over the locomotive but is not often used.

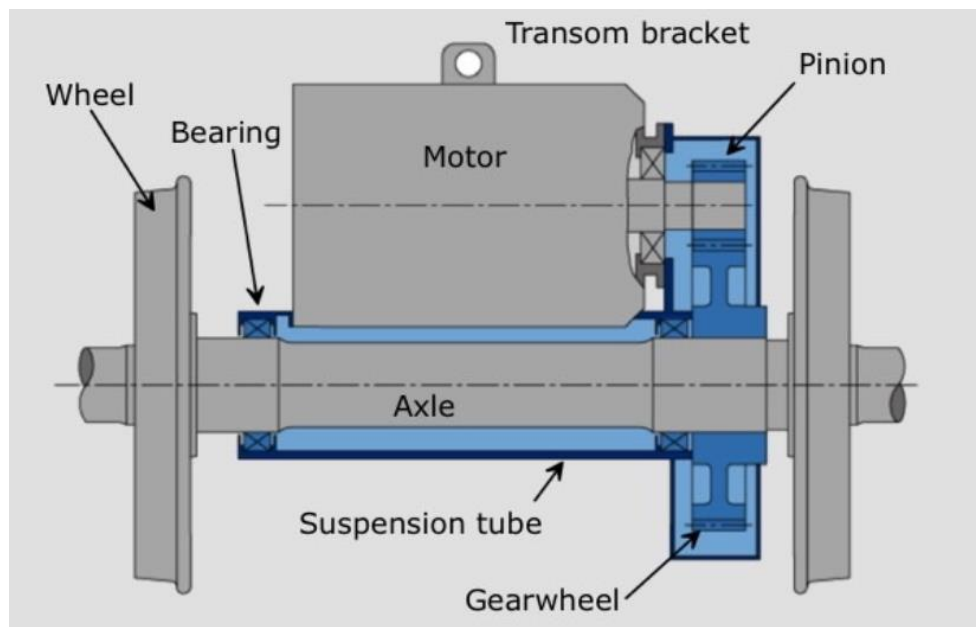


Fig 7- Axle control configuration.

In general, the traction motors are placed on each axle of the locomotive to drive the wheel.

The engine drives an AC main generator which generates AC current.

The AC current can be rectified to DC by diodes that powers DC traction motor. With DC motor the speed characteristic could be varied, allowing relatively smooth operator control of acceleration. For slow operation two motors could be run in series off the direct current supply. If higher speed is desired, the two motors could be operated in parallel, making a higher voltage available at each and allowing higher speed.

The AC current from generator can be rectified to DC and reconverted to AC which then powers the AC traction motor. The first conversion from AC to DC current by diodes is made because the DC rectification provides “clean” current that can be used by inverters to provide proper frequency needed by the traction motor.

Efficiency of the traction motor is usually 81% electrical generator converts 90% of the engine’s output into electrical energy and traction motor converts 90% of electrical energy into mechanical energy to the wheels.

The special hybrid diesel railcar architecture equipped with energy storage system on-board that permits to storage braking energy with an energy saving system (ESS) and helps in improving fuel economy and allows driving the trains for short-haul. This particular ESS is called Regenerative Braking system (RBs). RBs is a more efficient energy saving railcar application.

1.2.1.1 Regenerative Braking system

When a conventional vehicle applies its brakes, kinetic energy is converted to heat as friction between the brake pads and wheels. This heat is carries away in the airstream and the energy is effectively wasted. The total amount of energy lost in this way depends on how often, how hard and for how long the brakes are applied.

Regenerative braking refers to a process in which a portion of the kinetic energy of the vehicle is stored by a storage system. Energy normally dissipated in the brakes is directed by a power transmission system to the energy storage system during deceleration. That energy is held until required again by the vehicle, whereby it is converted back into kinetic energy and used to accelerate the vehicle [7].

Regenerative Braking scheme is shown in Fig 8.

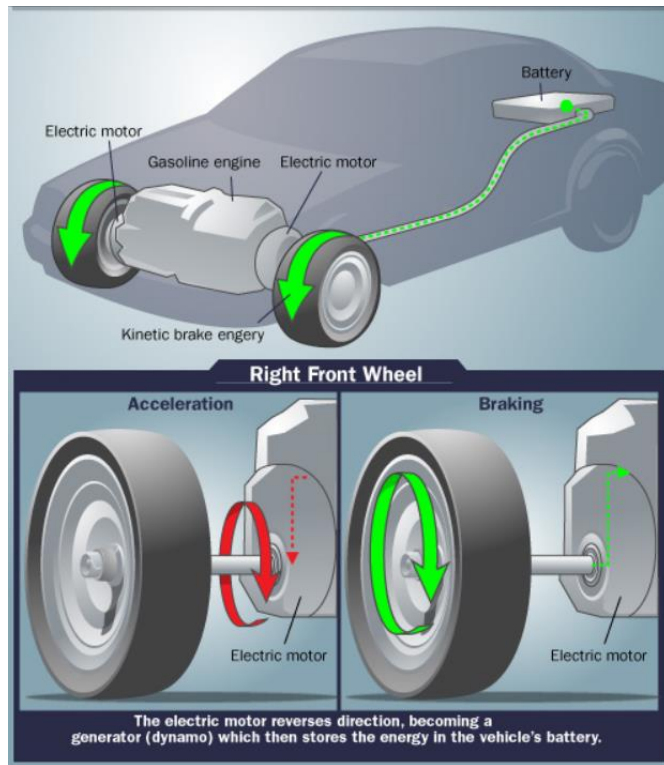


Fig 8-How Regenerative Braking works [8].

A significant amount of energy is consumed by braking. Braking a 1500 kg vehicle from 100 km/h to zero speed consumes about 0.16 kWh of energy in a few tens of meters. If this amount of energy is instead consumed in coasting by only overcoming the drags (rolling resistance and aerodynamic drag) without braking, the vehicle will travel about 2 km. The braking energy in typical urban areas may reach up to more than 25% of the total traction energy.

Thus, it is concluded that effective regenerative braking can significantly improve the fuel economy of EVs and HEVs [3].

Kinetic energy that is involved during braking phase is given by Eq. (1.8):

$$E_{kinetic} = \frac{1}{2} * mass * speed^2 \quad (1.8)$$

Since railway vehicle has a mass of the order of magnitude of tons and speed can reach some hundreds of kilometers per hour, it amounts to a huge amount of energy [9].

To capture this energy and store it on-board, it is necessary to have some energy storage systems. Battery, ultracapacitor or combination of the two or even a flywheel storage unit are the most important energy storage systems that are utilized in the RBs.

The aim of this project thesis is to study the most common energy storage system in a Regenerative Braking system: electro-chemical battery.

2 Batteries

Batteries are the most important energy storage devices utilized in HEVs. The performance, cost, safety and reliability of the vehicle is closely tied to the characteristics and usage of its battery.

Battery can work in two ways: to produce electrical power through chemical energy or to produce chemical energy through electrical power. The batteries that can work in both ways are called rechargeable.

This project thesis is focus on rechargeable batteries, also called secondary batteries.

Battery is made up from groups of electrochemical cells, that are the smallest electrochemical units.

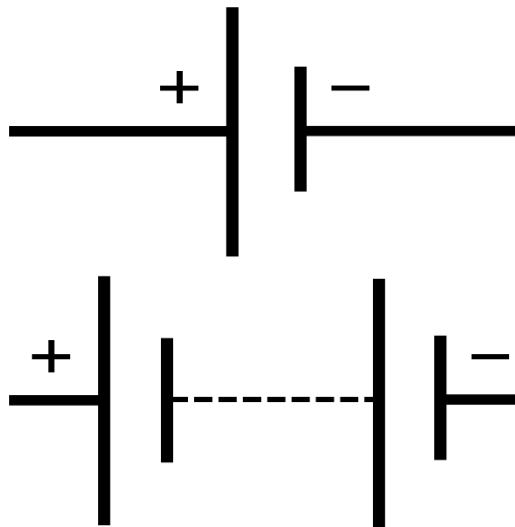


Fig 9- Schematic symbol for a cell and a battery.

The cycle of a rechargeable battery can be divided in discharge and charge configurations.

In discharge configuration chemical energy is directly transformed into electrical power, and the cell is called a galvanic cell; in charge configuration electrical power is provided to produce chemical energy that is stored to be used when requested, here the cell is called an electrolytic cell.

The main elements of an electrochemical cell are: anode, cathode and electrolyte, separator and current collectors. Anode and cathode are called electrodes. The Fig 10 shows a schematic diagram of an electrochemical cell.

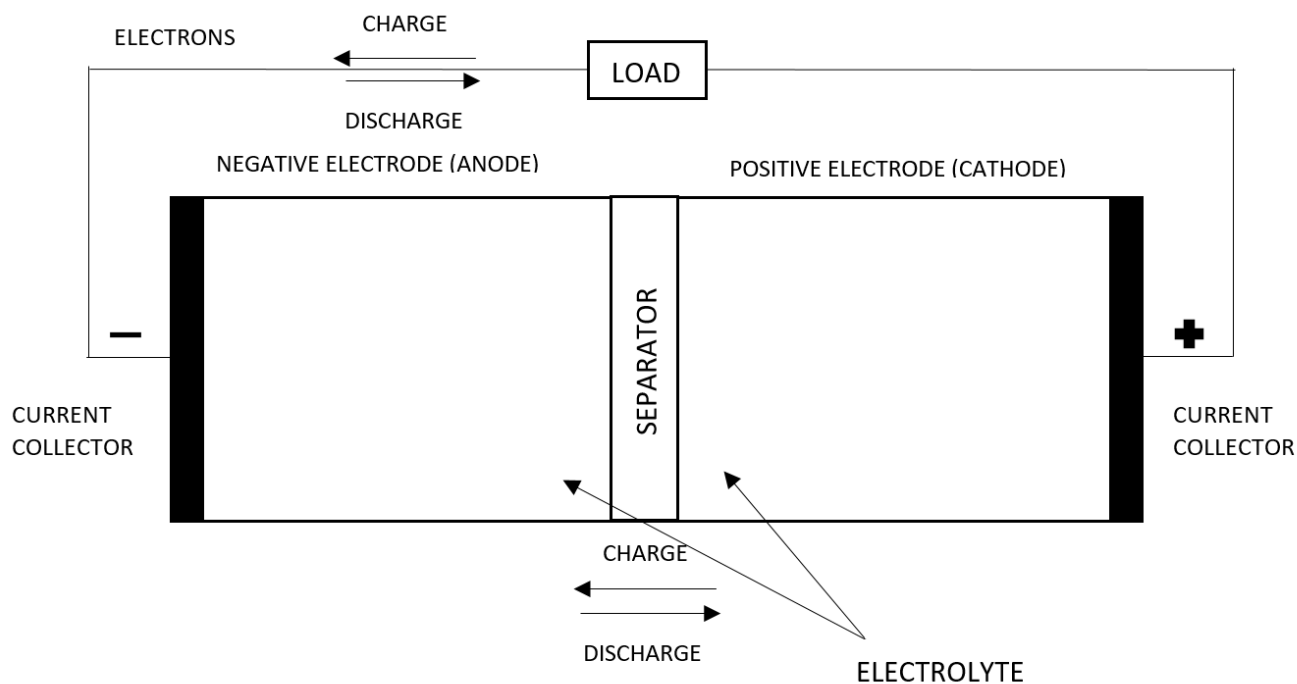


Fig 10-Schematic battery diagram.

During discharge cathode accepts electrons from external circuit and delivered ions: half-reaction of reduction occurs. During charge cathode gives up electrons to external circuit and half-reaction of oxidation occurs.

Electrolyte is an ionic conductor that provides the medium for internal ionic charge transfer between the electrodes. In general, it is made of a liquid solvent in which solute is dissolved that provide ionic conductivity. Electrolyte must be an electronic insulator. During discharge, ions delivered from reduction reaction moves through it from cathode to anode. During charge, ions moves from anode to cathode.

Separator is an insulator that divides physically the two electrodes. It is made of polymers such as polypropylene and polyethylene. It is moistened with electrolyte and forms a catalyst that promotes the movement of ions from cathode to anode on charge and in reverse on discharge.

Current collectors are electronic conductors though which electrons moves from electrode to external circuit or vice versa. Current collector of negative electrode is usually made of copper, while current collector of positive electrode is usually made of aluminum.

The operating conditions determine the efficiency of electrochemical cells and hence require rigorous understanding. Behind the operation of every electrochemical cell, there are series of thermodynamic and chemical equations that should be well understood.

2.1 Chemistry and kinetics

The maximum amount of work that can be performed during a chemical process is related to variation of Gibbs free energy of the species involved into reaction.

According to Nernst equation (2.1):

$$\Delta G = z_f * F * OCV \quad (2.1)$$

Where:

- z_f is charge number of specie that is equal to number of electrons delivered or gained;
- F is Faraday constant equal to $96487 \frac{C}{mol}$;
- OCV is open circuit voltage [V]. It will be discussed later.

Gibbs free energy ΔG is function of thermodynamic states (2.2):

$$\Delta G = \Delta H - T * \Delta S \quad (2.2)$$

Where :

- ΔH is enthalpy [$\frac{J}{kg}$];
- ΔS is entropy [$\frac{J}{kg * K}$];

Fixing enthalpy and entropy values, spontaneity of reaction is dependent to temperature value.

There are four cases:

1st case: $\Delta H < 0$ and $\Delta S < 0$ reaction is spontaneous at low $T \rightarrow \Delta G < 0$;

2nd case: $\Delta H < 0$ and $\Delta S > 0$ reaction is always spontaneous at every $T \rightarrow \Delta G < 0$;

3rd case: $\Delta H > 0$ and $\Delta S < 0$ reaction is never spontaneous at every $T \rightarrow \Delta G > 0$;

4th case: $\Delta H < 0$ and $\Delta S > 0$ reaction is spontaneous at high $T \rightarrow \Delta G < 0$;

Gibbs free energy of formation ΔG_f is expressed in terms of reactants and products (2.3):

$$\Delta G_f = G_f(\text{products}) - G_f(\text{reactants}) \quad (2.3)$$

For a generic reaction (2.4):



Change of Gibbs free energy can be expressed by (2.5):

$$\Delta G_f = \Delta G_f^0 + R * T * \frac{[C]^{\nu_c} [D]^{\nu_d}}{[A]^{\nu_a} [B]^{\nu_b}} \quad (2.5)$$

Where:

- ΔG_f^0 is Gibbs free energy at standard conditions (298.15 K and 1 bar);
- R is the universal gas constant equal to $8.314 \left[\frac{J}{mol \cdot K} \right]$;
- $[C]^{\nu_c}$ and the others similar terms represent the molar concentration of reactants and products, powered by their stoichiometric coefficients.

An important term is represented by OCV, that is present in equation (2.1).

OCV is the maximum potential difference that is present between the two electrodes when the circuit is open. In this configuration the two electrodes aren't electrically connected and they can't exchange electrons and ions as no redox reactions occur.

Substituting equation (2.5) in (2.1), OCV can be expressed by (2.6):

$$OCV = -\frac{\Delta G(T, P)}{zf * F} = -\frac{\Delta G(T, P_0)}{zf * F} + \frac{\bar{R} * T}{zf * F} * \ln \frac{[A]^{\nu_a} [B]^{\nu_b}}{[C]^{\nu_c} [D]^{\nu_d}} \quad (2.6)$$

In terms of partial pressures (2.7):

$$OCV = -\frac{\Delta G(T, P_0)}{zf * F} + \frac{\bar{R} * T}{zf * F} \frac{\prod_i^n \left(\frac{P_i}{P_0}\right)^{\nu_i}}{\prod_i^m \left(\frac{P_i}{P_0}\right)^{\nu_i}} \quad (2.7)$$

Thus, OCV depends on the partial pressure of reactants and products and temperature.

When electrochemical cell works as galvanic cell, OCV and useful power increase with increment of reactants partial pressure and with reduction of temperature.

When electrochemical cell works as electrolytic cell, OCV and absorbed power decreases with reduction of reactants partial pressure and with increment of temperature.

Another parameter that influence electrochemical cell efficiency is the velocity of reaction. The branch of chemical that studies how fast is, is chemical kinetics. The main parameter to determine velocity of reaction is called “rate of reaction”.

Rate of reaction represents the speed at which reactants are converted into products.

Rate of reaction is expressed by the following equation (2.8), referred to the generic reaction (2.4):

$$r = -\frac{1}{\nu_a} \frac{dC_a}{dt} = -\frac{1}{\nu_b} \frac{dC_b}{dt} = \frac{1}{\nu_c} \frac{dC_c}{dt} = \frac{1}{\nu_d} \frac{dC_d}{dt} \quad (2.8)$$

Where:

- ν is stoichiometric coefficient;
- C is concentration of chemical species in $[\frac{mol}{m^3}]$.

According to law of mass action, rate of reaction is also defined by following equation (2.9):

$$r = k * \prod_i^n C_i^{mi} \quad (2.9)$$

Where:

- K is the reaction rate constant;
- C_i is concentration of reactant “i”;
- mi derives from fitting parameters and satisfies $\sum_i mi = reaction\ order$ (it is equal to stoichiometric coefficient in some case).

A critical parameter that influence rate of reaction is the rate constant k .

According to Arrhenius equation, k is defined as:

$$k = A * e^{-\frac{E_a}{RT}} \quad (2.10)$$

Where:

- A is a pre-exponential that derives from empirical data.
- E_a is activation energy, that represents minimum energy of collision between particles able to activate the reaction. It is measured in Joule. if E_a is low, reaction occurs more easily. An expedient to reduce activation energy is represented by the presence of catalyst. If E_a decreases, k increases.
- R is universal gas constant equal to $8.314 [\frac{J}{mol*K}]$;

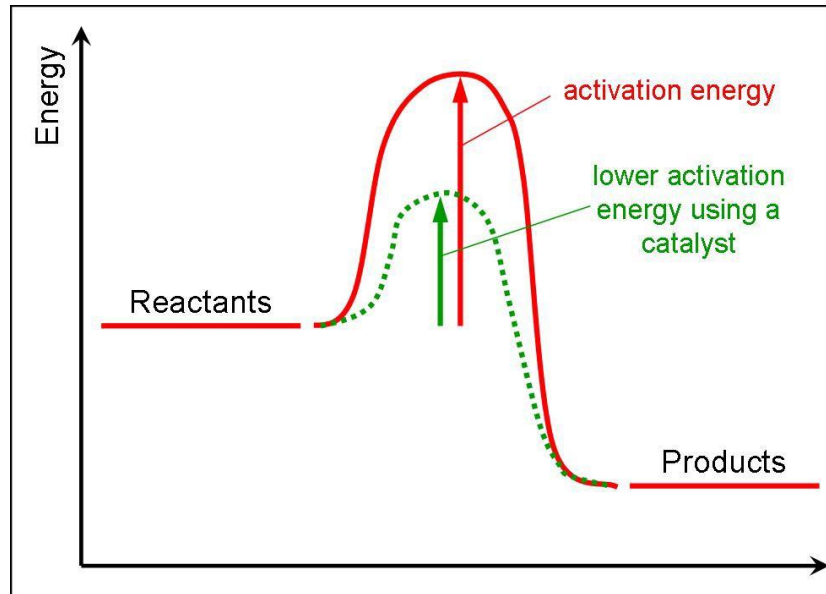


Fig 11- Activation energy.

As can be seen from above equation, temperature is an important parameter that influence the speed of reaction. If temperature value increases, rate of reaction increases. The reason is simple: when a mixture is heated up, the kinetic energy of particles increases, and they move faster and collide frequently. This increases the speed of reaction and thus the reaction rate.

2.2 Polarization curve

Propagation of charges, ions and electrons, are due to difference of potential.

Current flow is given by (2.11):

$$i = -\sigma * \nabla E \quad (2.11)$$

Where:

- σ is conductivity of the matrix electrodes [$\frac{S}{m^2}$];
- E is electric potential [V];

The maximum potential difference is when there is no external load, no current and the circuit is open and is called the open circuit voltage. When the circuit is closed, system is not in ideal condition and the real potential across the cell is lower or higher than OCV. The potential drop is due to charge and mass transport phenomena that occurs when the circuit is closed, and electrons and ions are changed between electrodes. The diagram that explain this concept is represented by polarization curve. Polarization curve is a plot of current density i [$\frac{A}{m^2}$] versus electrode potential E [V].

Considering the generic polarization curve (Fig 12):

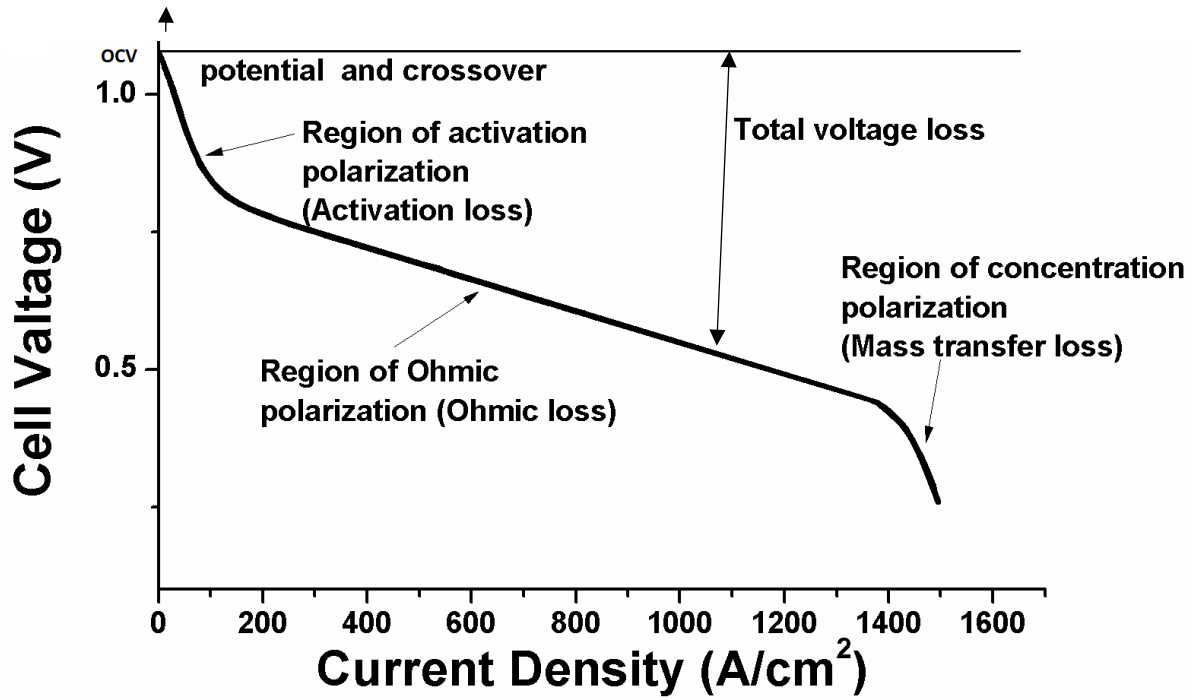


Fig 12-Polarization curve.

Total voltage losses are due to three major factors: activation losses, ohmic losses and diffusion process losses.

Activation losses are the main cause of voltage drop. This loss is related to the activation of electro-chemical reaction. Kinetic process depends on the rate of reaction. Referring rate of reaction to potential drop η , we obtain (2.12):

$$r = k * \exp\left(\frac{\alpha * v_i * z_i * \eta * F}{R * T}\right) \quad (2.12)$$

Where α is transfer coefficient and it depends on β (symmetry factor) and n_{rsd} (number of electrons transferred).

From definition of rate of reaction in terms of potential drop, Butler-Volmer equation can be defined (2.13):

$$i = i_0 * \left(e^{\frac{\beta * F * \eta_{act}}{R * T}} - e^{\frac{-(1-\beta) * F * \eta_{act}}{R * T}} \right) \quad (2.13)$$

Where i_0 is current density exchanged when reaction is at equilibrium.

Butler-Volmer equation explicitly relates current density and activation voltage drop: a smaller value of i_0 means grater voltage drop and, vice versa, higher value of i_0 means lower voltage drop.

Another important loss to consider is ohmic loss. An electro-chemical cell is composed by electrodes and electrolyte. Electrodes represent a resistance to the flow of electrons; the electrolyte offers resistance to the flow of ions. Ohmic losses are caused by both flow of electrons at cathode and flow of ions through the electrolyte. The cell interconnects also contribute to the ohmic losses.

Ohm law is given by (2.14):

$$\Delta V = R * I \quad (2.14)$$

Where:

- I is current [A];
- R is resistance [ohm];
- V is potential [V];

Referring to current density and resistivity,(2.14) can be rewritten (2.15):

$$\Delta V = \rho * i * L = ASR * i \quad (2.15)$$

Where ASR is Area Specific Resistance that represents mainly the resistivity and thickness of electrolyte that ions must traverse. It is important to notice that resistivity ρ depends by material properties and temperature, as shown from equation (2.16) :

$$\rho = \rho_0 * [1 + \gamma * (T - T_0)] \quad (2.16)$$

Where:

- γ is temperature coefficient and depends from material;
- ρ_0 is resistivity at T_0 (in general $T_0 = 20 \text{ }^\circ\text{C}$).

The behavior of the material is different, for conductor materials if temperature increases, resistivity decreases, and voltage drop due to ohmic losses is lower, for semiconductor materials if the temperature increases, resistivity increases and ohmic drop is higher.

Voltage drop due to molecular diffusion processes is related to the diffusion of reactants molecules that must reach point of reaction. The molecular diffusion determines the reactants molecule concentration in any point of the electrodes that influences number of reactions and the current produced.

Diffusivity process is related to diffusive coefficient of the species (2.17):

$$D_i^{eff} = \left(\frac{p}{\tau}\right)^n * D_i \quad (2.17)$$

Where:

- D_i^{eff} is effective diffusivity coefficient of specie "i" [m^2/s].
- D_i is diffusive coefficient specie "i" in bulk condition;
- p is porosity;
- τ is tortuosity;
- n is fitting parameter.

Tortuosity is defined in (2.18):

$$\tau = p^{-brugg} \quad (2.18)$$

Where *brugg* is Bruggeman coefficient.

The description of diffusion is given by Fick's law (2.19):

$$N_i = -D_i * \nabla c_i \quad (2.19)$$

Where:

- N_i is the molar flux [$\frac{mol}{sec*m^2}$] of *i* specie;
- ∇c_i is concentration gradient [$\frac{mol}{m^3}$];
- D_i is diffusion coefficient.

Another important quantity is the transport number, that determines how fast concentration gradients will form under load. Transport number is the fraction of the total electrical current carried in an electrolyte by a given ionic species. While the activity coefficient determines the voltage drop associated with a given concentration gradient

It is clear that the molar flow due to diffusion is proportional to the concentration gradient.

2.3 Reactions

As described in previous section, in any electro-chemical process, electrons flow from one chemical substances to another, driven by an oxidation-reduction (red-ox) reaction.

A redox reaction occurs when electrons are transferred from a substance that is oxidized to one that is being reduced. The reductant is the substance that loses electrons and is oxidized in the process; the oxidant is species that gains electrons and is reduced in the process. A redox reaction can be described as two half-reactions, one representing the oxidation process and one the reduction process.

Chemical reactions occur into electrodes, in particular oxidation half-reaction takes place at negative electrode, while reduction half-reaction takes place at positive electrode. In discharging configuration, negative electrode is represented by anode and positive electrode by cathode. Whereas in charging configuration the vice versa is valid.

Considering a generic redox reaction, the total reaction is represented by (2.20):



The two half-reaction are:

Oxidation reaction (2.21):



Reduction reaction (2.22):



The kinetics, chemistry and reactions are depended on the materials and characteristics of the different typologies of battery.

2.4 Li-ion battery

There are many types of batteries utilized in hybrid vehicle. The most important are: Lead-Acid (Pb-acid), Nickel-Metal hybrid (Ni-MH) and Lithium-ion batteries (Li-ion). Their theoretical voltage is determined from electrode materials.

Referring to main battery parameters, the table and plot below makes a comparison between the different type of battery:

Table 4-Comparison between types of batteries [10].

	Pb-acid	Ni-MH	Li-ion
Voltage [V]	1.93	1.35	4.1
Specific energy [Wh/kg]	166	240	410
Energy efficiency	0.65-0.70	0.55-0.65	~0.80

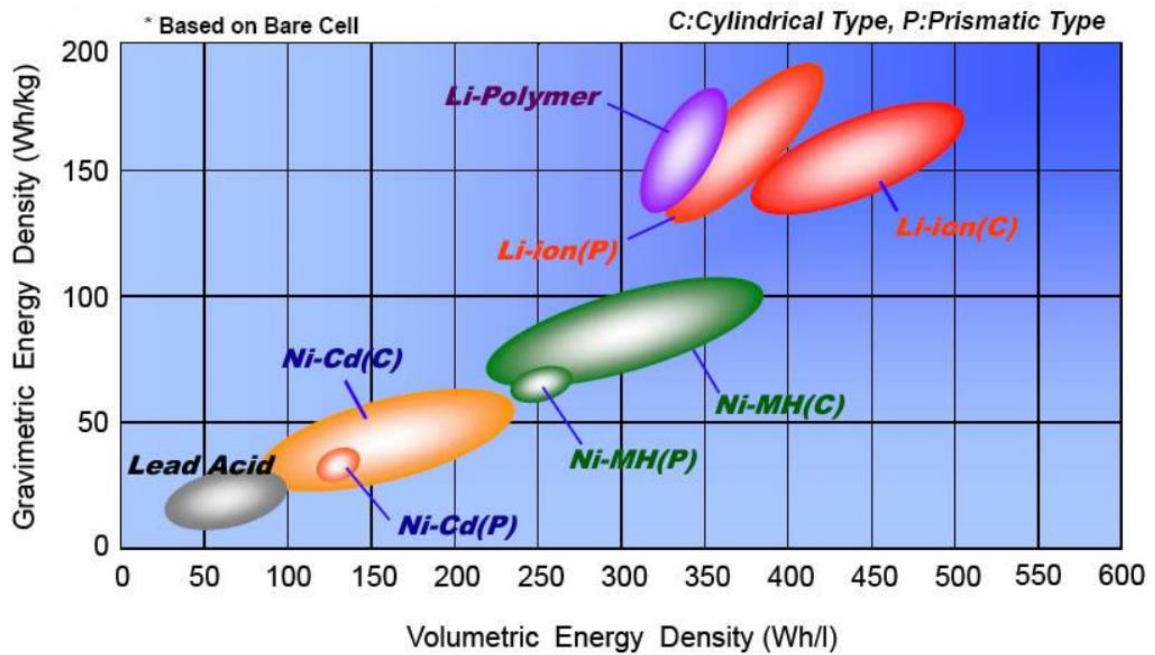


Fig 13-Comparison types of batteries: energy density, size and weight [11].

As we can see from Table 4, Li-ion batteries have high energy density, which makes them attractive for hybrid vehicles applications, in particular, for railcars.

Li-ion battery, with its continuous improvement of technology and performance, has become the first choice for electric vehicles in recent years.

Hybrid electric vehicles (HEV) requires batteries with high power, fast charge capability and long-life capabilities.

Lithium is the lightest metallic element and has a considerably high potential and energy density. These are some of properties that make Li-ion chemistry a very good candidate or electric vehicle applications [12].

Lithium-ion batteries have some advantages and limitations [13] :

Advantages are:

- High specific energy and high load capabilities;
- Long cycle and extend shelf-life and maintenance-free;
- High capacity, low internal resistance;
- Low self-discharge.

Limitations:

- Requires protection circuit to prevent thermal runaway if stressed;

- Degrades at high temperature and when stored at high voltage;

Today, a wide range of Li-ion chemistries are available, and they are identified with respect to the composition of their anode and cathode.

Table 5 shown major Li-ion battery materials:

Table 5-Comparison of Li-ion battery cathode and anode materials [12]

Material	Specific capacity [mAh/g]	Voltage [V]	Characteristics ✓ <i>Pro</i> ○ <i>cons</i>
LiCoO ₂ Lithium cobalt oxide (cathode)	160	3.7	✓ Good capacity and cycle life ○ Expensive, unsafe during fast charging
LiMn ₂ O ₄ Lithium Manganese Oxide (cathode)	130	4.0	✓ Acceptable rate capability and low cost ○ Poor cycle and calendar life
LiFePO ₄ Lithium Iron Phosphate (cathode)	140	3.3	✓ Good cycle life, power capability, low cost and improved abuse tolerance ○ Low capacity and calendar life
NMC Lithium Nickel Manganese Cobalt Oxide (cathode)	180	4.2	✓ High capacity and lowest cost ○ Life cycle
NCA Lithium Nickel Cobalt Aluminum Oxide (cathode)	185	4.2	✓ Highest capacity and low cost ○ Safety
Graphite (anode)	372	<0.1	✓ Low cost, flat and low potential profile ○ Low volumetric density, high sensitivity to electrolytes and easy exfoliation

LTO Lithium Titanate (anode)	168	1.0-2.0	<ul style="list-style-type: none"> ✓ Highest cycle life ○ High cost and low energy density
Silicon (anode)	3700	0.5-1.0	<ul style="list-style-type: none"> ✓ Very high energy ○ In early experimental stage and large volume expansion

As it was explained before, an electrochemical cell is composed of anode, cathode, electrolyte and current collectors. In the case of Lithium-ion battery, it can be schematized as in Fig 14 :

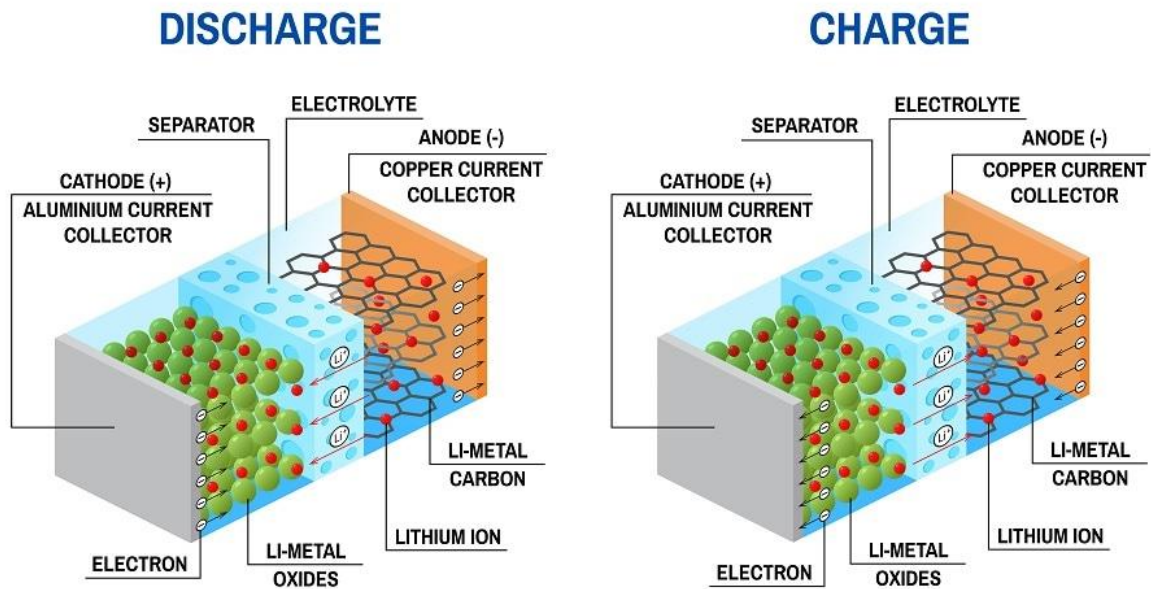


Fig 14-Lithium-ion electrochemical cell: discharge and charge configuration.

Discharging process: At anode oxidation reaction occurs and Li^+ ion and electrons are delivered. Li -ions starts to travel from anode to cathode, while electrons passing through external circuit Fig 15:

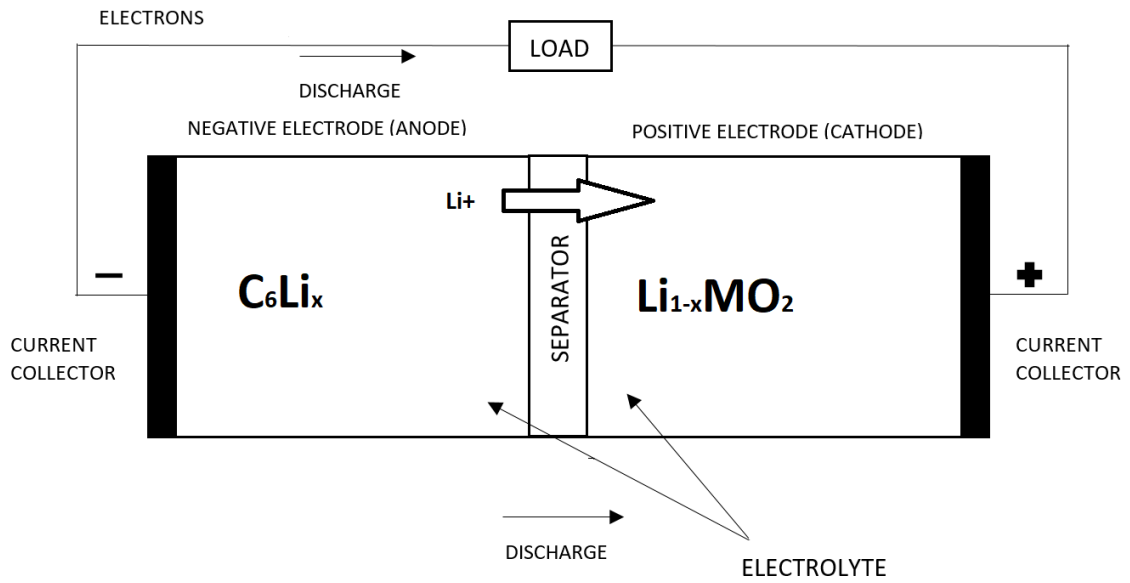


Fig 15-Li-ion discharge process.

Oxidation reaction (2.23):



At cathode reduction reaction occurs and Li ions and electrons are accepted Fig 16:

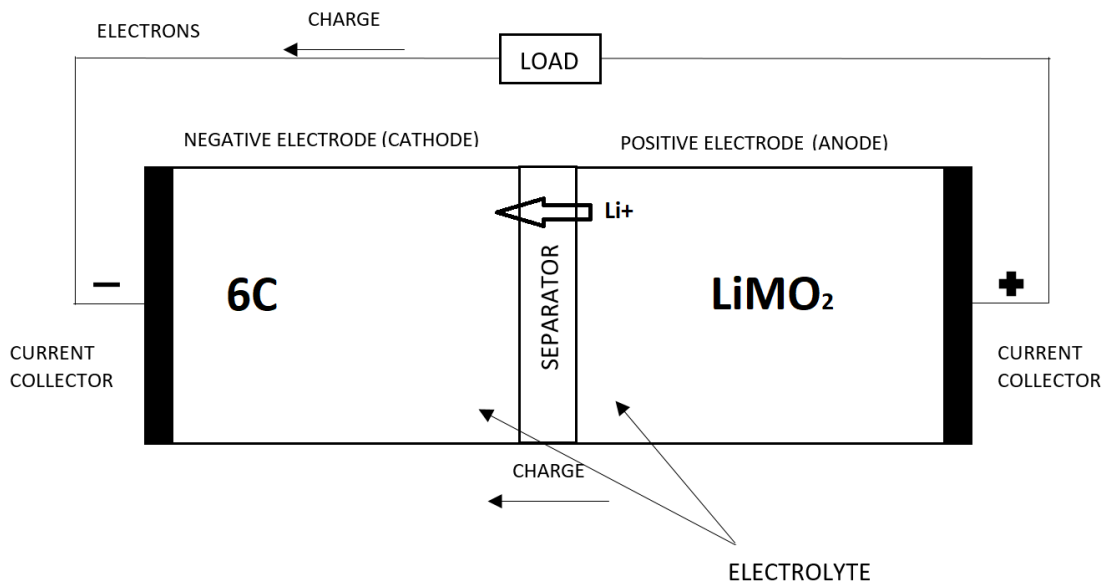
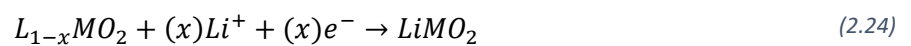


Fig 16-Li-ion charge process.

Reduction reaction (2.24):



Complete redox reaction is (2.25):



To facilitate lithium ion transport between the active materials of electrodes using the electrolyte within the cell, electrode materials need to be porous in nature. Being able to control the porosity increases the intercalations between the electrode and the electrolyte and increases the intra-electrode conductivity, with an adequate lithium-ion intercalation. In chemistry, the term “intercalation” refers to reversible inclusion or insertion of a molecule or ion into compounds with layered structures.

Electrode materials with high electrochemical intercalation potential can be used to develop a high energy density.

During ion intercalation, solid electrolyte interphase (SEI) layer is created on electrode surface. SEI at anode usually consist of reduction products of electrolytes formed through reactions between electrode and electrolytes due to electrons leakage from the anode.

On one hand, SEI formation allows Li^+ transport and blocks electrons to prevent further electrolyte decomposition and ensure continued electrochemical reactions; on the other hands SEI formation and growth consume active lithium and electrolyte material, leading to capacity fade, an increase in battery resistance and poor power density.

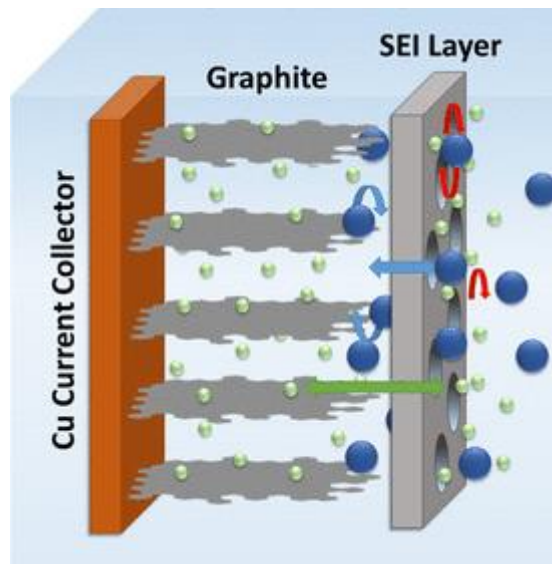


Fig 17- SEI scheme.

Battery researches attribute different issues as underutilization, capacity fade, thermal runaway and low energy density with Solid-Electrolyte Interphase layer growth.

2.4.1 Battery configurations

There are three main configurations of Li-ion cells in electrical vehicles by winding and stacking up the anode-separator-cathode sandwich layer are: the cylindrical shape and the prismatic shape, whereas the prismatic shape can be further divided into hard-case cell and prismatic pouch cell.

The cylindrical cell is one of the most widely used. The advantages are ease of manufacture and good mechanical stability. It has good cycling ability, offers a long calendar life and it is economical.

The prismatic design improves the space utilization and increases the flexibility while cylindrical cells are more economical and easy to produce due to the manufacturing maturity even though at the expense of low space efficiency.

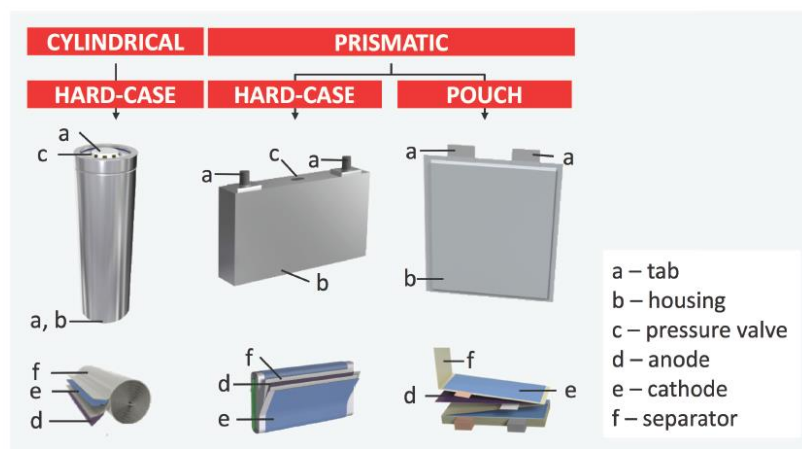


Fig 18- Schematic and pictures of different battery configuration: cylindrical and prismatic [14].

The pouch cell offers a simple, flexible and lightweight solution to battery design. It makes most efficient use of space. It is light and cost-effective but the exposure to humidity and high temperature can reduce its life. Shape of cells is chosen based on their demand.

Battery is composed by many numbers of cells depending on type of load to provide adequate power and energy.

The electrochemical cells can be connected in series or in parallel assembling a battery module. Many battery modules can be connected in series or parallel assembling a battery pack. Focusing on series and parallel connections, connecting two or more cells or batteries in parallel, the total capacity will be two or more times the value of the nominal capacity, as shown in Eq. (2.26).

$$Q_{tot} = n_p * Q_n \quad (2.26)$$

Where:

- Q_{tot} is total capacity [Ah];
- n_p is number of branch in parallel;
- Q_n is nominal capacity [Ah];

While connecting two or more cells in series, the total voltage will be two or more times the value of the nominal voltage, as shown in Eq.(2.27).

$$V_{tot} = n_s * V_n \quad (2.27)$$

Where:

- V_{tot} is total voltage [V];
- n_s is number of branch in series;
- V_n is nominal voltage [V];

3 Thermal modeling

As can be seen from equations that govern battery's electrochemical behavior, temperature is one of the most important parameters that influences its performance. Starting from the Gibbs free energy definition Eq.(1.8), passing through constant rate Eq. (2.10), keeping the battery temperature within desired ranges improves the battery efficiency. Freezing and overheating of the electrochemical system in the battery should be avoided to prevent any reduction in power capability, charge/discharge capacity and premature aging of the battery [12].

Thus, discrepancy between the optimum and operating conditions of the batteries need to be reduced significantly by implementing battery thermal management systems (BTMs).

3.1 Thermal issues in Li-ion battery

The temperature at which the battery is discharged/charged has a pronounced effect on its service life (capacity) and voltage characteristics. Both high and low battery operating temperature cause performance degradation and in extreme event dangerous failures.

3.1.1 High temperature and low temperature performance degradations

Performance degradations can be summarized as follow:

- capacity fade and power loss under high temperatures;
- reduction in chemical activity and increase in the internal resistance under low temperatures.

The Fig 19 shows the usual effect of lower discharge temperature that result in a reduction of capacity as well as an increase in the slope of the discharge curve. The reason is that at higher temperatures, the internal resistance decreases and, as a result, the ampere-hour capacity and energy output increase.

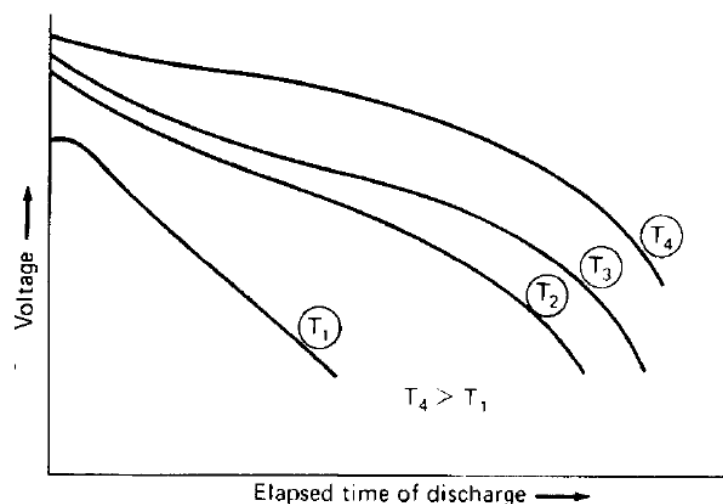


Fig 19- Effect of temperature on battery capacity. T1 to T4 increasing temperatures [15].

Despite apparent positive effect of high temperatures on battery capacity, chemical activity also increases and may be rapid enough during the discharge to cause a net loss of capacity. This phenomenon is known as “self-discharge”.

The Fig 20 shows the loss of capacity at higher temperatures at low discharge rates or long discharge times due to self-discharge or chemical deterioration. It is also seen that higher capacity may be obtained as a result of the battery heating at high rate discharge [15].

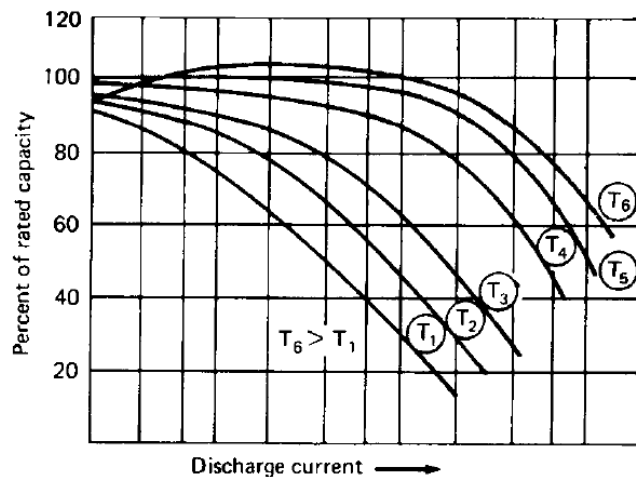


Fig 20-Effect of discharge load on battery capacity at various temperatures. T1 to T6 increasing temperature, T4 normal room temperature [15].

Another situation that need to be analyzed: high temperature storage and charging/discharging. Charging/discharging or storage of Li-ion cell at high temperatures can lead to a failure of the cell. The reasons can be:

- SEI layer breakdown: the SEI layer can breakdown and dissolve into the electrolyte if the cell temperature rises above 120°C. An exothermic chemical reaction between the negative electrode and the electrolyte can start at this temperature.
- Electrolyte vaporization: under high temperature, the electrolyte can vaporize, and the consequence is an increase of cell’s internal pressure. This increase can lead to cell’s vent mechanism and expulsion of the vaporized electrolyte from the cell.
- High rate of charge and discharge: during high charging/discharging rate, the positive electrode can chemically oxidize the electrolyte, the exothermic oxidation process releases heat and increases the temperature. If the process is allowed to continue, the cell temperature become sufficiently high and cause degradation of the separator, resulting in a cell internal short.

Fig 21 shows the capacity fade due to high temperature of a cell during its operation:

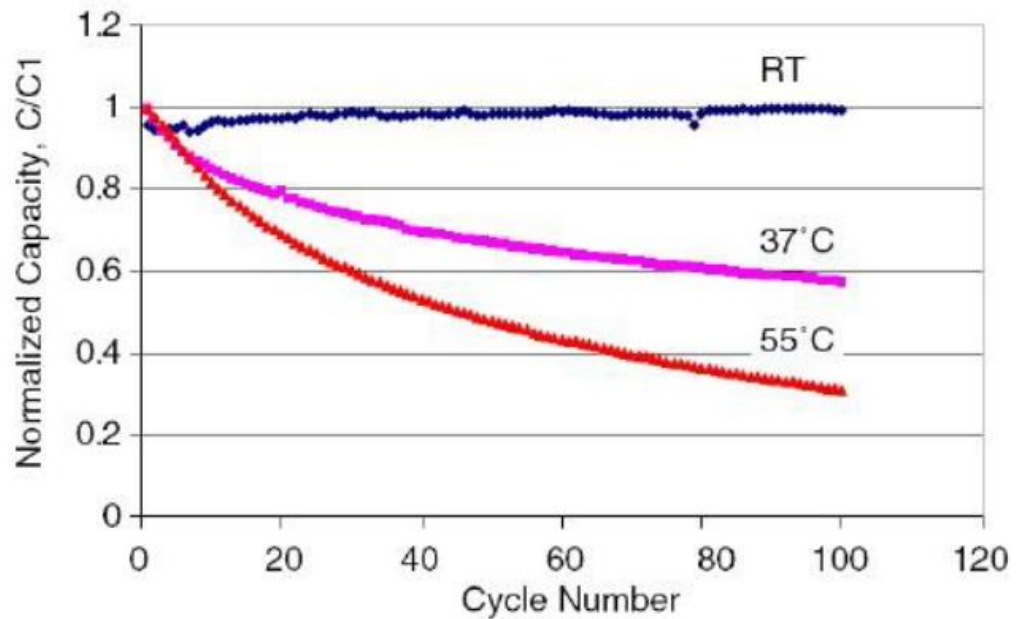


Fig 21- Normalize discharge capacity with cycle number at 25°C, 37°C and 55°C [16].

Many studies have demonstrated that the cell performance decreases under low temperature.

There are three different hypotheses about the deterioration of low temperature performance of lithium ion batteries:

- The ionic conductivity of electrolyte is too low at low temperature;
- The low conductivity of SEI film formed at the interface of solid and liquid at low temperature;
- The solid phase diffusion coefficient of Li^+ ions in carbon anode material is too low at low temperature.

The ionic conductivity of the electrolyte is one transport property that helps to determine how fast a cell can be charged or discharged. Conductivity of SEI film and solid phase diffusion coefficient determine how slow or fast of kinetics of charge transfer. Electrochemical impedance spectroscopy studies, that were conducted at low temperature, demonstrated an increase of the cell impedance due to an increase of the interfacial resistance of the cathode/electrolyte interface [17]. Another issue is the formation of the lithium plating: the lithium dendrites grow on the negative electrode surface and decrease the charge capacity of the cell as some of the cyclable lithium intercalated in the graphite is lost. Furthermore, it may penetrate the separator thus results in internal short-circuits [14].

All of these issues reduce the delivered power and energy density of the batteries at low temperatures. Citing one of the study conducted about how low temperature influence the

performance of Li-ion batteries, the battery tested at 25 °C has $\approx 800 \frac{W}{l}$ and $100 \frac{Wh}{l}$, while at -40°C has $\approx 10 \frac{W}{l}$ and $5 \frac{Wh}{l}$ [18].

Battery behavior at low temperature makes the utilization of Li-ion batteries in the cold environments inappropriate.

3.1.2 Thermal runaway

The consequences of a failure event in a Li-ion battery tend to be more severe compared to other rechargeable battery chemistries for two reasons. First, Li-ion batteries have a higher energy density than other battery chemistries; therefore, more heat can be generated by the chemical reaction between the positive and negative electrodes. Second, Li-ion batteries use a flammable organic solvent as the electrolyte that can ignite and release additional heat if exposed to the air. It is this combination of high-energy density and a flammable electrolyte that makes safety a much larger issue for Li-ion battery systems than it has been for other battery chemistries.

Another undesirable condition due to the elevated battery temperature is thermal runaway. This condition induces a series of exothermic reactions which in turn raises the temperature further until irreparable incidents happen. The consequences of thermal runaway are fire and explosion and they are serious problems that arouse concerns from public. Battery Thermal runaway is caused by particular abuse conditions such as mechanical and electrical abuse that carry to increase temperature batteries.

Fig 22 shows some accidents due to TR.

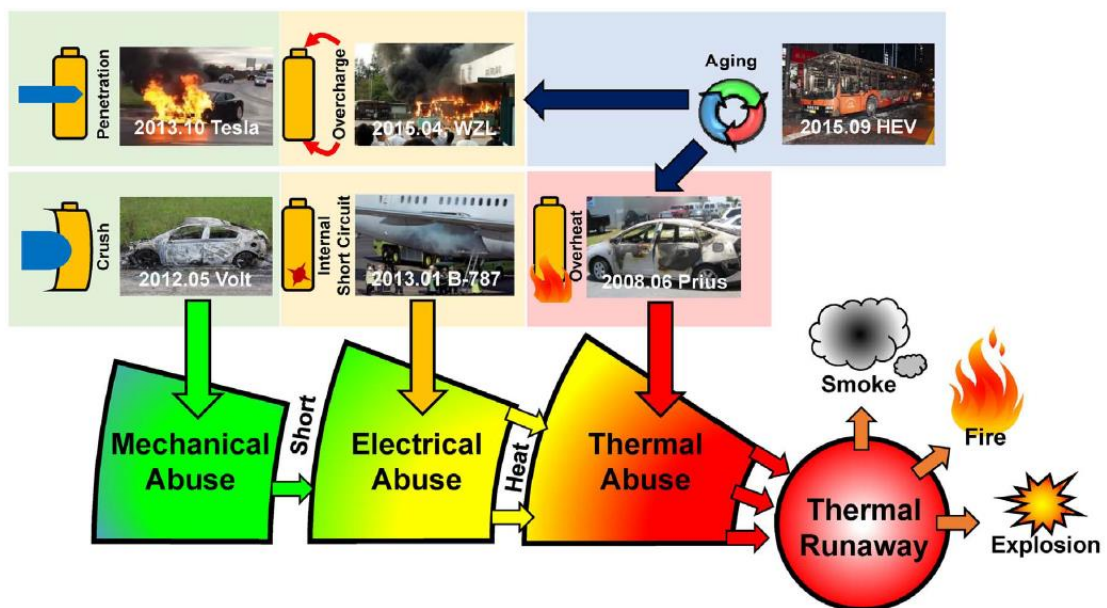


Fig 22-Accidents related with lithium ion battery failure and correlated abuse conditions [19].

Mechanical abuse is due to a destructive deformation and displacement caused by vehicle collision and consequent crash or penetration of the battery pack.

The main causes of electrical abuse are [4]:

- External short circuit: the electrode with voltage difference are connected by conductors. In a fully charged multicell Li-ion battery, this can generate high peak currents. Under worst-case conditions, this can lead to cell venting with the release of flammable electrolyte, generation of toxic gases or rupture of the cell. This can start a chain reaction causing neighboring cells to fail due to the heat generated.
- Internal short circuit: it can occur between two current collectors, Cu current collector and positive electrode active material, Al current collector and negative electrode active material, active material on both the electrodes.

3.1.3 Temperature gradient

There is a great discrepancy between the battery at the center of module and those near the edge. The convection coefficient is higher at the surface of the outer battery thus provides better dissipation conditions than inner cell in the pack. Apart from the temperature distribution among cells, the temperature imbalance within a cell is important to consider. The heat generation rates are not uniform inside the cell. This causes the local deterioration which has an adverse effect in the performance of the whole cell and may result in the battery failure. In summary, the temperature non-uniformity both cell to cell and within the cell have a negative effect in the performance of the battery pack. This condition doesn't permit to reach best performance. The acceptable condition inside the battery pack is usually a maximum temperature deviation below 5°C among the cells [14].

After describing the main degradation phenomena of Lithium ion batteries that depends from temperature, the heat generation inside electrochemical cells is analyzed in the next section.

3.2 Heat generation rate

The process of conversion of electrical energy to chemical energy and vice versa produces heat, which results in increased cell temperature. The operation of a lithium-ion cell is based on several highly coupled phenomena involving multiple physical processes. For example, exothermic electrochemical reactions produce heat, which causes temperature rise. Since temperature directly affects the rates of electrochemical reactions and electrical impedances, therefore, the thermal performance of the cell in turn affects electrochemical and electrical performance. High energy content in Li-ion batteries plays a large effect on thermal phenomena that affect performance and safety of battery.

However, the factors influencing the thermal behavior of cell are extremely complex. Multiple mechanisms including electricity, electrochemistry, heat transfer are coupled and the involved parameters change with time, temperature, State of Charge etc...

Many researchers such as Newman and his coworker conducted studies to model work of electrochemical systems. The models, based on different physical mechanism, can be classified as electro-thermal model [20]. Focusing on heat generation at a single cell level, an energy balance is required to calculate the heat generated by the cell and the temperature changes in a cell. Since most lithium cells are very thin (less than 300 μm thick), temperature gradients perpendicular to the electrodes are negligible. The form of the energy balance used in modeling batteries is described by (3.1) [21]:

$$\dot{Q} = I \left(V_{oc} - V + T \frac{\partial V_{oc}}{\partial T} \right) + C_p \frac{dT}{dt} \quad (3.1)$$

Where:

- \dot{Q} is the rate of the heat transferred to the system from its surrounding [W];
- V_{oc} is open-circuit potential and V is cell potential [V];
- $I(V_{oc} - V)$ is the heat generated due to the presence of the resistance to the passage of current;
- $I T \frac{\partial V_{oc}}{\partial T}$ is the heat generated due to the reversible heat effects;
- $C_p \frac{dT}{dt}$ is the product of heat capacity at constant pressure and temperature variation.

There is a more general form of the energy balance which includes heats of multiple reactions, mixing, phase change and changes in heat capacity. Heat required to form concentration gradients during the passage of current is released upon relaxation of those gradient after interruption of the current.

The equation (3.1) can be rewrite:

$$\dot{Q} = I \left(V - V_{oc}(c_s) + T \frac{\partial V(c_s)}{\partial T} \right) + C_p \frac{dT}{dt} + \int \sum_i (H_i - H_i(c_s)) \frac{\partial c_i}{\partial t} dv \quad (3.2)$$

Where:

- the term c_s refers to the local lithium concentration in the solid averaged over the cross-sectional area of the electrode;
- H_i is molar enthalpy of species "i" and c is concentration;
- The integral is over the entire cell.

After analyzing how heat is generated inside a cell, it is important understand how to dissipate it properly. This is the task of the Battery thermal management system (BTMs).

3.3 Battery thermal management system (BTMS)

The BTMS is an important and integral part of a battery management system (BMS). BMS has a great impact on safe operation, optimization of the strategy for vehicles, choice of the charging mode and reduction of operating costs. It should provide real-time monitoring of battery states and fault diagnosis and inform the vehicle control unit (VCU). Then the VCU can adopt the corresponding control strategy to achieve effective and safe use of the battery. In order to achieve an efficient operation of the vehicles as well as to extend the cycle life of the batteries, the BMS should include the following functions [22]:

- Battery cell voltage measurement;
- Battery temperature measurement;
- Battery pack current measurement;
- Battery total voltage measurement;
- Thermal management;
- Battery pack state of health (SOH) estimation;
- Battery pack SOC estimation;
- Analysis of battery fault and online alarm;
- Communication with on-board equipment;
- Communication with battery charger which can realize the safe charge;
- Recording of discharge and charge times.

The following Fig 23 schematizes BTMs key functions:

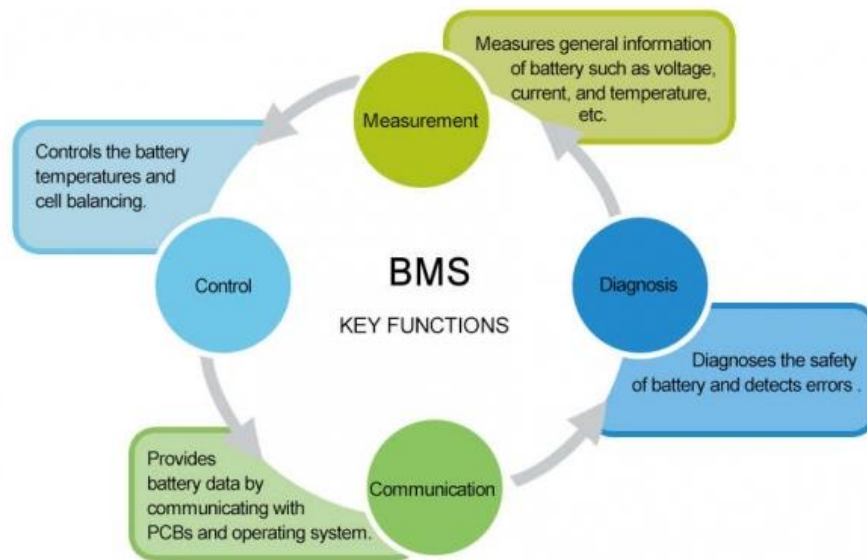


Fig 23- Scheme of BMS key functions [23].

Summarizing, BMS takes the imprint of “chemical battery” during charging and discharging and establishes the “digital battery” that communicates with the user. Fig 24 shows scheme of battery that is composed by stored energy, empty portion and inactive part that is permanently lost. BMS is programmed to measure these portions and to control them [24].

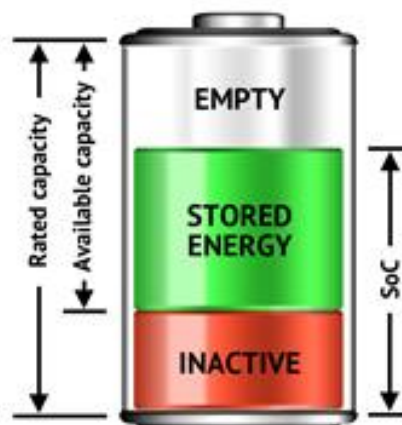


Fig 24- The three parts of the battery.

One of the main functions of BMS is temperature measurements. Temperature measurement is the real-time monitoring of the operating temperature of the battery pack. Currently, the measurement

methods include use of a thermocouple, metal thermal resistance temperature detector, thermistor, analog integrated temperature sensor and intelligent temperature sensor.

- The thermocouple is widely used in temperature measurement. Its main features include wide measurement range, stable performance, simple structure, good dynamic response, small measurement error. Its temperature range is 0 °C to 1600 °C.
- A thermal resistance detector is a common temperature detector in the middle-low temperature region. Its principles are based on the fact that the resistance of a conductor or semiconductor will change as the temperature changes. Its temperature range is -200 °C to 600 °C;
- The thermistor is a temperature measurement device comprising solid semiconductors with a high resistance temperature coefficient. Its temperature range is -50°C to 400°C;
- The intelligent temperature sensor can output data and control data. It has good characteristics, such as high measurement accuracy, fast conversion time, programmability, multipoint measurement in parallel, convenient measurement and installation. Its temperature range is -40°C to 150°C.

Because of the different numbers of temperature measurements required in different battery packs, the number of a temperature measurement module need flexible adjustment.

The fluctuations of the temperature, as it has been said before, are kept under control by Battery thermal management systems.

To optimize the performance of a battery and pack/module, the thermal energy management system should have:

- Optimum operating temperature range for every cell and all battery modules, rejecting heat in hot climates/ adding heat in cold climates;
- Small temperature variations within a cell and modules;
- Compact and lightweight, easily packaged, reliable, low-cost and easy for service;
- A provision for ventilation if the battery generates potentially hazardous gases.

Fig 25 shows a generic battery thermal management system:

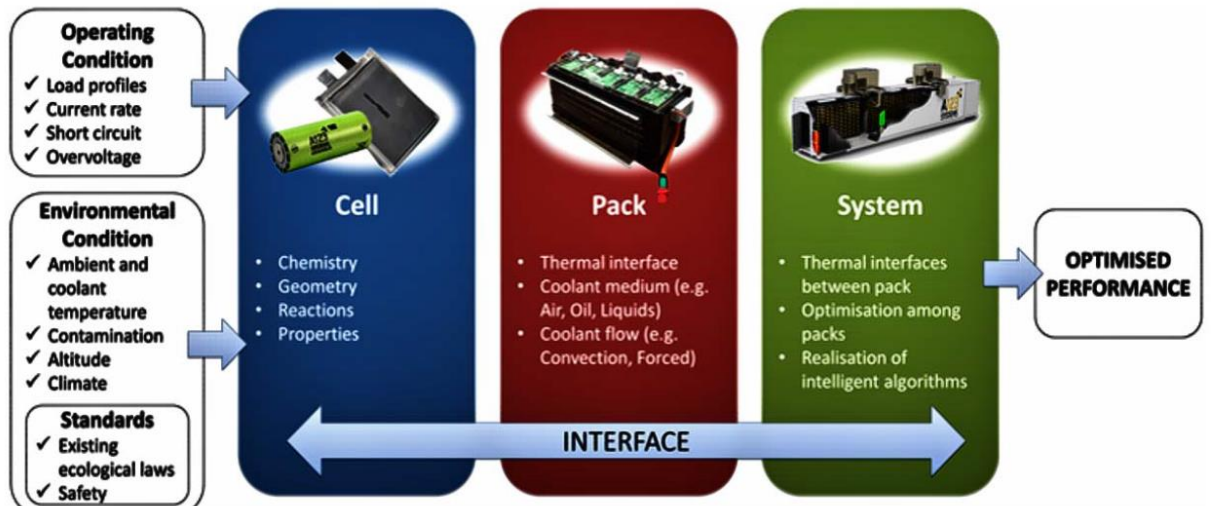


Fig 25- Battery Thermal Management system (BTMs) [25].

The thermal management strategies can be either internal or external. Internal cooling allows to remove heat directly from the source. This approach includes forced circulation of the electrolyte or thermos-electric coolers. However, conventional thermal management systems for lithium-ion batteries remove heat from the exterior surface of the battery (external BTMs). External BTMs can be classified into passive, in which only ambient environment is used, and active, in which a built-in source provides heating and/or cooling. The medium can be [26]:

- Air: either natural or forced air convection can be used. This method can't efficiently dissipate heat in large-scale batteries. Passive air cooling is possible for batteries of low energy density, an active air cooling is requested for high energy density batteries such as lithium-ion batteries;

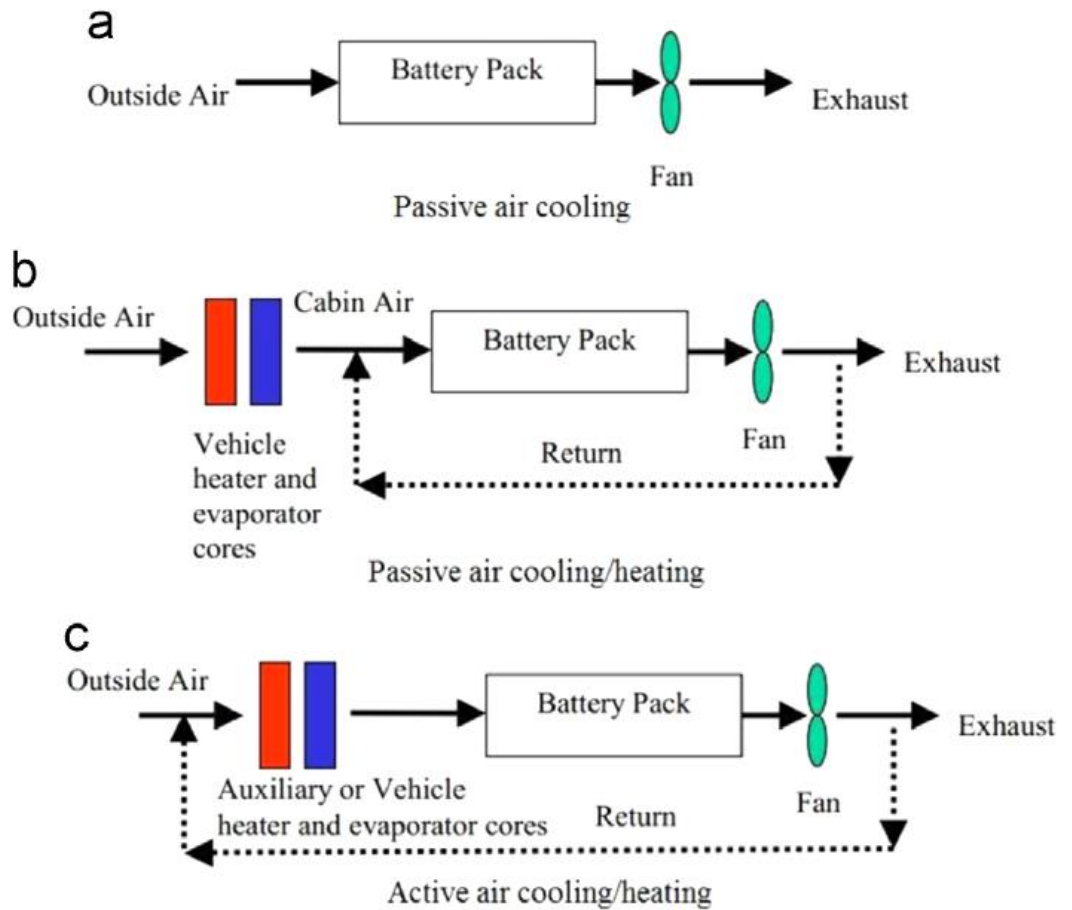
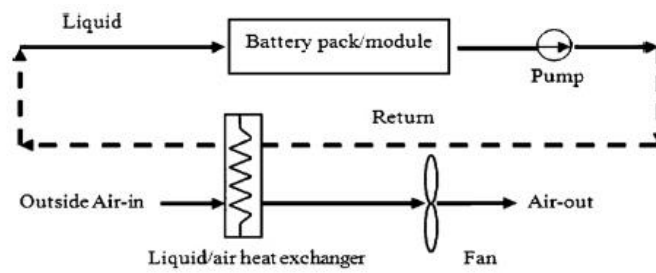
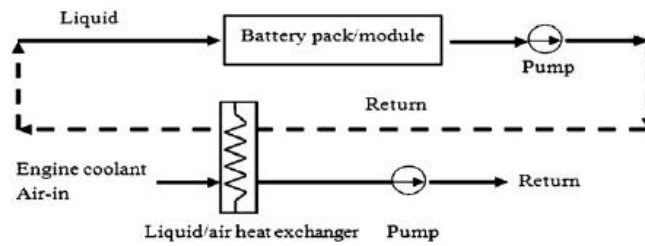


Fig 26- a) Passive air cooling scheme; b) passive air cooling/heating scheme; c) active air cooling/heating scheme [26].

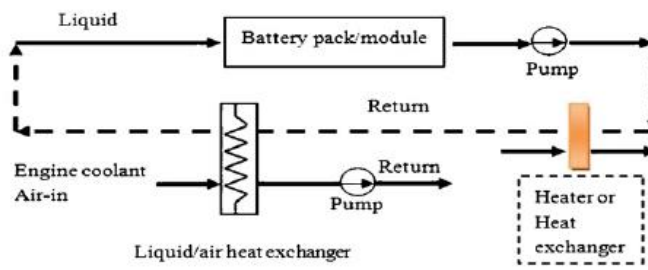
- Liquid: liquid has high thermal conductivity and heat capacity. These qualities make it a better solution in BTM. It can be divided into passive and active methods. The medium can be refrigerant (such as water, glycol, oil) or coolant (acetone). The use of oil permits to achieve the heat transfer coefficient 1.5 to 3 times higher than air, while water or water/glycol more than 3 times. This indicates that the temperature difference will be reduced to 1/3 of than obtained from air [26].



(a) Passive liquid cooling



(b) Active moderate cooling/heating



(c) Active cooling (high temperature)/heating (cold temperature)

Fig 27- Thermal management using liquid: a)Passing liquid cooling; b) active moderate cooling/heating; c) active cooling(high temperature) /heating (cold temperature) [27].

- PCM: this kind of material normally has a large latent heat of fusion and a desirable melting point that can store or release large amount of heat. The heat transfer route starts from the battery, which generates heat, and goes to the PCM and then to the battery case in contact with the ambient air. PCM eliminates the need for active cooling/heating during the majority operating time because it delays the temperature rise when the ambient is cold and maintains the battery below ambient during hot days.

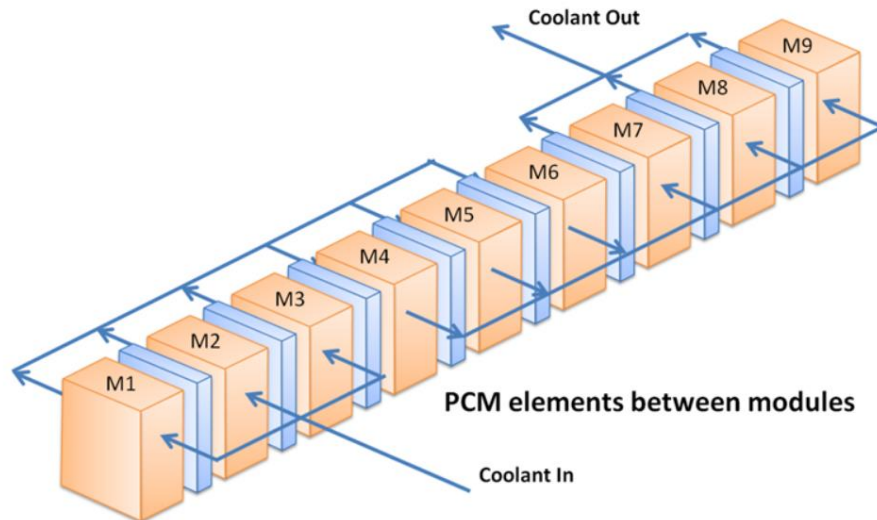


Fig 28- Battery cooling layout with additional PCM elements [28]

- Heat pipe: heat pipes are considered versatile for the efficient cooling and thermal management. The mechanism of a heat pipe is that the heat can be transferred through latent heat of vaporization from the evaporator to the condenser, and the working fluid from the evaporator to the condenser, and the working fluid can be passively transported back to the evaporator by capillary pressure developed within a porous wick lining.

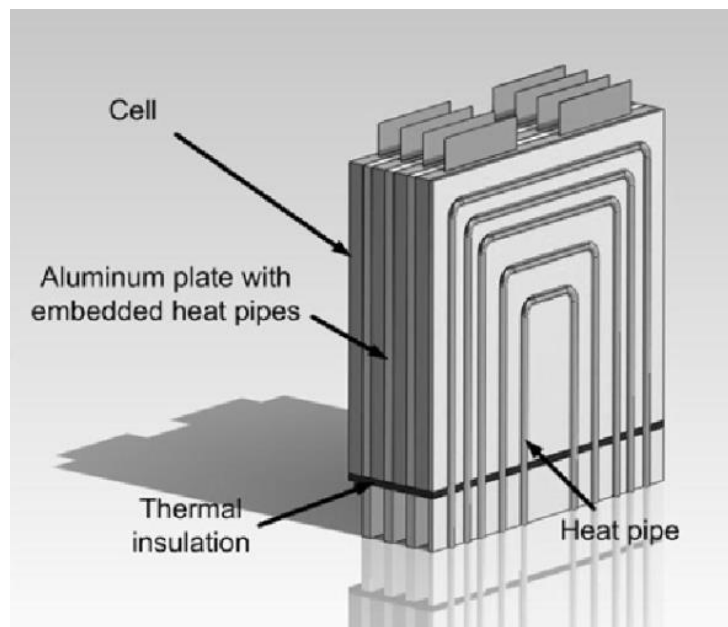


Fig 29- Heat pipes cooling system [29].

To size the proper thermal management system of a battery, heat generation rate of the smallest electrochemical cell should be known.

3.4 Predicted models

For the optimal design of lithium-ion battery and its thermal management system, models that predict the performance of the battery have been developed by many researchers. These models provide information on battery charging/discharging and transient behavior and health status of the battery as a function of different stress factors such as temperature, discharge rate, etc. However, the batteries behaviors are time-variant and strongly non-linear, for these reasons accurate simulation models are difficult to obtain. Common battery models can be grouped into three main groups: mathematical models, electrochemical models, equivalent circuit models.

3.4.1 Mathematical models

Mathematical models are based on experimental data to predict the future behavior of lithium-ion batteries, without consideration of physicochemical principles. Polynomial, exponential, power law, logarithmic and trigonometric functions are commonly used. One example of mathematical model is represented by stochastic methods. The computational simplicity of these models enables very fast computations, but since these models are based on fitting experimental data for a specific set of operating conditions, predictions can very poor for other battery operating conditions.

3.4.2 Equivalent circuit models

The equivalent circuit model is developed by using resistors, capacitors and voltage sources to form a circuit network. Typically, a large capacitor or an ideal voltage source is selected to represent the open-circuit voltage (OCV), the remainder of the circuit simulates the battery's internal resistance and dynamic effects such as terminal voltage relaxation. The equivalent circuit model is developed starting from data obtained by electrochemical impedance spectroscopy (EIS), which contains the data to model the battery. The development of equivalent circuit model uses an impedance-based modeling concept [30].

Impedance spectra is obtained by applying an AC signal " I_{ac} " with different defined frequencies and evaluating the system responses.

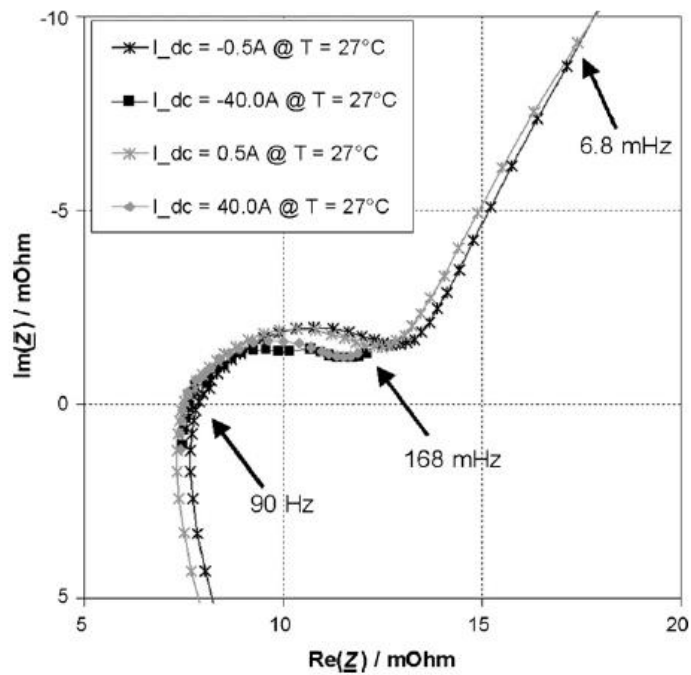


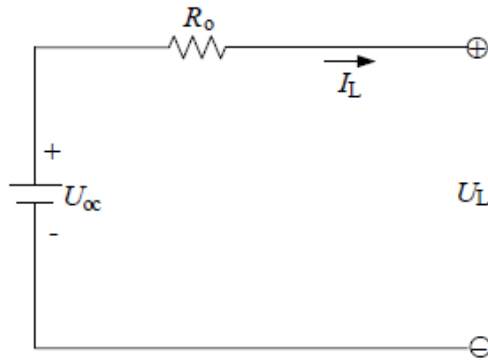
Fig 30- Impedance spectra at various direct currents I_{dc} [30].

The spectra show various behaviors and, based on these, different types of electric circuit features are used to model battery:

- Inductive behavior “L” caused by the metallic connectors of the battery;
- Pure ohmic resistance “ R_i ” reflects the limited conductance of the contacts, the active masses and electrolyte and charged double layers inside the battery.
- Parallel connection of non-linear resistor “ R_{ct} ” and capacitors “ C_{dl} ” are used to model non-linear behavior of charge-transfer process. In particular, the non-linear resistors behavior is described by Butler-Volmer equation (2.13).

There are many equivalent circuit models: R_{int} , RC [31], Thevenin and PNGV,

The R_{int} model implements an ideal voltage source U_{oc} to define the battery open-circuit voltage. Both resistance R_o and open-circuit voltage U_{oc} are functions of SoC (State of charge), SoH (State of health) and temperature. I_L is load current with a positive value when discharging and a negative value when charging, U_L is the terminal voltage, it is present in Fig 31.



$$U_L = U_{oc} - I_L R_o$$

Fig 31-Schematic diagram of the Rint model.

The RC model consist of two capacitors (C_c and C_b) and three resistors (R_t , R_e and R_c). The capacitor C_c represents the surface effect of a battery; the capacitor C_b represents the ample capability of a battery to store charge chemically. SoC can be determined by the voltage across the bulk capacitor. U_b and U_c are the voltages across C_b and C_c respectively. This model is represented in Fig 32.

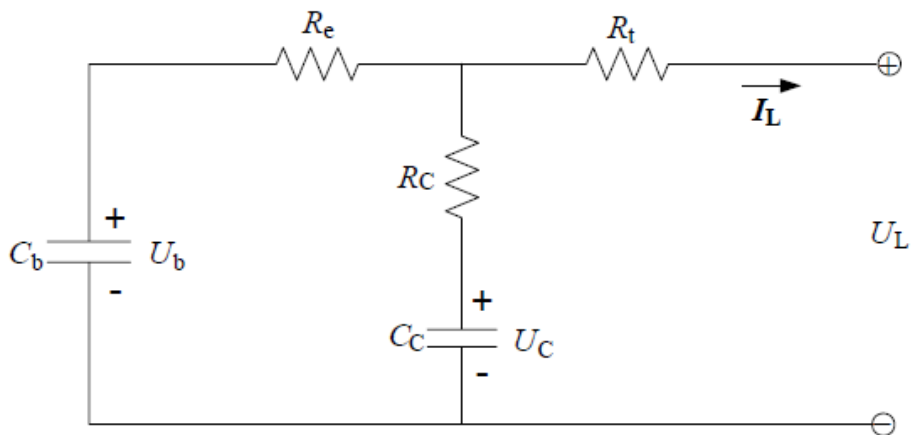
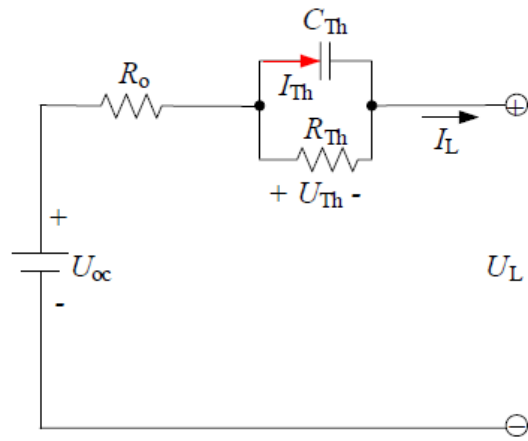


Fig 32-Schematic diagram of the RC model.

The Thevenin model connects a parallel RC network in series based on the Rint model. It is composed of open-circuit voltage U_{oc} , internal resistance and equivalent capacitances. Internal resistances are divided into ohmic resistance R_o and polarization resistance R_{th} . Transient behavior of the battery during its charging and discharging cycle is represented by equivalent capacitance C_{th} , U_{th} is the voltage across C_{th} and I_{ht} is the outflow current of C_{th} . The model is represented in Fig 33.



$$\begin{cases} \dot{U}_{Th} = -\frac{U_{Th}}{R_{Th} C_{Th}} + \frac{I_L}{C_{Th}} \\ U_L = U_{oc} - U_{Th} - I_L R_o \end{cases}$$

Fig 33- Schematic diagram of Thevenin model.

The PNGV model describes the internal resistance R_o , the changes of electromotive force with a capacitor C_o and battery polarization with a resistance R_1 and capacitor C_1 [32]. The PNGV model can be obtained by adding a capacitor in series based on Thevenin model to describe the changing of open-circuit voltage in the time accumulation of load current. The model is represented in Fig 34.

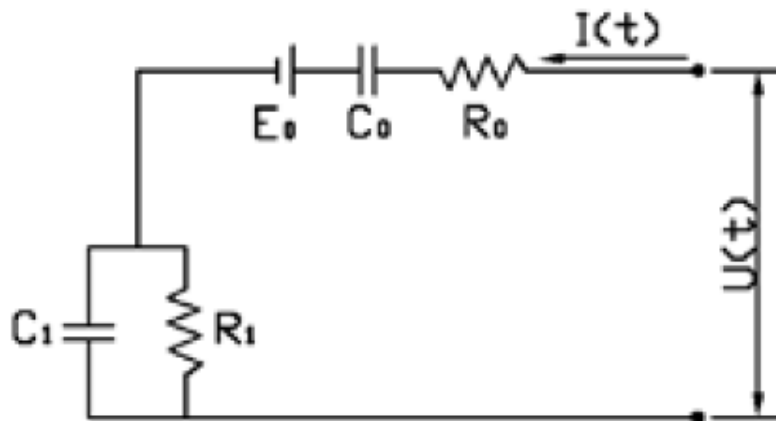


Fig 34- Schematic diagram of PNGV model.

3.4.3 Electrochemical models

The electrochemical models are based on the chemical processes that take place in the battery. These models develop continuum models that incorporate chemical/ electrochemical kinetics and transport phenomena to produce more accurate predictions. There are numerous electrochemical models and they have different complexity degree.

In Fig 31 the scheme of the different model types as functions of CPU time and accuracy is represented:

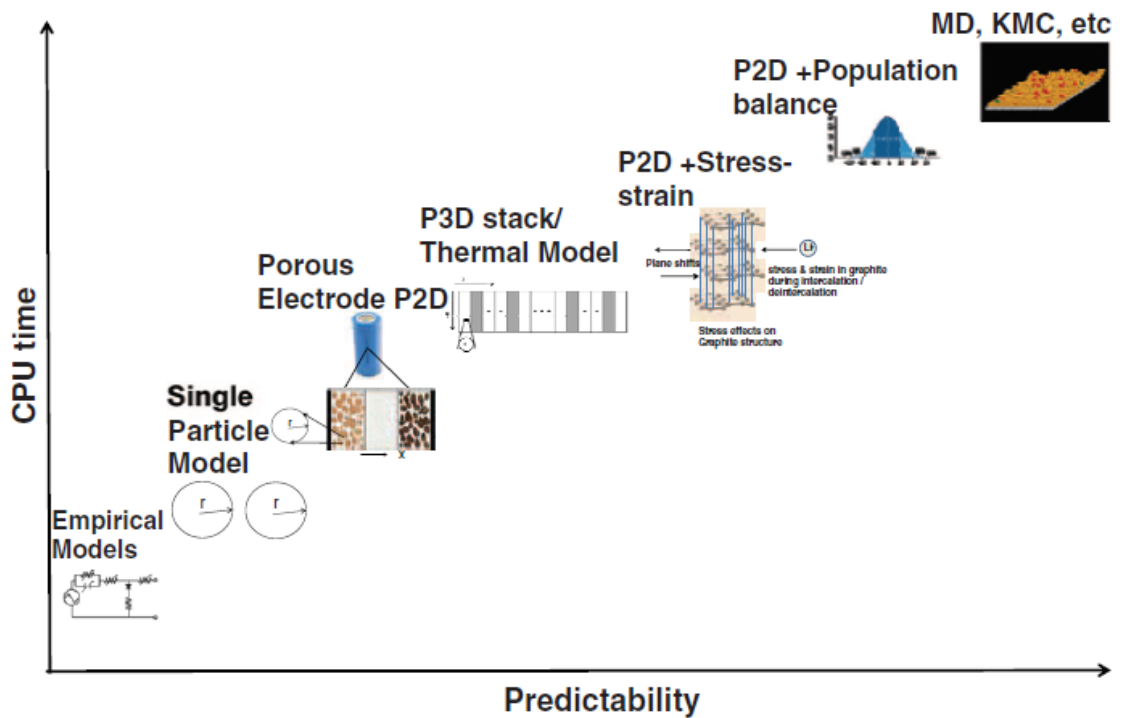


Fig 35- Electrochemical models scheme as function of CPU time and predictability [33].

3.4.3.1 Single particle model

The single-particle model takes into account the simplification of the effect of transport phenomena. The diffusion and intercalation phenomena are considered within the particle, while concentration and potential effect in the solution phase between the particles are neglected [33]. In this model each electrode is represented by a single-spherical particle whose area is equivalent to that of the active area of the solid phase in the porous electrode. The solid phase concentration is represented by a second order polynomial whose coefficients are expressed in terms of the average concentration [34]. The single particle model can be represented by Fig 36:

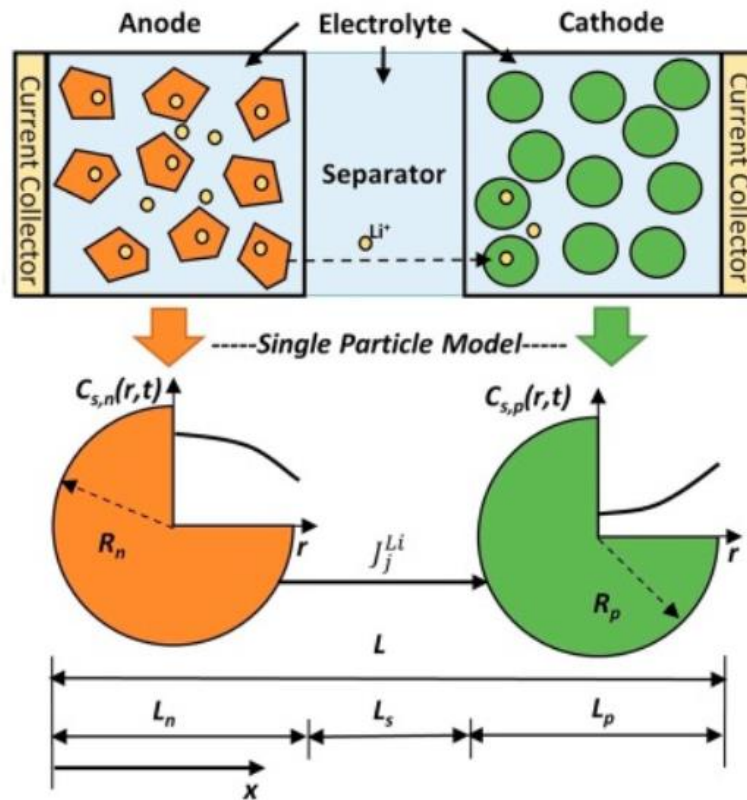


Fig 36- Schematic diagram that represents two single particles for each electrode [35].

The simplifications of the single-particle model reduce accuracy in simulating the cycling performance and contemporary these reduce time requested for the solution. Thus, single particle model is only valid for limited conditions such as low rates and thin electrodes.

3.4.3.2 Ohmic porous-electrode models

Increasing the complexity level, ohmic porous-electrode models are defined. These models take into account solid phase and electrolyte phase potentials and current, while spatial variation of the concentrations is neglected. In this approach it is assumed that the concentration within each spherical particle of each electrode can be approximated with a parabolic profile, similar to the single-particle model, other phenomena are included, for example the dependency of the conductivities as a function of porosity.

3.4.3.3 Pseudo-two-dimensional models

The pseudo-two-dimensional model is an expansion of ohmic porous-electrode models and includes diffusion in the electrolyte and solid phases, such models were developed by M. Doyle, T. Fuller and J. Newman [36]. The theory on which the models is based is the concentrated solution theory. Before this model, transport in the liquid electrolyte phase was described with dilute solution theory, in which an incorrect number of transport properties is defined because only interaction between the solute and the solvent are considered. For these reasons concentrated solution theory is appropriate. This theory provides the description of internal behavior of lithium-ion sandwich consisting of positive and

negative porous electrode, a separator, and current collectors. The physics-based model is used by most of battery researchers. The models resolve:

- Electrolyte concentration;
- Electrolyte potential;
- Solid-state potential;
- Solid-state concentration within the porous electrodes and electrolyte concentration;
- Electrolyte potential within the separator.

The pseudo-two-dimensional model considers one-dimensional transport from the lithium anode through separator into the composite cathode.

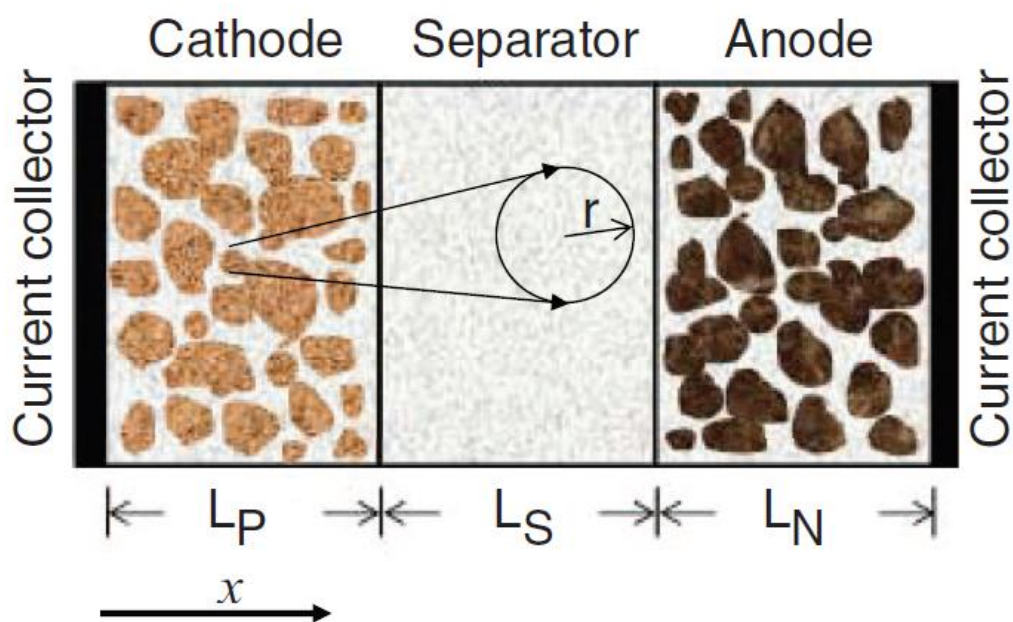


Fig 37-Schematic diagram of pseudo-two-dimensional model [33].

The separator consists of an inert polymer material that acts as the solvent for a lithium salt. As said, transport in the separator is modeled with concentrated solution theory. The electrical conductivity, the transference number of the lithium ion and the diffusion coefficient of the lithium salt characterize transport in the polymer. The equations that govern all these processes will be discussed in following chapter.

3.4.3.4 Electrochemical-thermal coupled models

Multiphysics electrochemical-thermal coupled models are necessary to accurately describe all the important phenomena that occur during the operation of lithium-ion batteries for high power/energy application such as in electric/hybrid vehicles. The pseudo-two-dimensional model previously described is coupled with 3D model to predict the electrical potential and temperature in the battery.

The coupling between the two models are made by the coupling between the generated heat source and the average temperature and can be summarized by the following Fig 38:

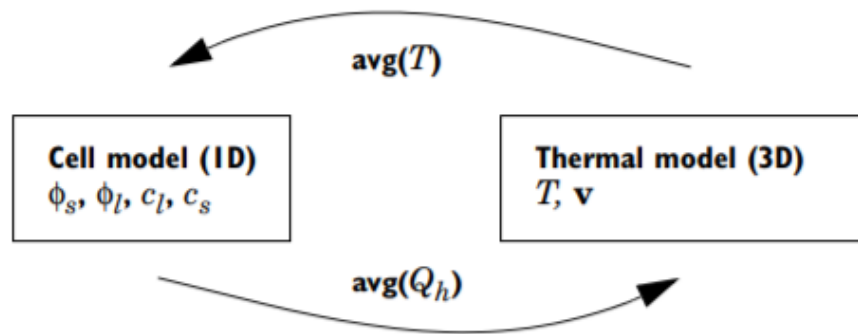


Fig 38- Schematic diagram of coupling between pseudo-two-dimensional model and 3D model [37].

The model developed in this project thesis is based on a pseudo two-dimensional approach for the electrochemical model coupled with 3D model to characterize thermal battery behavior.

4 Model development

Modeling and simulations are necessary tools for accelerated understanding, design optimization, design of automatic control of batteries and battery systems, in general to know the battery performance during operations. Computer simulations are very useful in this process because they can potentially lead to a great saving of time and materials. Using simulations for this purpose requires a mathematical model that is sophisticated enough to describe the system properly.

The battery model is developed in COMSOL Multiphysics® modeling software which has a built-in battery module called “Batteries & Fuel Cells” module. The “Batteries & Fuel Cells” module is a simulation software that can be used for modeling all types of fuel cells and batteries, with robust features for simulating all varieties of electrochemical behavior. It contains a number of physics interfaces that simulate either the electrochemical processes themselves or the surrounding processes that affect them. Models developed in the “Batteries and Fuel Cells” module may also be integrated with any other physics interfaces modules include in the COMSOL Product Suite. Critical information concerning the design and operation of electrodes and current collectors, cooling systems, the optimization of electrodes, separators and thermal management, with respect to performance and the deterioration of component due to aging or to other issues can be evaluated.

The model is based on the “pseudo two dimensional” approach for the electrochemical model and the “pseudo two-dimensional model coupled with a three dimensional one” for the thermal model. The bases of this approach have been shown in the paragraph “Electrochemical-thermal coupled models”.

To development of the study, two COMSOL Multiphysics® modules are necessary to obtain the battery heat generation: the first, “Battery and Fuel Cells”, simulates the electrochemistry of the battery. The second, “Heat Transfer in Solid”, simulates the heat conduction in the entire battery. The coupling between these two physics allows to evaluate the dependence of the chemical reactions from the temperature distribution and the temperature distribution from the chemical heat generation, as shown Fig 38.

During the first part of this work the electrochemical and thermal models will be developed for 18650 NMC-graphite cylindrical battery. Some parameters that include electrode specific parameters (such as diffusion coefficient, electrical conductivity, contact resistance), and kinetics parameters (such as transfer coefficients, concentration exponential etc.) needed for the simulations of lithium-ion cells are not convenient to evaluate from experimental measurements, for this reason it is needed research it calibrating the electrochemical and thermal models. This is possible through the comparison between simulation results and experimental data.

4.1.1 Electrochemical model

The electrochemical model is based on the study of Newman and other, explained in the paragraph “Pseudo-two- dimensional models”.

The model includes the following processes [38] [39]:

- Electronic current conduction in the electrodes.
- Ionic charge transport in the electrodes and electrolyte.
- Material transport in the electrolyte, allowing for the introduction of the effects of the concentration on ionic conductivity and concentration overpotential.
- The active electrode materials are made up of spherical particles with a uniform size.
- Volume change during cell operation is neglected, resulting in constant electrode porosities.
- The transport of lithium inside the active material particles is by diffusion with a constant diffusion coefficient.
- Interfacial chemical equilibrium exists in the electrolyte phase due to a large value of the mass diffusivity of electrolyte.
- Interfacial electrical equilibrium exists in both the electrolyte and solid active material phases due to either large values of their electronic conductivities or a small size of active material particles.
- Material transport within the spherical particles that form the electrodes.
- Charge transfer kinetics follows Butler-Volmer equation.
- No gas phase is present.
- Side reactions, significant only at relatively high temperatures, are ignored.

The chemical reaction taking place in the Lithium-Ion battery may be represented by a 1D geometrical model, that corresponds to the thickness dimension.

The computational domain is composed of 5 layers:

- Negative current collector.
- Negative electrode.
- Separator.
- Positive electrode.
- Positive current collector.

The one-dimensional domain is shown in Fig 39:



Fig 39- One dimensional geometry scheme.

These layers are made of following materials respectively:

- Copper.
- Graphite (Li_xC_6).
- Ethylene carbonate/diethylene carbonate in 1:1 (EC:DEC) (LiPF_6).
- Lithium Nickel Manganese Cobalt Oxide in $\text{LiNi}_{1/3}\text{Mn}_{1/3}\text{Co}_{1/3}\text{O}_2$ (NMC).
- Aluminum.

$\text{LiNi}_x\text{Mn}_y\text{CO}_2$ is the state of art choice of the cathode materials for the high-capacity Li-ion batteries in the electric vehicle applications. The composition of Ni, Mn, Co can be turned to optimize the capacity, cyclic rate, electrochemical stability and lifetime. Ni, Mn and Co contribute to the enhanced performance of NMC in different ways. Ni-rich compositions demonstrate high discharge capacity; Mn-rich compositions maintain better cycle life and thermal safety; while Co-rich compositions provide excellent rate capability [40].

The Table 6 shows the geometrical parameters of the one-dimensional model:

Table 6-Geometrical parameters.

	Unit	Negative Current Collector	Negative Electrode	Separator	Positive Electrode	Positive Current Collector
Length	μm	7.5	80	25	65	10

The Fig 40 shows the 1D geometry from COMSOL Multiphysics®:

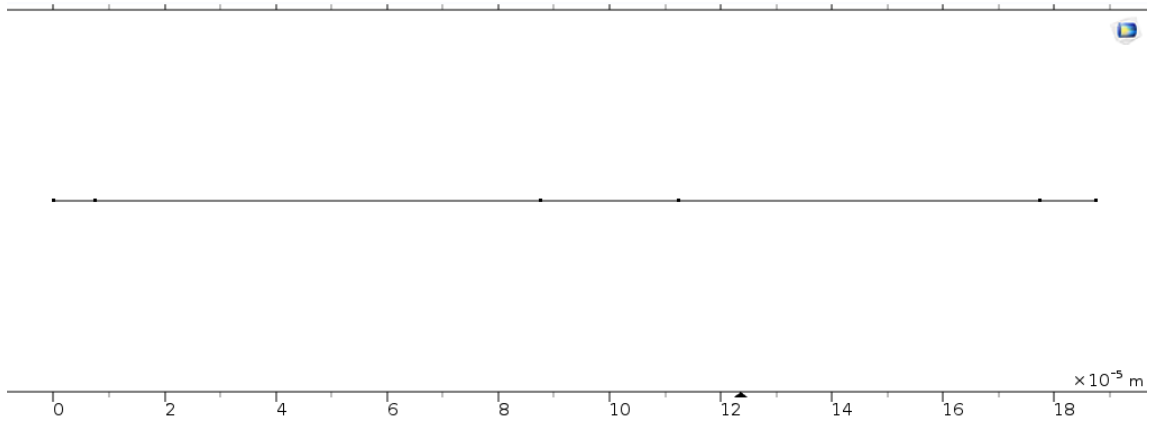


Fig 40-1D geometry COMSOL Multiphysics

The equilibrium potentials of positive and negative electrodes are shown in Fig 41 and Fig 42.

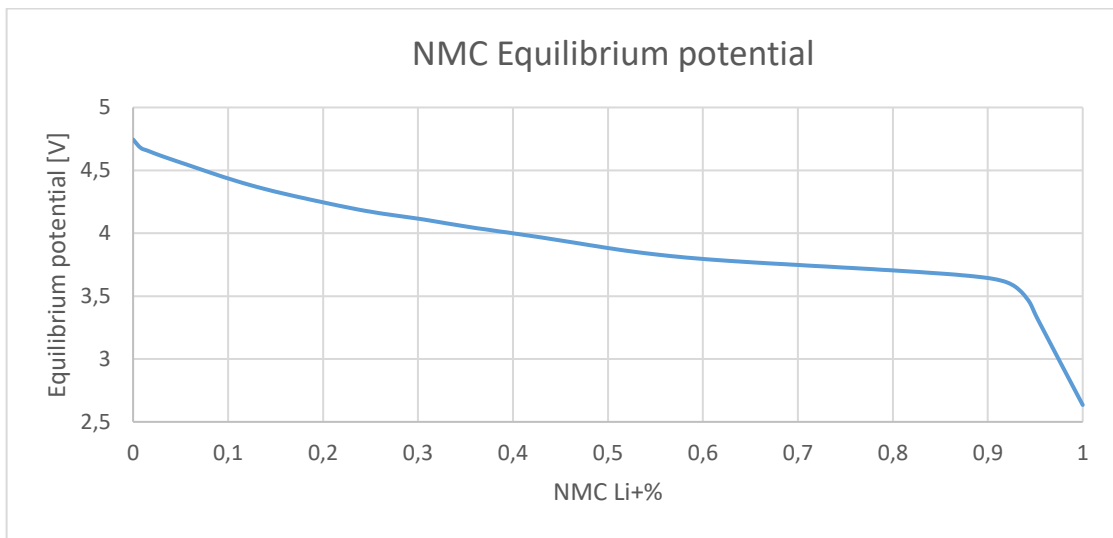


Fig 41- Equilibrium potential plot of NMC.

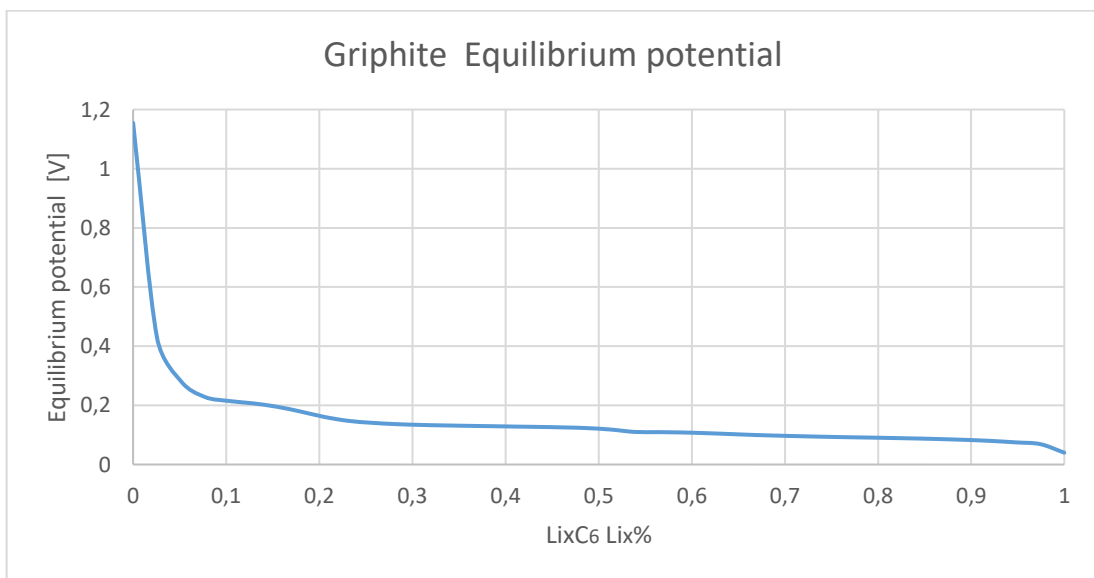
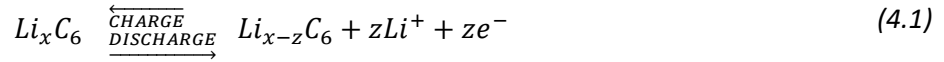


Fig 42-Equilibrium potential plot of graphite.

During the discharge process, lithium ions are extracted from the negative electrode, they move into the electrolyte and are transported across the separator to the positive electrode where they are inserted. The electrodes are porous in nature and immersed in the liquid electrolyte.

The electrochemical reactions that occur at the interface of the electrode and electrolyte in the both negative and positive during discharge/charge are (4.1) and (4.2):

At negative electrode (4.1):



At positive electrode (4.2) (Generical reaction):



The governing equations are implemented in the software. The final model equations are summarized below.

Reaction rates for insertion and de-insertion reactions are assumed to follow the Butler-Volmer equation previously defined in Eq.(2.13). In particular, the mathematical formulation of Butler-Volmer equation is (4.3):

$$i_s = i_0 \left(\exp\left(\frac{\alpha_a F \eta}{RT}\right) - \exp\left(-\frac{\alpha_c F \eta}{RT}\right) \right) \quad (4.3)$$

Where:

$$i_0 = F(k_c)^{\alpha_a} (k_a)^{\alpha_c} (c_{s,max} - c_s)^{\alpha_a} c_s^{\alpha_c} \left(\frac{c_l}{c_{s,ref}}\right)^{\alpha_a} \quad (4.4)$$

The overpotential η is defined as (4.5):

$$\eta = \varphi_s - \varphi_l - E_{eq} \quad (4.5)$$

The subscript “s” is refers to solid electrode phase, while the subscript “l” is refers to liquid electrolyte phase. The terms of (4.3), (4.4) and (4.5) are explained below:

- α_a is the anodic transfer coefficient;
- α_c is cathodic transfer coefficient;

- k_a is the anodic constant rate [m/s];
- k_c is the cathodic constant rate [m/s];
- $c_{s,max}$ is maximum concentration of the solid phase [mol/m³];
- c_s is maximum concentration of the solid phase [mol/m³];
- c_l is the concentration of the liquid electrolyte phase [mol/m³];
- $c_{l,ref}$ is the reference concentration of the liquid electrolyte [mol/m³];
- F is Faraday constant equal to $96487 \left[\frac{C}{mol} \right]$;
- φ_s is the solid phase potential [V];
- φ_l is the liquid phase potential [V];
- E_{eq} is the equilibrium potential [V];

The transport of electrons in the solid phase follows Ohm's law which can be expressed as (4.6):

$$i_s = -\sigma_s \nabla \varphi_s \quad (4.6)$$

Where σ_s is the electrical conductivity of the solid phase [S/m].

The transport of lithium ions in the electrolyte can be expressed as (4.7):

$$i_l = -\sigma_l \nabla \varphi_l + \frac{2\sigma_l RT}{F} \left(1 + \frac{\partial \ln f}{\partial \ln c_l} \right) (1 - t_+) \nabla \ln c_l \quad (4.7)$$

Where i_l consists of two terms, the first term following Ohm's law and the second accounting for the ionic concentration gradient, f is the average molar activity coefficient, t_+ is the transferring number of lithium ions in the liquid phase.

Diffusion in and out of the particle can be expressed as (4.8):

$$\frac{\partial c_s}{\partial t} = \nabla (-D_s \nabla c_s) \quad (4.8)$$

Where D_s represents the diffusion coefficient of lithium in the solid phase [m²/s].

With boundary conditions (4.9) and (4.11):

$$\frac{\partial c_s}{\partial r} \Big|_{r=0} = 0 \quad (4.9)$$

$$-D_s \frac{\partial c_s}{\partial r} \Big|_{r=r_p} = \frac{-\nabla i_s}{F} \frac{3\varepsilon_s}{r_p} \quad (4.10)$$

- ε_s is the volume fraction of electrode solid phase [-];
- r_p is the average particle radius [m].

The mass conservation of lithium ions in the electrolyte is given by (4.11):

$$\varepsilon_l \frac{\partial c_s}{\partial t} = \nabla(-D_l \nabla c_l) - \nabla \left(\frac{i_l t_+}{F} \right) + \frac{-\nabla i_l}{F} \quad (4.11)$$

Where

- ε_l is the volume fraction of electrolyte phase [-];
- D_l is the diffusivity coefficient of lithium ion in the electrolyte [m²/s].

The diffusivity coefficients are corrected with the Bruggeman coefficient (4.12):

$$f_l = \varepsilon_l^{brugg} \quad (4.12)$$

The parameters needed to resolve the electrochemical model are chosen from the experimental measurements, literature and from the model validation study. The parameters chosen from the literature and from experimental measurements are shown in Table 7.

Table 7- Electrochemical parameters.

Parameter	Value	Unit	Description
i	15.9	A/m ²	1C battery current density
i_{batt_1C}	2.15	A	1C battery current
C_{s0_neg}	29237	mol/m ³	Initial concentration negative electrode material
C_{s0_pos}	9894	mol/m ³	Initial concentration positive electrode material
C_{l_0}	1000	mol/m ³	Initial electrolyte salt concentration
r_{p_neg}	1e-5	m	Particle radius negative electrode
r_{p_pos}	2.5e-7	m	Particle radius positive electrode
a_{A_neg}	0.5	-	Reaction rate coefficient negative electrode
a_{C_pos}	0.5	-	Reaction rate coefficient negative electrode
$C_{s_max_neg}$	31370	mol/m ³	Maximum graphite concentration
$C_{s_max_pos}$	49470	mol/m ³	Maximum Lithium ion concentration

The other parameters not measured and needed to electrochemical simulation are defined in “Model validation ” paragraph.

4.1.2 Thermal model

The thermal model has been implemented in COMSOL Multiphysics® using “Heat Transfer in Solid” interface. As it is shown in “Electrochemical-thermal coupled models” paragraph, the electrochemical and thermal model are coupled: simultaneously electrochemical and thermal model exchange data.

The electrochemical and thermal model is developed for 18650 cylindrical battery. It is possible exploit the axial-symmetry of the cylindrical geometry to reduce the computational domain from 3D to 2D.

The geometry consists of three domains:

- Battery canister - Steel;
- Battery mandrel insulation around which the battery cell sheets are wound - Nylon;
- Active battery material domain - wound sheets of cell material.

Table 8- 2D Battery dimensions.

Unit	Cell height	Cell length	Cell thickness	Canister thickness	Mandrel radius
mm	65	18	0.187	0.25	2

The Fig 43 shows the geometry from COMSOL Multiphysics®:

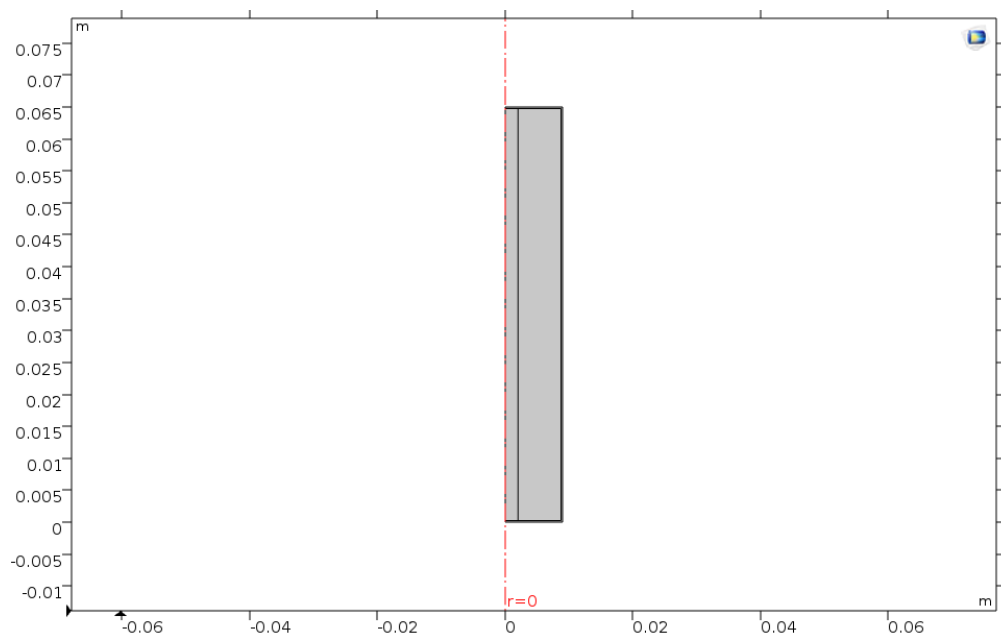


Fig 43-2D battery geometry.

The Fig 44 shows the scheme of the battery highlighting the different components:

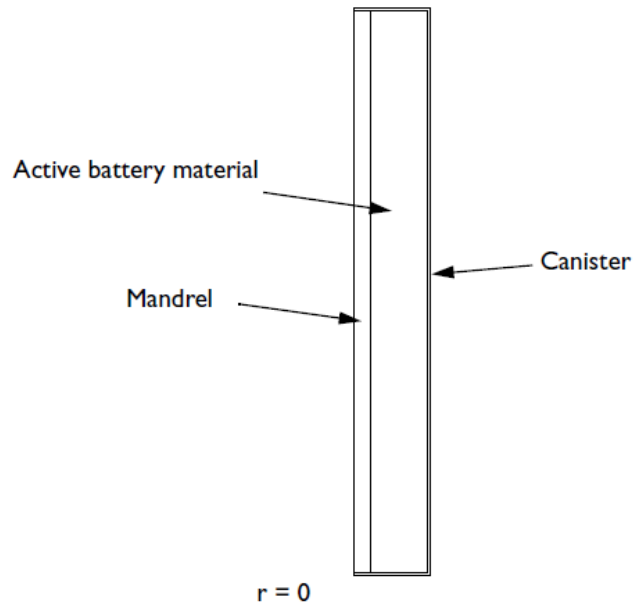


Fig 44-Battery components [41].

The final model equations are summarized below.

The energy balance can be expressed as (3.1) and rewrite in a compact form:

$$\rho c_p \frac{\partial T}{\partial t} - k \nabla^2 T = q_{rea} + q_{act} + q_{ohm} \quad (4.13)$$

There are three parts of heat generation sources:

- The heat generation due to electrochemical reaction is:

$$q_{rea} = I T \frac{\partial V_{oc}}{\partial T} = I T \frac{\Delta S}{F} \quad (4.14)$$

- The heat generation due to active polarization is:

$$q_{act} = I \eta \quad (4.15)$$

- The heat generation due to ohmic losses is:

$$q_{ohm} = -i_l \nabla \varphi_l - i_s \nabla \varphi_l \quad (4.16)$$

The active battery materials are assumed to consist of one or several cells wound spirally into a cylinder. As an effect of this, the thermal conductivities are anisotropic in the thermal model, with a higher thermal conductivity along the battery sheets, the cylinder length direction, rather than in the normal direction to the sheets, the radial direction.

In the radial direction the thermal conductivity is calculated as follow:

$$k_{T,r} = \frac{\sum L_i}{\sum \frac{L_i}{k_{T,i}}} \quad (4.17)$$

Where:

- L_i are the thicknesses of the different layers of the cell [m].
- $k_{T,i}$ are the thermal conductivities of the materials constituting these layers [W/(m*K)].

The thermal conductivity in the cylinder length direction is calculated according to:

$$k_{T,ang} = \frac{\sum L_i k_{T,i}}{\sum L_i} \quad (4.18)$$

The density and heat capacity for the active battery material are calculated similarly according to:

$$\rho_{batt} = \frac{\sum L_i \rho_i}{\sum L_i} \quad (4.19)$$

$$C_{p,batt} = \frac{\sum L_i C_{p,i}}{\sum L_i} \quad (4.20)$$

The average temperature that is the output of the 2D axial-symmetric thermal model is defined as input of 1D electrochemical one.

Table 9-Temperature variable.

T	nojac(comp2.aveop1(comp2.T))	K	Average temperature in active battery material
----------	------------------------------	---	--

While the heat generation that is the output of the 1D electrochemical model is defined as input of the 2D axial-symmetrical heat transfer model and it represents the heat source located in the active battery domain.

Table 10-Heat source variable.

Qh	nojac(comp1.aveop2(comp1.liion.Qh))* (L_neg+L_sep+L_pos+L_posCC+L_negCC)/L_batt	W/m ³	Average heat source From 1d battery model
-----------	--	------------------	--

The heat convective flux is imposed on the external boundaries:

$$q_0 = h(T - T_{ext}) \quad (4.21)$$

Where:

- T_{ext} is equal to 293.15K.
- h [W/(m²*K)] is the convective heat transfer coefficient that will be determined in “Model validation ” paragraph.

The Fig 45 shows the scheme of the heat transfer problem:

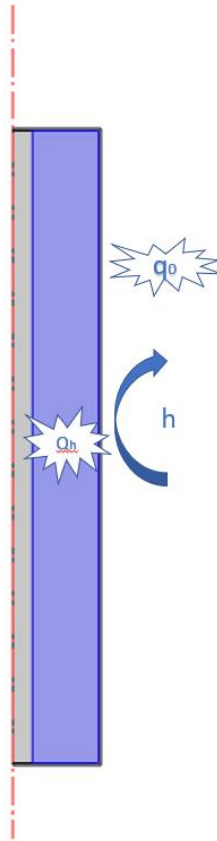


Fig 45-Heat transfer problem scheme.

The parameters needed to resolve the thermal model are chosen from experimental measurements, literature and from “model validation” study. The parameters defined from experimental measurements and literature are shown in Table 11.

Table 11-Thermal parameters.

Parameter	Value	Unit	Description
T_{init}	293.15	K	Initial temperature
ρ_{pos_cc}	2700	kg/m ³	Positive current collector density
ρ_{neg_cc}	8960	kg/m ³	Negative current collector density
$C_{p_pos_cc}$	900	J/kgK	Negative current collector specific heat at constant pressure
$C_{p_neg_cc}$	385	J/kgK	Positive current collector specific heat at constant pressure
K_{T_pos}	0.3	W/mK	Positive electrode thermal conductivity
K_{T_neg}	1.04	W/mK	Negative electrode thermal conductivity
K_{T_sep}	1.21	W/mK	Separator thermal conductivity
$K_{T_pos_cc}$	283	W/mK	Negative current collector thermal conductivity
$K_{T_neg_cc}$	400	W/mK	Positive current collector thermal conductivity

The other parameters not measured and needed to thermal simulation are defined in “Model validation” paragraph.

4.2 Model validation

Physical and chemical parameters are needed for the simulation of lithium-ion cells. Although finding some parameters such as physical dimension and chemistry of materials are practicable from experimental measurements, it is not convenient to measure some others. These parameters include design parameters, such as porosity, particle size, electrode specific parameters like diffusion coefficients, electrical conductivity, contact resistance. Parameter estimation might be a useful approach to find kinetic and transport parameters from the experiment charge/discharge data [42].

In order to validate the models, the simulation results are compared with experimental ones.

Thermal validation is carried out for 1C, 1.5C and 2C rates, along with the electrochemical validation for 0.05C, 0.1C, 0.2C, 0.5C, 1C, 1.5C and 2C rates.

4.2.1 Steps

The steps followed to estimate the unknown cell parameters are developed according to two methods:

1. firstly, by performing a parameter study on cell parameters within a known range from literature studies;
2. secondly, to improve the accuracy of the simulation results, COMSOL optimization module is used.

These methods are applied for all C-rates to estimate the best parameter values to reach a simulation results much closer to experimental data.

Once found the parameters for all C-rates, these are set in a new parametric study that put together all C-rates in only study to found the same value for every parameter suitable for thermal model validation (1C, 1.5C and 2C) and for the electrochemical validation (0.05C, 0.1C, 0.2C, 0.5C, 1C, 1.5C and 2C).

The estimated electrochemical parameters are shows in Table 12:

Table 12-The estimated electrochemical parameters.

Parameter	Unit	Description
Ds_neg	m ² /s	Solid phase Li-diffusivity negative electrode
Ds_pos	m ² /s	Solid phase Li-diffusivity positive electrode
Epsl_neg		Solid phase vol-fraction negative electrode

Epsl_pos		Solid phase vol-fraction positive electrode
K_neg	m/s	Reaction rate coefficient negative electrode
K_pos	m/s	Reaction rate coefficient positive electrode
brugg	-	Bruggman coefficient
R_film	Ωm^2	Negative electrode Film resistance

Once found the unknown electrochemical parameters, the thermal and characteristic material unknown parameters are estimated according to the methods explained above and they are shown in Table 13.

Table 13- Thermal and characteristic material estimated unknown parameters.

Parameter	Unit	Description
rho_neg	kg/m ³	Negative electrode density
rho_pos	kg/m ³	Positive electrode density
Cp_neg	J/kgK	Negative electrode specific heat at constant pressure
Cp_pos	J/kgK	Positive electrode specific heat at constant pressure
h	W/m ² K	Convective heat transfer coefficient

The parametric study is applied to find the appropriate range values, once that the ranges are found, the optimization study is implemented.

The optimization technique is typically formulated as the minimization of the sum-of-squared differences between the model outputs and their experimentally measured values for each cycle “i”

(4.22):

$$\min_{\theta_i} \sum_{j=1}^{n_i} [y_i(t_j) - y_{model,i}(t_j, \theta_j)]^2 \quad (4.22)$$

Where:

- $y_i(t_j)$ is the experimentally measured value at time t_j for cycle i .
- $y_{model,i}(t_j, \theta_j)$ is the computed output from the battery model at time t_j for cycle “i” for the vector of model parameters θ_j .

- n_i is the number of time points in cycle “ i ”.

The objective function of the optimization study is represented by $[y_i(t_j) - y_{model,i}(t_j, \theta_j)]^2$. For the model validation, two objective functions are used (4.23) and

(4.24):

- For electrochemical model validation (4.23):

$$\min_{\theta_i} \sum_{j=1}^{n_i} [E_i(t_j) - E_{model,i}(t_j, \theta_j)]^2 \quad (4.23)$$

Where experimentally measured " $E_i(t_j)$ " and computed output " $E_{model,i}(t_j, \theta_j)$ " are represented by battery voltage values [V].

- For thermal model validation
- (4.24):

$$\min_{\theta_i} \sum_{j=1}^{n_i} [T_i(t_j) - T_{model,i}(t_j, \theta_j)]^2 \quad (4.24)$$

Where experimentally measured " $T_i(t_j)$ " and computed output " $T_{model,i}(t_j, \theta_j)$ " are represented by battery temperature values [K].

The optimization method utilized and present in the COMSOL library is “Nelder-Mead” method. This method is one of the best-known algorithms for multidimensional unconstrained optimization without derivatives. It is widely used to solve parameter estimation. The general algorithm is given by:

- Construct the initial working simplex.
- Repeat the following steps until the termination test is satisfied.
- Calculate the termination test information.
- If the termination test is not satisfied, then transform the working simplex.
- Return the best vertex of the current simplex and the associated function value.

The results of the model validation study are shown in the following paragraph.

4.2.2 Results and discussion

The model validation is solved by using Finite Element Method (FEM). The performance and accuracy of the calculation depends heavily on the mesh and solver. The mesh used in FEM analysis is reported in Fig 46.

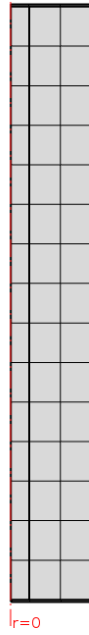


Fig 46- Mesh used for FEM analysis.

The maximum mesh element size is equal to $4.3e-3[m]$, the minimum mesh element size is equal to $1.95e-5 [m]$.

The validation starts from the parametric study applied to electrochemical model for 0.05C, 0.1C, 0.2C, 0.5C, 1C, 1.5C, 2C.

For lower C-rates the temperature variation is neglected, and the process is considered isothermal. The validation is conducted with the study of the battery discharge processes.

The Fig 47 shows the electrochemical validation results for 0.05C, 0.1C, 0.2C, 0.5C rates.

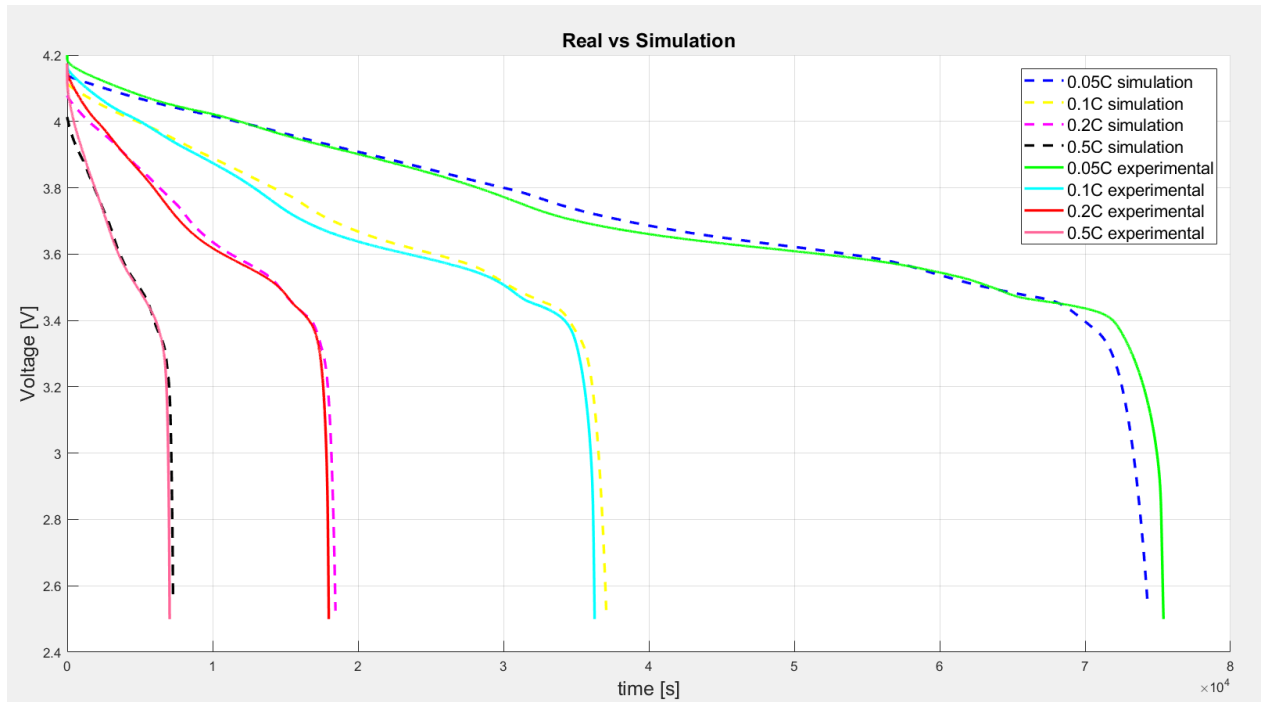


Fig 47- Electrochemical validation 0.05C, 0.1C, 0.2C, 0.5C.

The Fig 48 shows the electrochemical validation results for 1C, 1.5C and 2C.

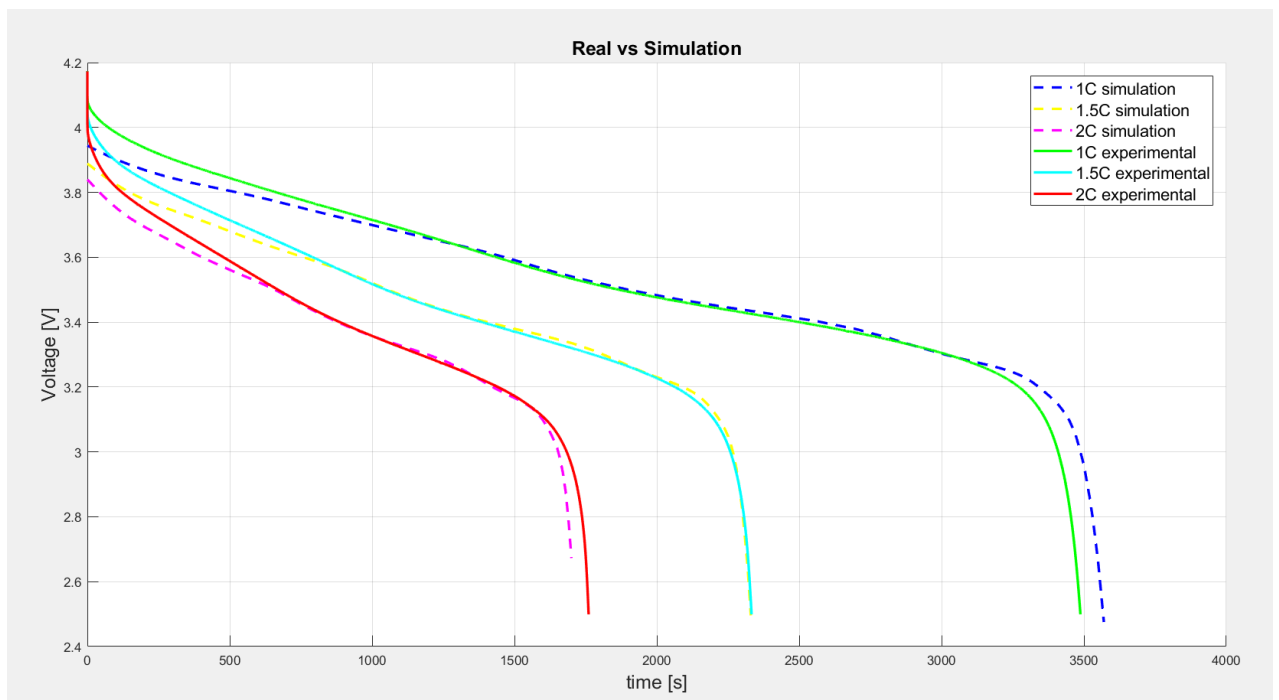


Fig 48- Electrochemical validation 1C, 1.5C and 2C.

The electrochemical model predicts the voltage very well at lower and higher C-rates.

The electrochemical parameters found applied the methods described above are listed in Table 14 .

Table 14- Electrochemical parameter values for the validation.

Parameter	Value	Unit	Description
Ds_neg	5e-12	m ² /s	Solid phase Li-diffusivity negative electrode
Ds_pos	3.25e-12	m ² /s	Solid phase Li-diffusivity positive electrode
Epsl_neg	0.711		Electrolyte phase vol-fraction negative electrode
Epsl_pos	0.633		Electrolyte phase vol-fraction positive electrode
Epss_neg	1-epsl_neg-0.026		Solid phase vol-fraction negative electrode
Epss_pos	1-epsl_pos-0.073		Solid phase vol-fraction positive electrode
K_neg	5e-12	m/s	Reaction rate coefficient negative electrode
K_pos	5e-12	m/s	Reaction rate coefficient positive electrode
brugg	6	-	Bruggman coefficient
R_film	25e-3	Ωm ²	Negative electrode Film resistance

To find these parameter values a lot of simulations have been made. The following figures show some intermediate simulations, other examples are illustrated in the “APPENDIX” section.

The Fig 49 and Fig 50 confront the results of the study for the research of the best values of epsl_pos, epsl_neg and consequently epss_pos and epss_neg. The Fig 49 represents the voltage of the pre-optimization study, while Fig 50 represents the voltage of the post-optimization study.

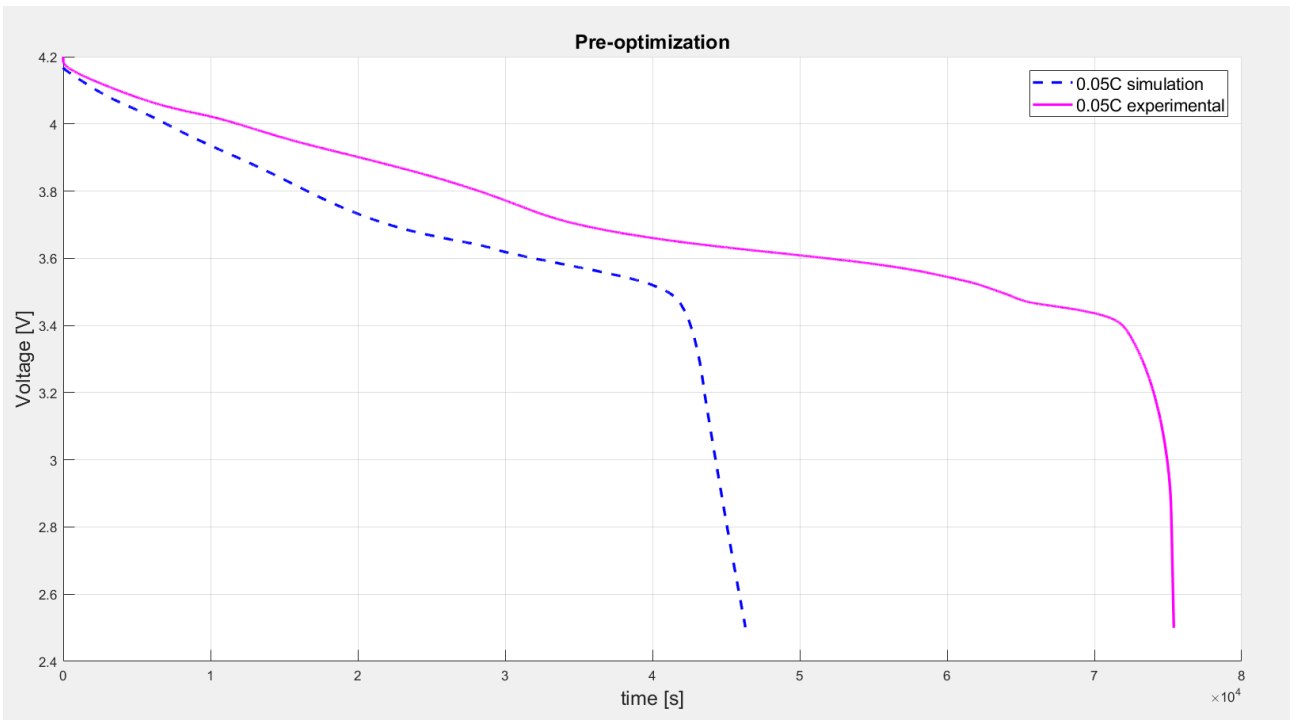


Fig 49- 0.05C pre-optimization study.

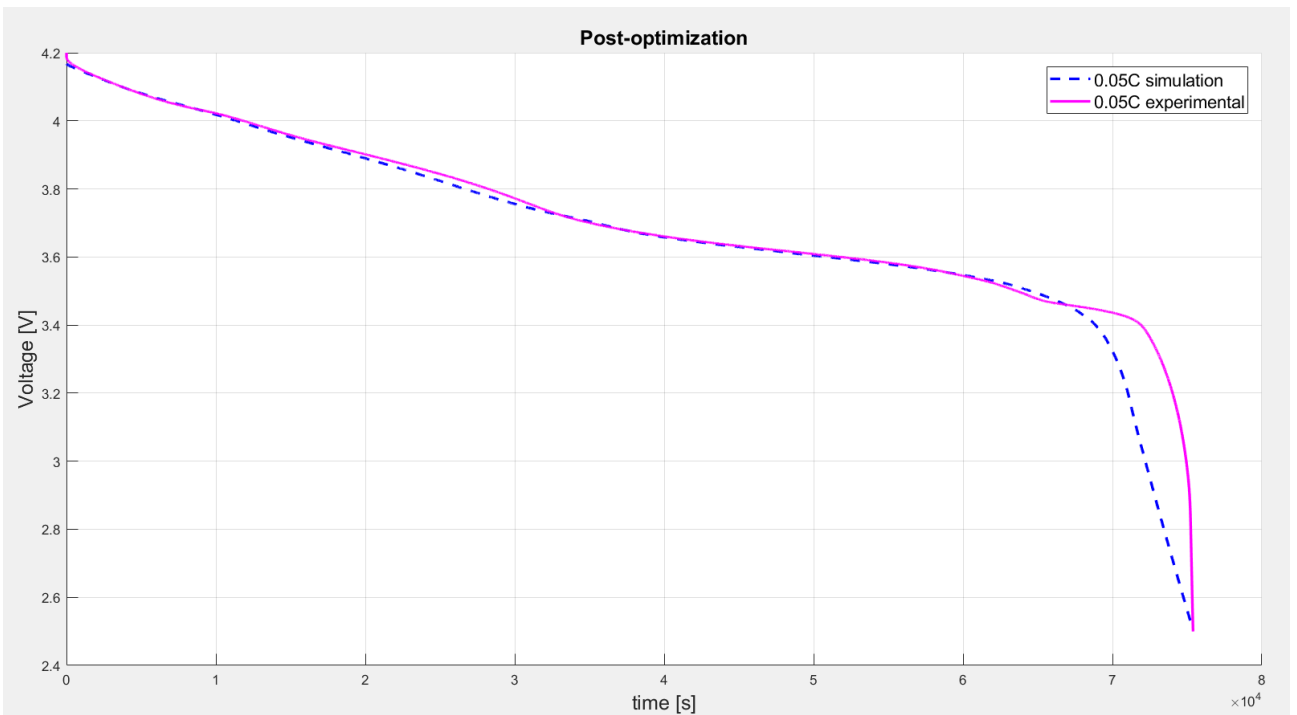


Fig 50-0.05C optimization study.

The optimization study has been conducted according to Table 15 with objective function equal to Eq.(4.23):

Table 15-Optimization study parameters.

Parameter	Initial value	lower boundary	Upper boundary
Epsl_neg	0.686	0.357	0.800
Epsl_pos	0.684	0.444	0.800

Pre-optimization study has been conducted with epsl_neg equal to 0.503 and epsl_pos equal to 0.517, while the optimization study result reports epsl_neg equal to 0.711 and epsl_pos equal to 0.633. It is clear that increasing the volume fraction value of the electrolyte phase, the volume fraction value of solid phase decrease, for this reason the discharge curve is less flat and discharge process is faster.

Thermal model validation is conducted for 1C, 1.5C and 2C and the results are shown in Fig 51.

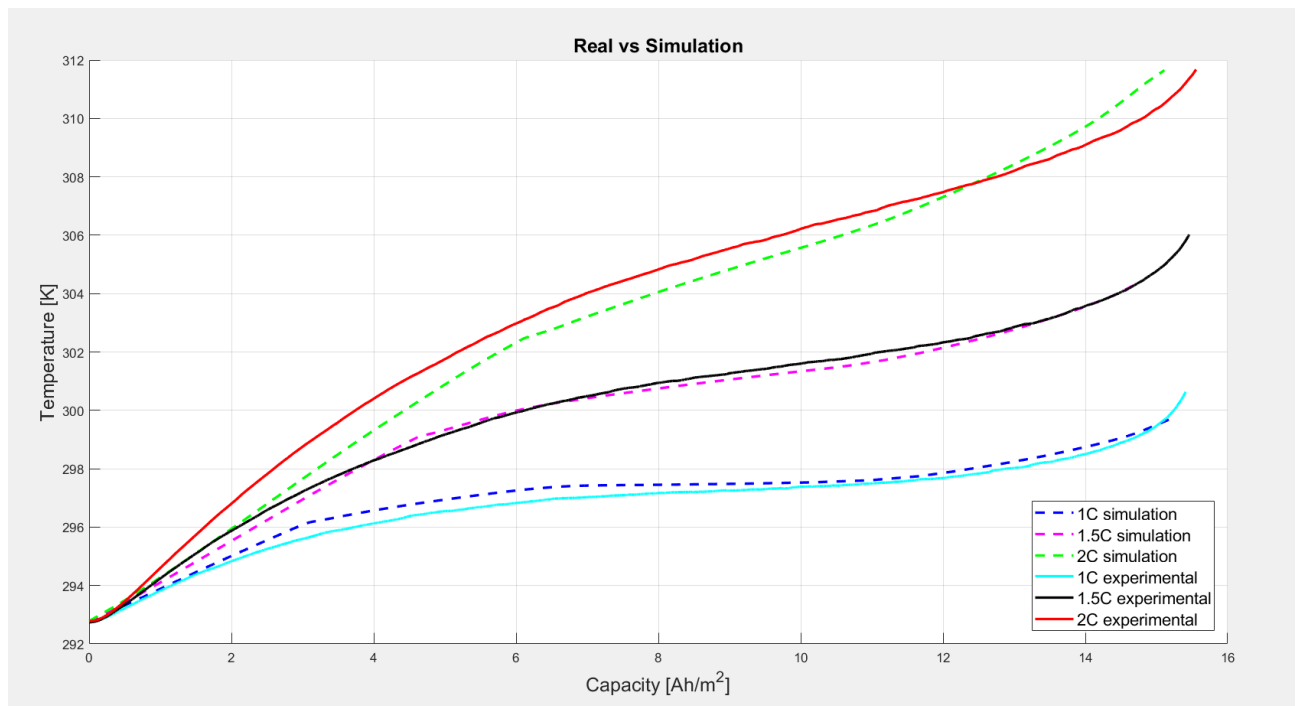


Fig 51-Thermal model validation 1C, 1.5C and 2C

The thermal parameters found by applying the methods described above are listed in Table 16.

Table 16- Thermal model validation parameters.

Parameter	Value	Unit	Description
rho_neg	1891.99	kg/m ³	Negative electrode density
rho_pos	2451.88	kg/m ³	Positive electrode density
Cp_neg	520.12	J/kgK	Negative electrode specific heat at constant pressure
Cp_pos	727.32	J/kgK	Positive electrode specific heat at constant pressure
h	variable	W/m ² K	Convective heat transfer coefficient

The heat transfer coefficient has been varied in function of the time because during the experimental tests the battery has been positioned into a box where a fan was actioned during the process.

To find these parameter values a lot of number of simulations have been made. Starting from parametric studies a possible range of values has been identified, then applying the optimization studies the best values have been identified.

The following figures show some intermediate simulations. The Fig 52 and Fig 53 Fig 49 confront the results of the study for the research of the best values of k_neg, k_pos, Ds_neg and Ds_pos. The Fig 52 represents the Temperature of the pre-optimization study, while Fig 53 represents the Temperature of the post-optimization study:

.

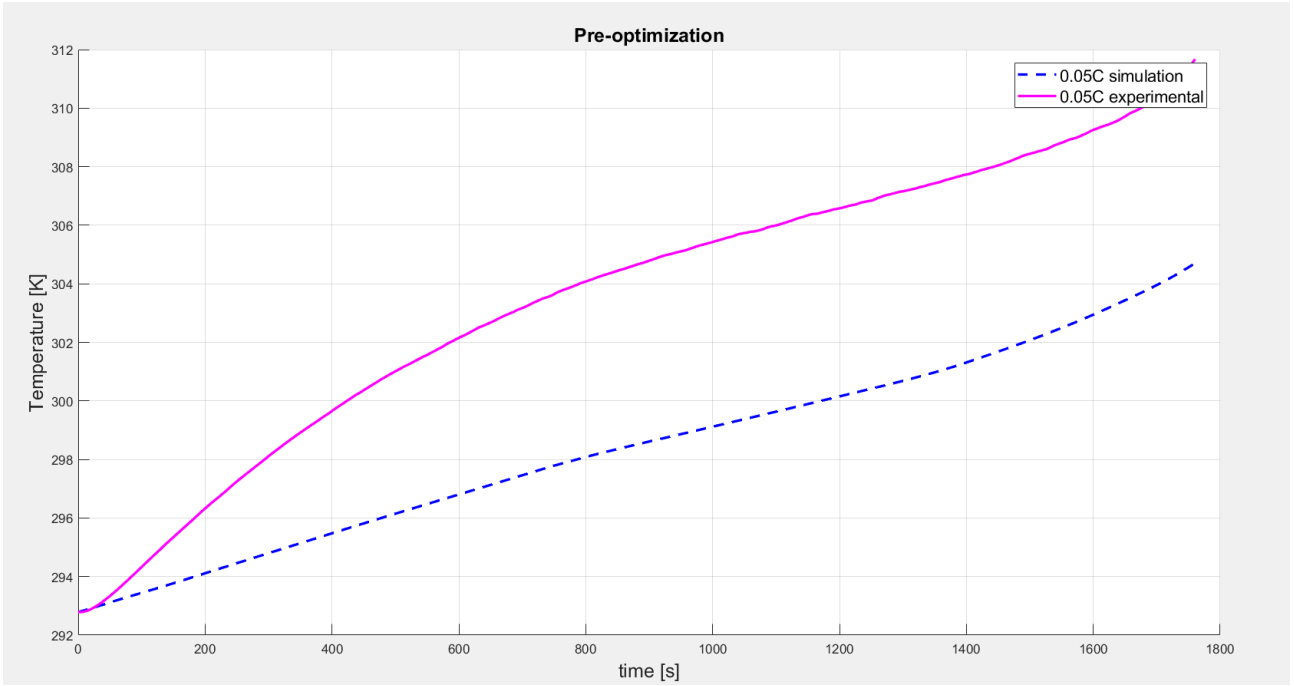


Fig 52- 2C pre-optimization study.

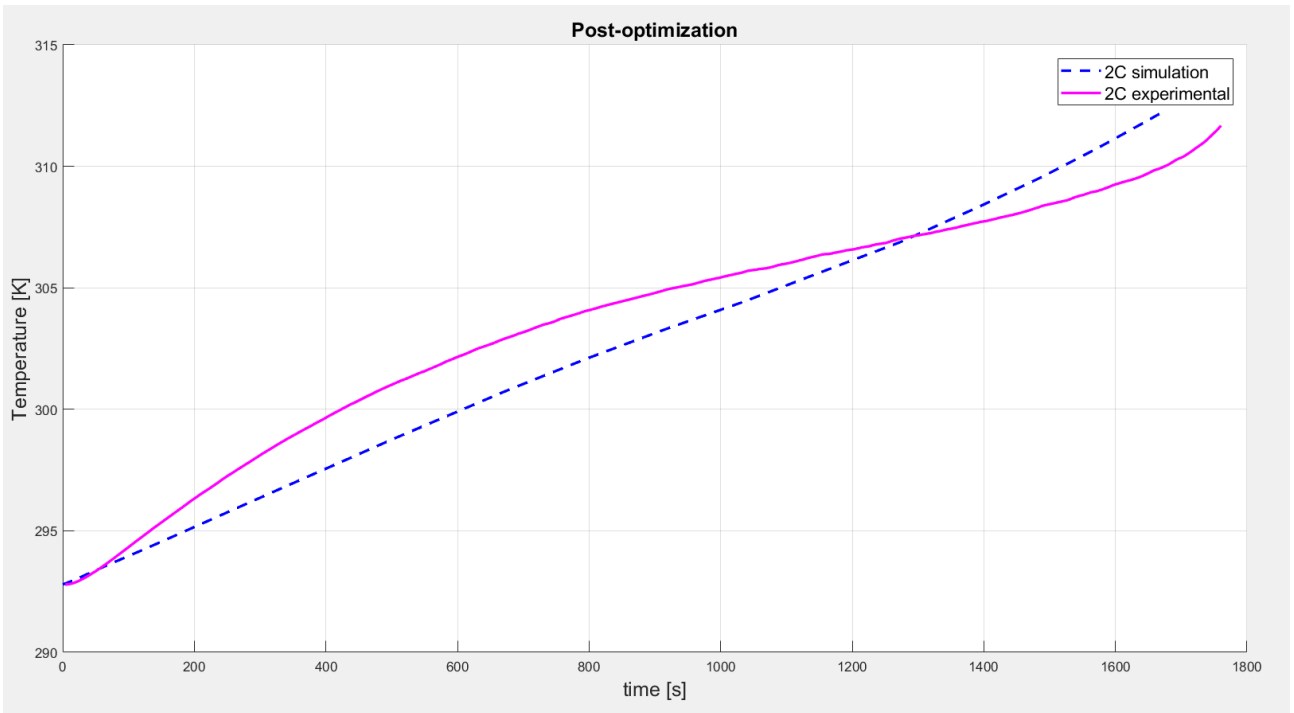


Fig 53-2C optimization study.

The optimization study has been conducted according to objective function equal to Eq.(4.23) and (4.23):

Table 17-Optimization parameter values.

Parameter	Initial value	lower boundary	Upper boundary
K_neg [m/s]	2e-12	3e-12	7e-12
K_pos [m/s]	4.64e-12	3e-12	7e-12

Pre-optimization study has been conducted with k_neg equal to 3e-12 [m/s], k_pos equal to 3e-12 [m/s], while the optimization study result reports k_neg equal to 3.33e-12 [m/s] and k_pos equal to 2e-12 [m/s].

With a decrease of constant rates k_neg and k_pos, the temperature values increases. Recalling the Arrhenius equation (2.10), it is clear that k and T are inversely proportional.

(4.25)

$$k = Ae^{-\frac{E_a}{RT}}$$

Passing to logarithm and rewrite the expression:

$$\ln k = \ln A - \frac{E_a}{RT} \quad (4.26)$$

With a decrease of k, an increase of T corresponds.

These kinds of parametric and optimization studies have been conducted for all C-rates and intersecting the results to find the same parameters values for all C-rates.

Once that the electrochemical and thermal models for this kind of electrochemical cell are validated, it is possible apply them to the same kind of battery utilized for a railway regenerative braking system.

4.3 Case study: battery pack to regenerative braking system

As it is said in “The battery pack to regenerative braking system” paragraph, this project thesis is an evolution of the study conducted by my colleague Giuseppe Boccardo in his thesis work [9]. The application of electrochemical and thermal validated models is referred to the battery pack utilized in a regenerative braking system to track the railway for about 19.46km that comprise underground and non-underground sections in the urban area of Turin. Data calculated in his study take into account the quantities explained in “1.2.1.1 Regenerative Braking system” paragraph.

The main data needed to sizing battery pack are shown in Table 18.

Table 18-data to sizing battery pack [9].

Total energy demand [kWh]	196
Desired Voltage [V]	950

The Table 19 shows the characteristics of NMC-graphite battery:

Table 19- NMC-graphite battery Characteristics

Nominal capacity [Ah]	2.1
Nominal Voltage [V]	3.7

The battery energy is equal to:

$$W = V * Q \quad (4.27)$$

Where:

- V is Voltage [V];
- Q is capacity [Ah].

It is hypothesized the following battery pack configuration.

Number of cells in a single module:

- Cells connected in series 12;
- Cells connected in parallel 10.

Number of module in the battery pack:

- Modules connected in series 22;
- Modules connected in parallel 13.

This configuration has been hypothesized using the Eq. (2.26) and (2.27) to satisfy the voltage and energy requested.

- The voltage of single module is equal to 44V;
- The battery pack energy has been calculated considering a DOD (Depth of discharge) equal to 80% and its value is equal to 245 kWh.

4.3.1 Results and discussion

The validated electrochemical and thermal models are used in the regenerative braking battery pack just described. The only different between the battery studied for the validation thermal model in the previous paragraph and the battery used in this application is the pouch geometry rather than cylindrical one. The choice of the pouch geometry is due to the most efficient use of the space and to the achievement of a 90/95 percent packaging efficiency, the highest among battery packs. Important properties considering the number of cells in the battery pack and the consequent volume occupied from a cylindric battery pack.

The electrochemical and thermal models are valid thanks to the fact that the electrical and materials parameters and the thickness of components of the cell are maintained unvaried.

Thermal characterization of the pouch battery pack starts from the study of a single pouch cell.

The pouch cell geometry and its properties are described in “Battery configurations” paragraph. The overview of the 3D pouch cell developed in COMSOL Multiphysics® is shown in Fig 54 and its vertical section is shown in Fig 55.

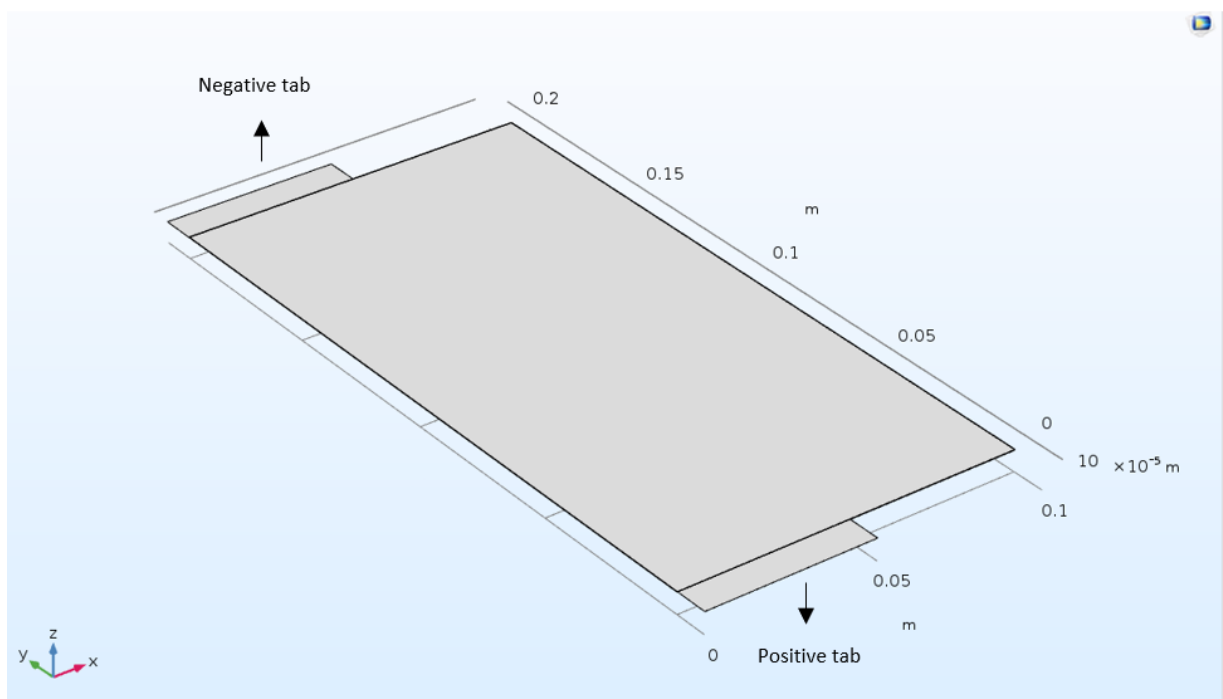


Fig 54- Pouch cell geometry.

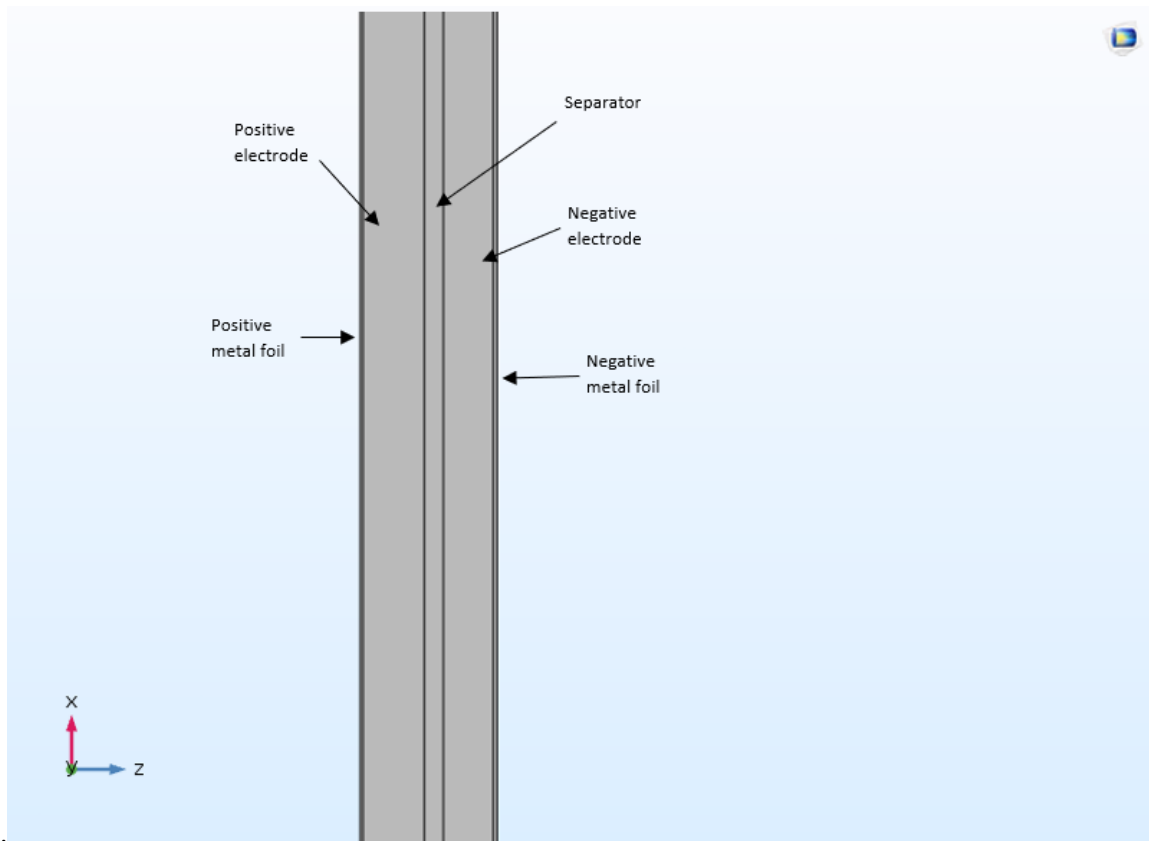


Fig 55- Cell vertical section.

The Table 20 shows the geometric parameters of the pouch cell.

Table 20- Pouch cell geometric parameters.

Unit	Cell height	Cell width	Cell thickness	Tab width	Tab height
mm	200	100	0.187	50	10

The mesh used in FEM analysis for the heat transfer calculation is reported below. The mesh size is chosen from COMSOL Multiphysics® using “physics-controlled mesh” tool.

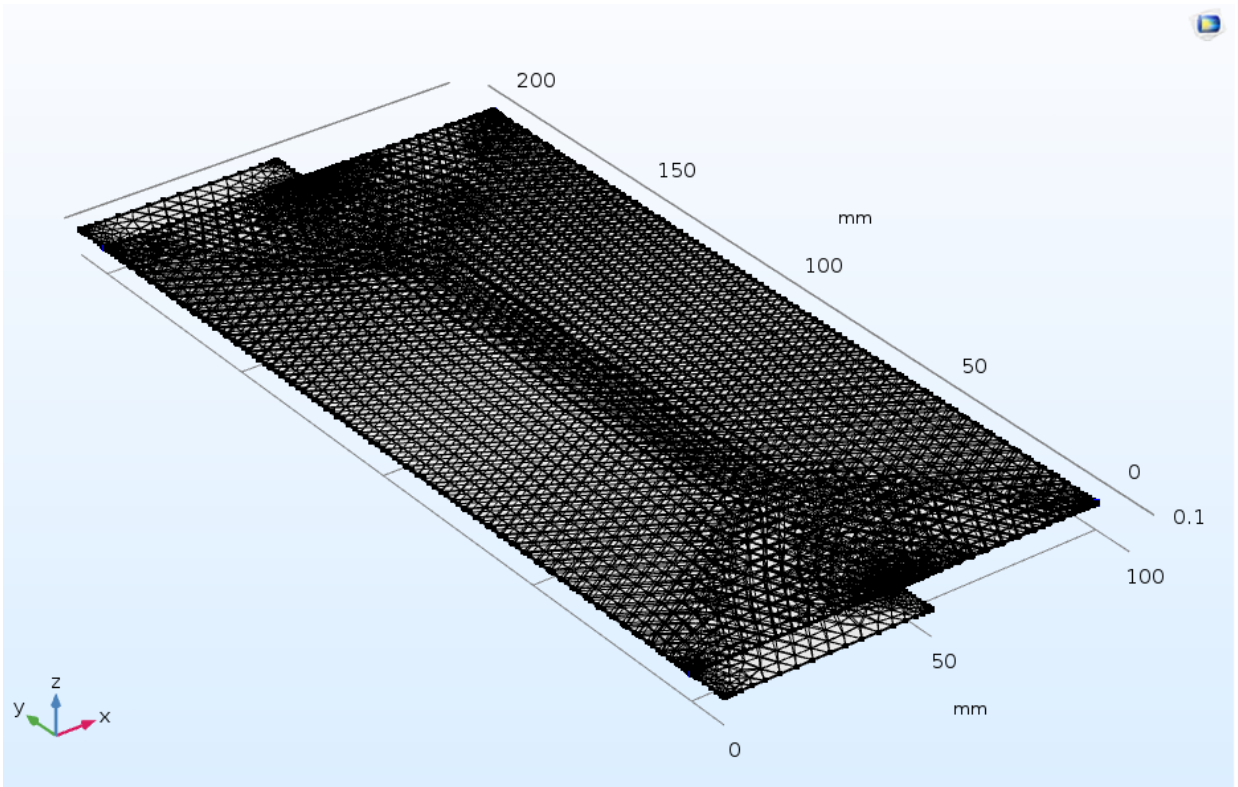


Fig 56-Mesh used for FEM analysis.

The electrochemical and thermal model have been implemented and the results are reported below.

The Fig 57 shows the 1C-rate discharge curve.

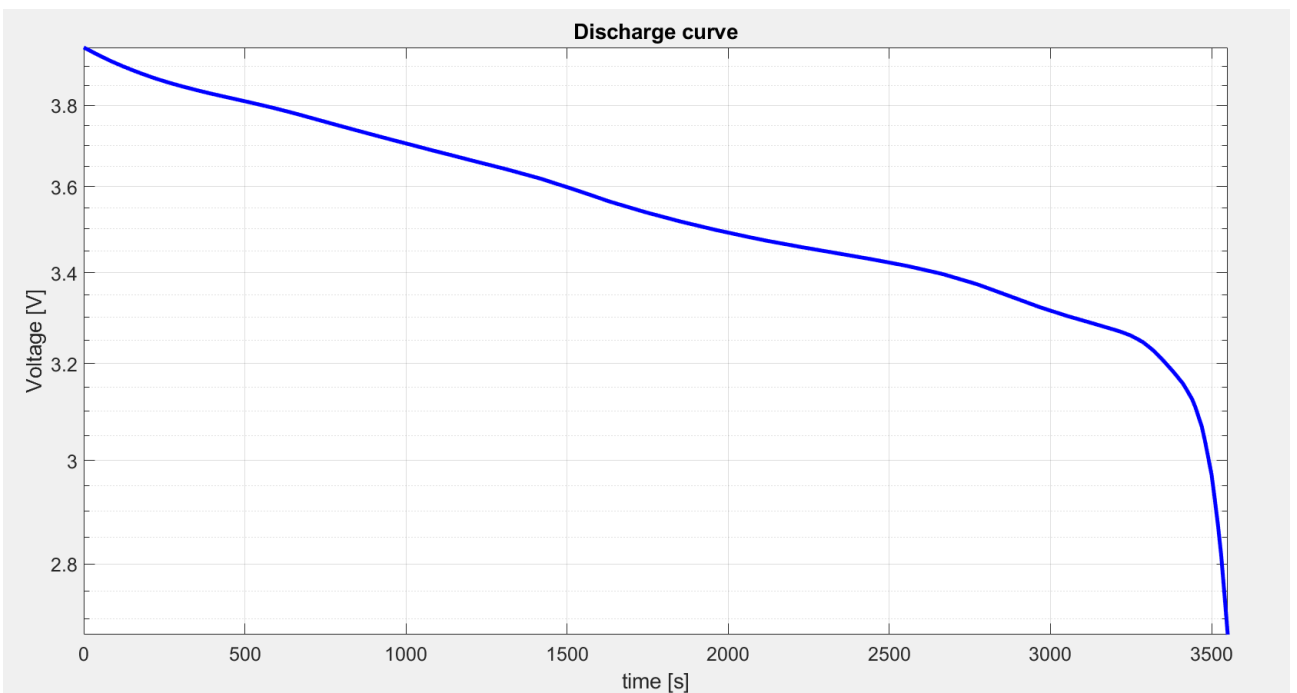


Fig 57- 1C-rate discharge process.

Comparing the discharge curve of the pouch cell and the discharge curve of the cylindrical cell, it is clear that the curves have the same behavior. As it is said before, the electrochemical parameters used

in the both simulations are the same, consequently the result is that the evolution of the voltage is the same.

The Fig 58 shows the temperature evolution during discharge process at 1C-rate.

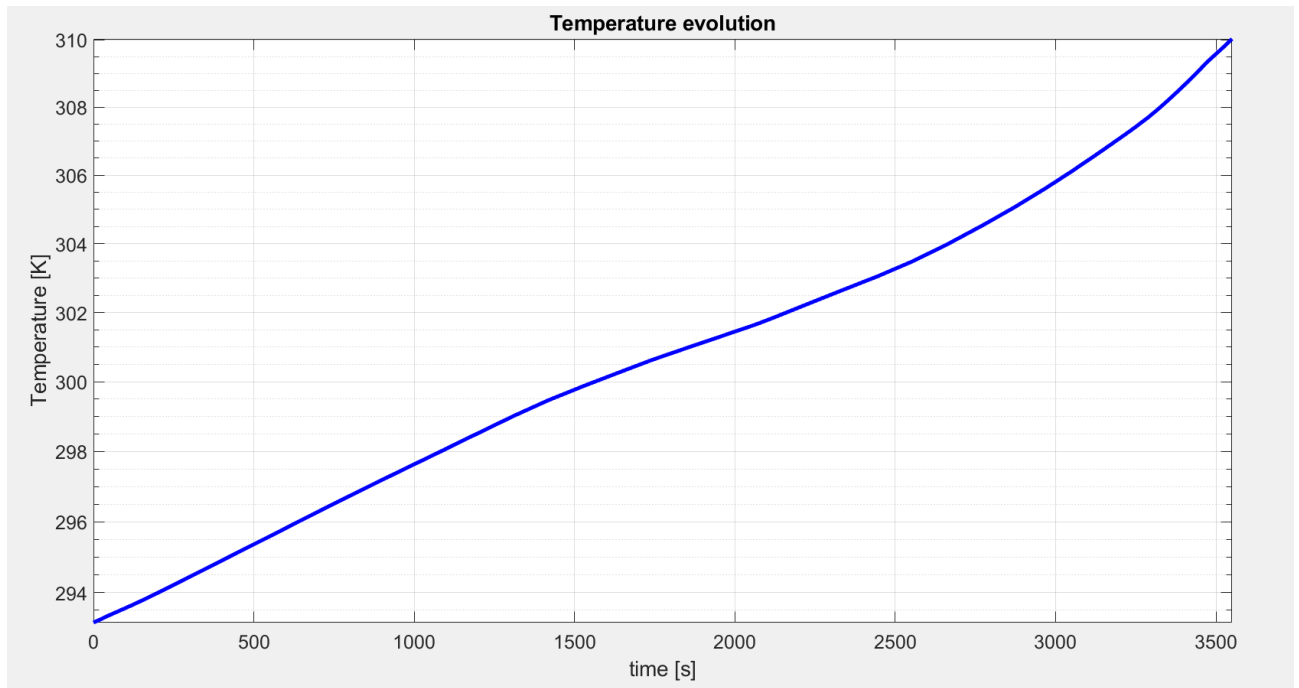


Fig 58- Single cell temperature evolution during discharge and charge cycle @1C-rate.

Comparing the temperature evolution curve of the pouch cell and the temperature evolution of the cylindrical cell, it is clear that the curves have not the same behavior. The thermal and material parameters of the cells used in both simulations are the same, but the heat transfer coefficient has been imposed equal to zero (adiabatic condition) for the pouch cell, this implicates an increase of temperature during the time. This choice has made to calculate the heat generation from the cell without any cooling system, thanks to this data will be possible to design an appropriate cooling battery system.

The Fig 59, Fig 60, Fig 61 show the surface temperature distribution at different time steps during discharge process.

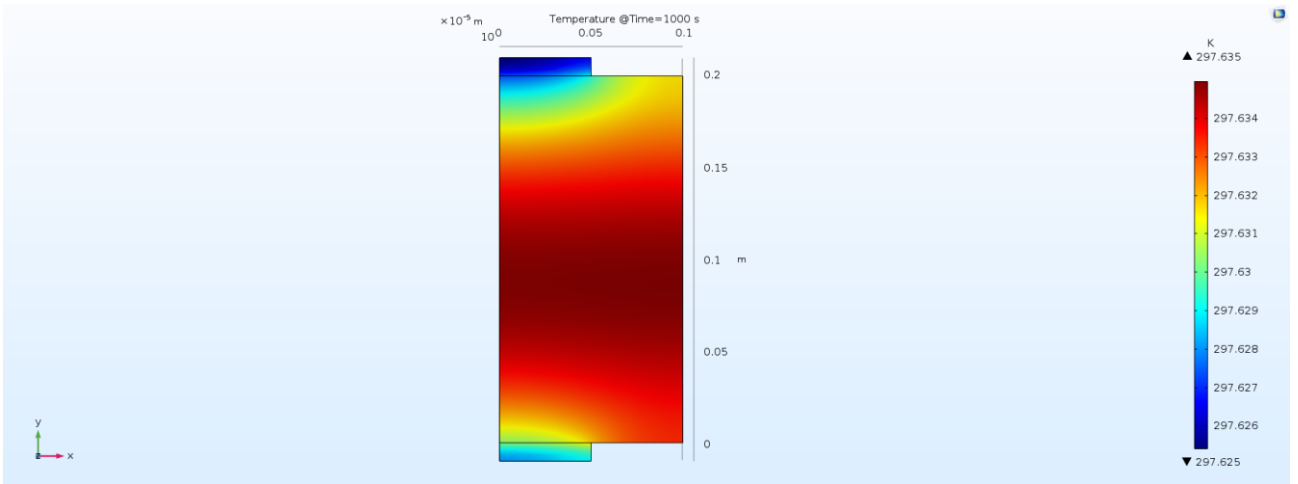


Fig 59-Temperature distribution @t=1000s.

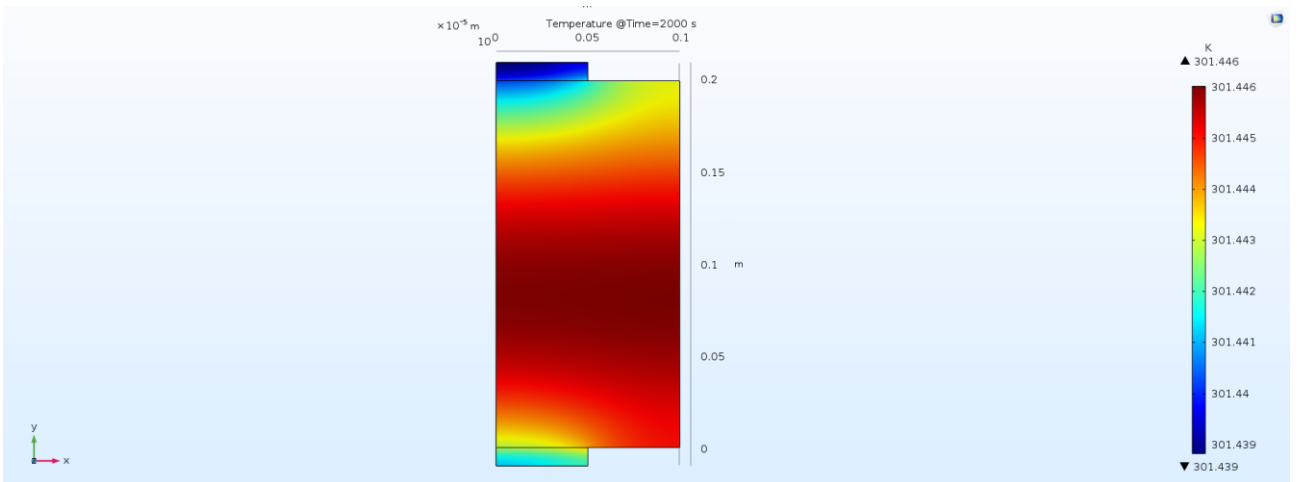


Fig 60-Temperature distribution @t=2000s.

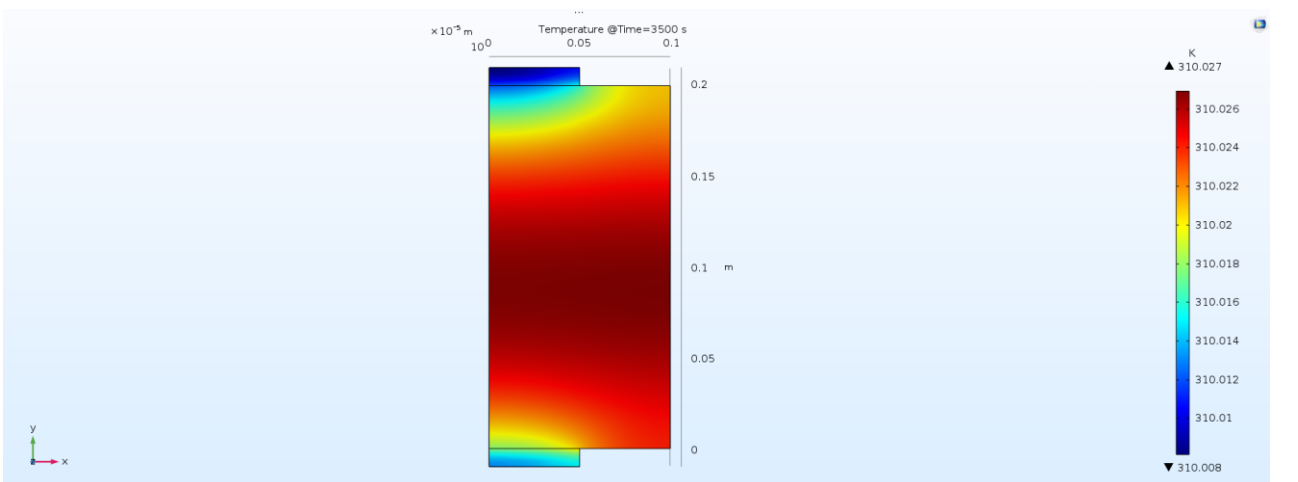


Fig 61-Temperature distribution @t=3550s.

The temperature has a uniform distribution in the body of the cell and a decrease in the tabs. The surface of the cell is covered by the current collector metal foils. These are in contact with the active battery material, where the heat source is located, for this reason the surface temperature is almost uniform, while the tabs are not in contact with the active battery material and the temperature is a little bit lower, because the conductivity of the metal foils is high. In particular, aluminum (inferior tab) has a thermal conductivity higher than copper (superior tab).

The heat generated from the cell during discharge process is shown in Fig 62.

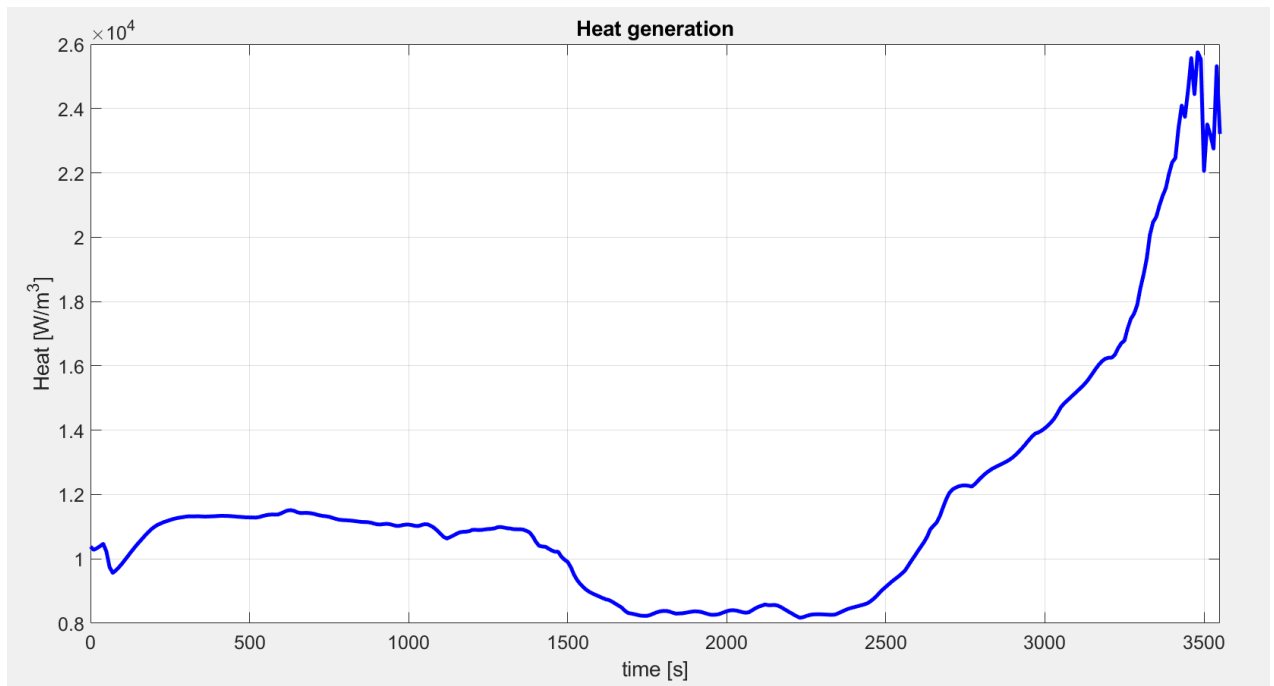


Fig 62-Heat generation @1C-rate.

Defined the single cell heat generation for the discharge process, thermal characterization study has been expanded to an entire discharge and charge cycle. The results displayed below: voltage evolution is represented in Fig 63 and the temperature evolution is shown in Fig 64.

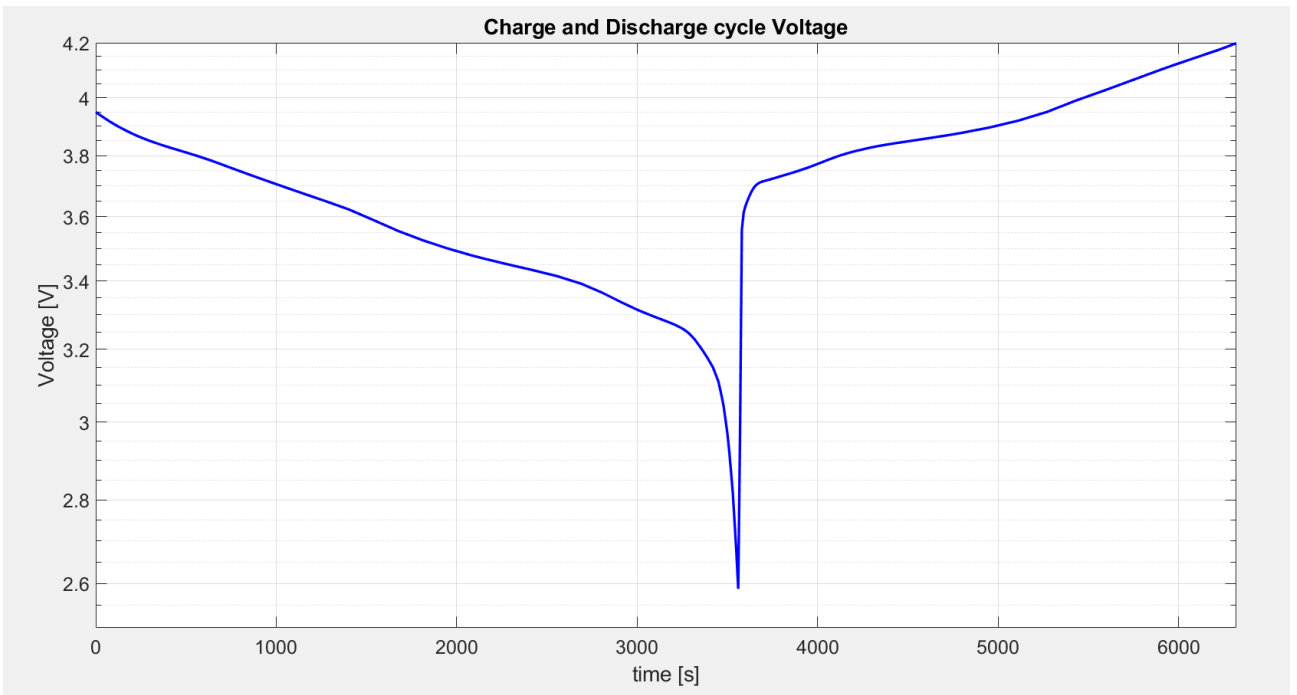


Fig 63- Discharge and charge cycle curve.

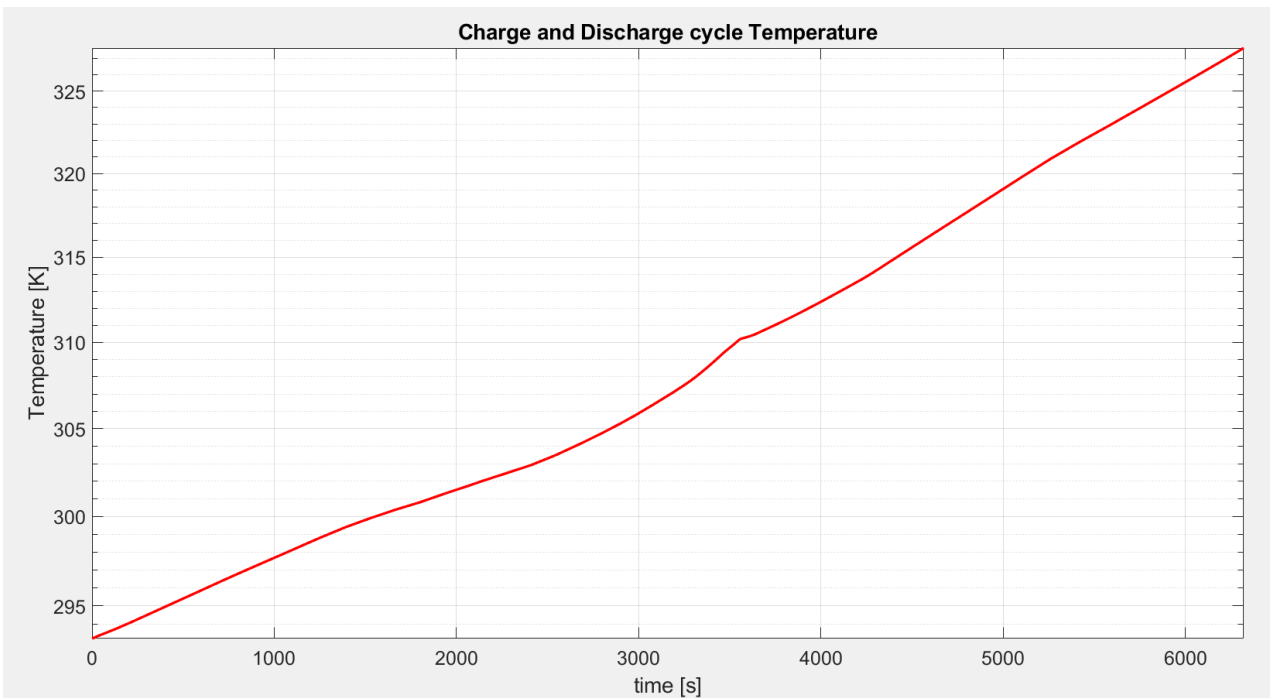


Fig 64-Single cell temperature evolution during discharge and charge cycle.

The heat generation during discharge and charge processes are comparable, in particular, the heat generation and the consequent temperature increase are higher during the discharge process respect to the charge process.

To take into account the cases in which a peak of current is requested, the simulation at 2C rate are conducted: for the discharge process the results are shown in Fig 65 and Fig 66.

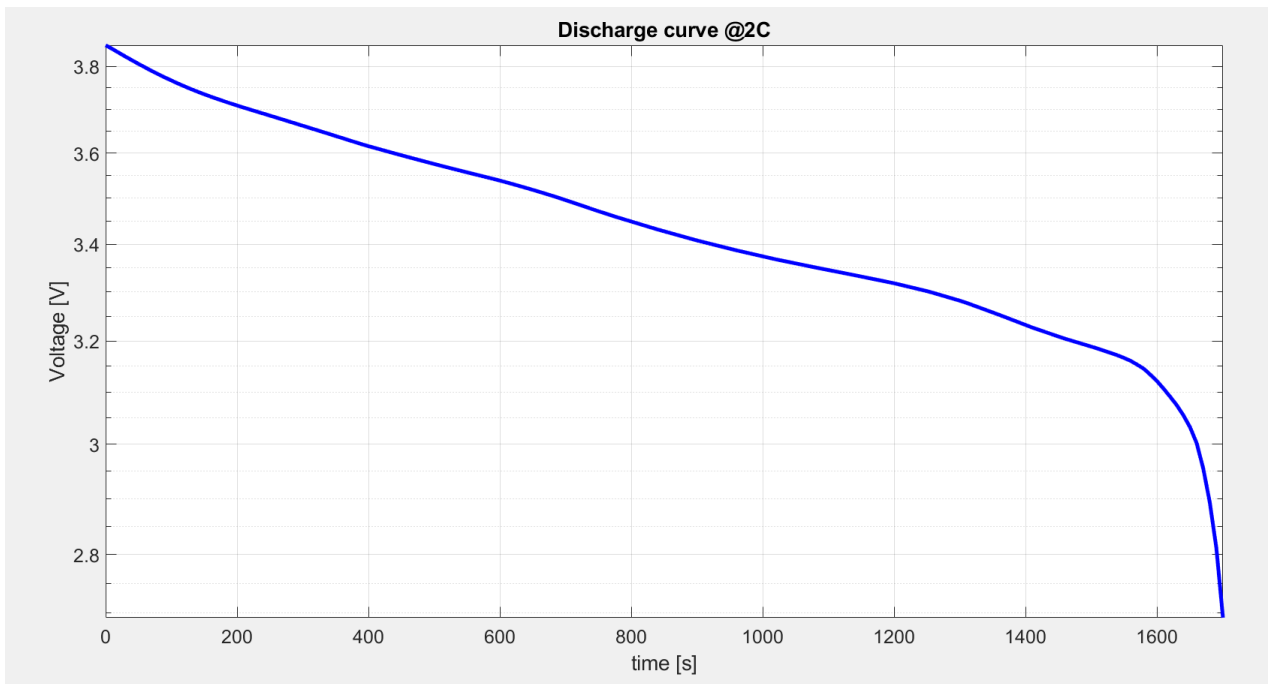


Fig 65-2C-rate discharge process.

Obviously, with the increase of the C-rate, the discharge process is faster. The temperature evolution of the single cell at 2C rate is reported in Fig 66.

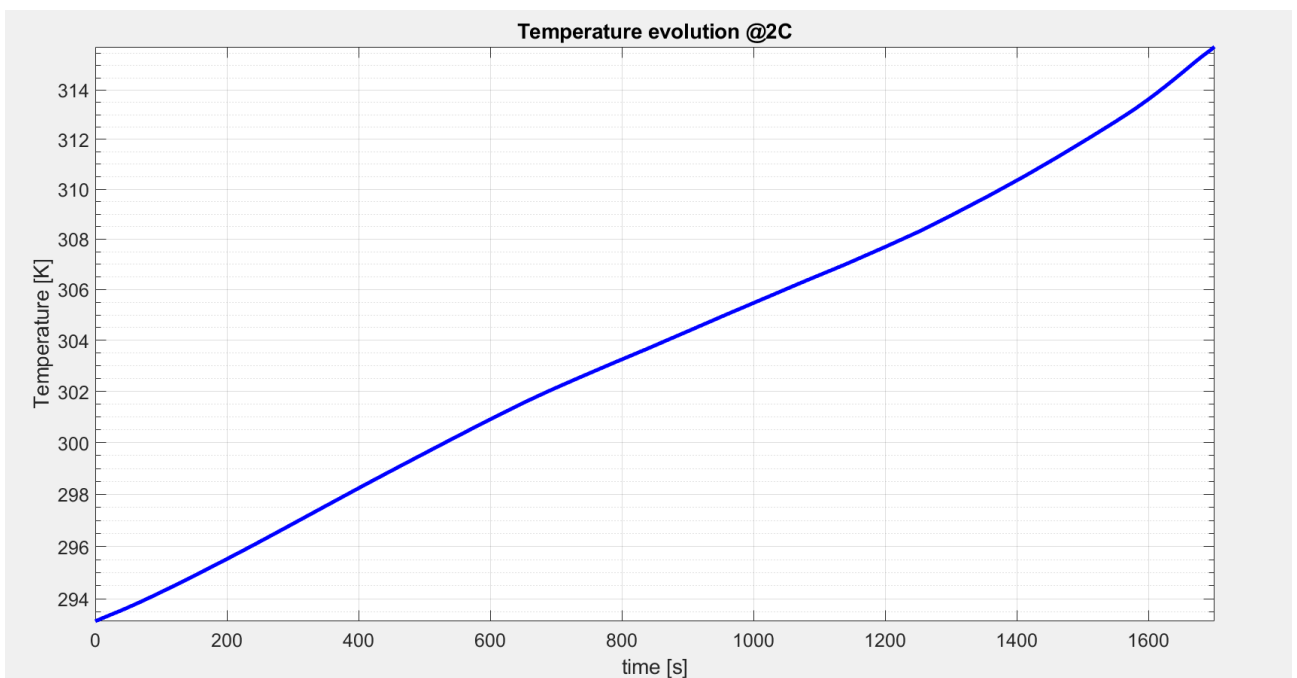


Fig 66- Single cell temperature evolution during discharge and charge cycle @2C-rate.

The increase of C-rate leads to an increase of temperature. It is a consequent of the heat generation during the process. The heat generation is shown in Fig 67.

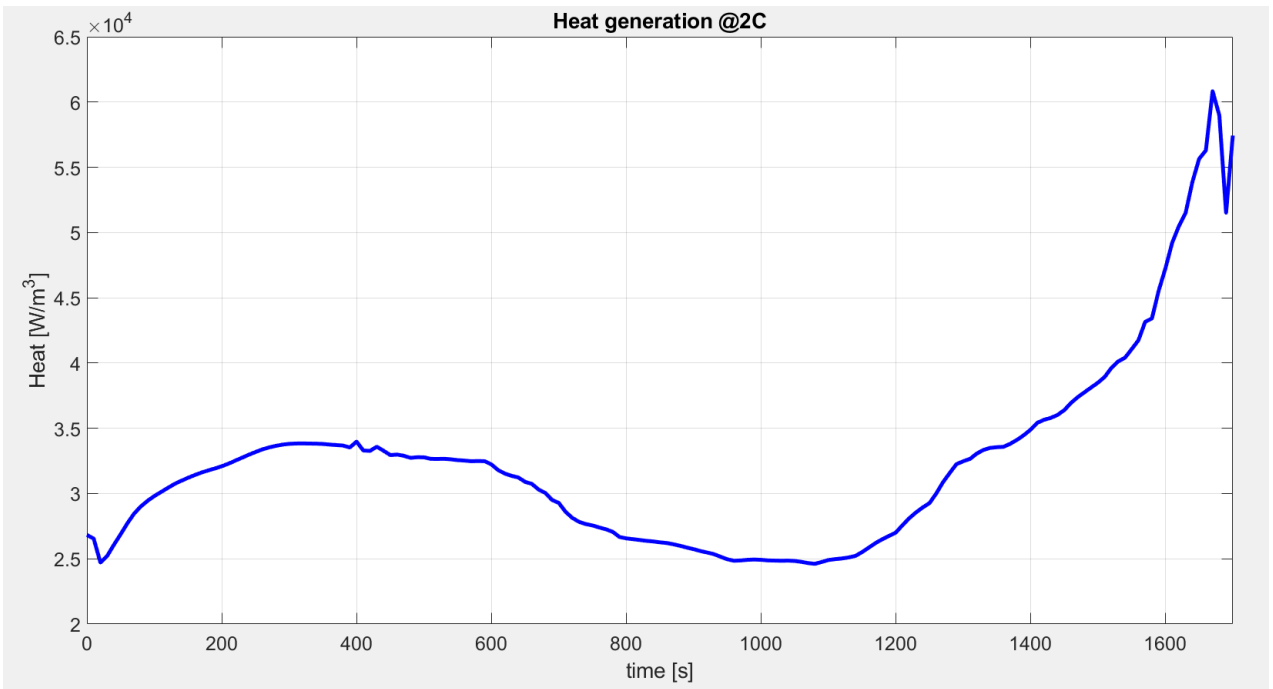


Fig 67- Heat generation during discharge process @2C-rate.

To describe thermal behavior of single cell, the discharge and charge cycle at 2C rate has been simulated. The Fig 68, Fig 69 and Fig 70 and show the voltage curve, temperature evolution and heat generation respectively.

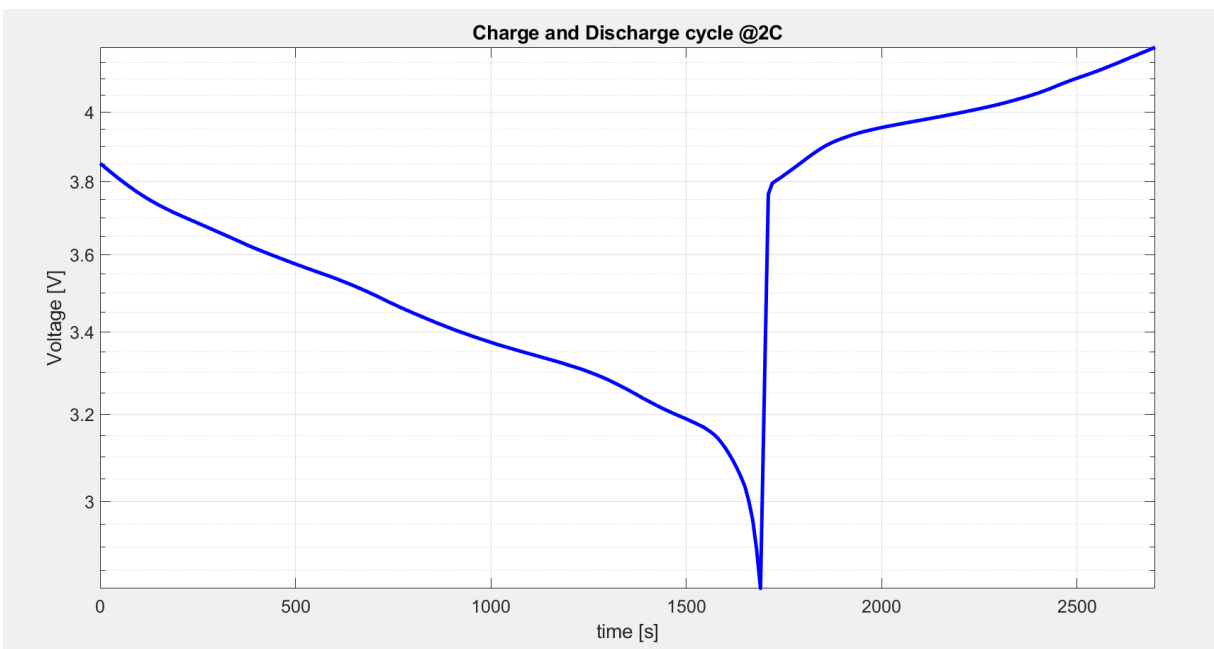


Fig 68- Discharge and charge cycle curve @2C.

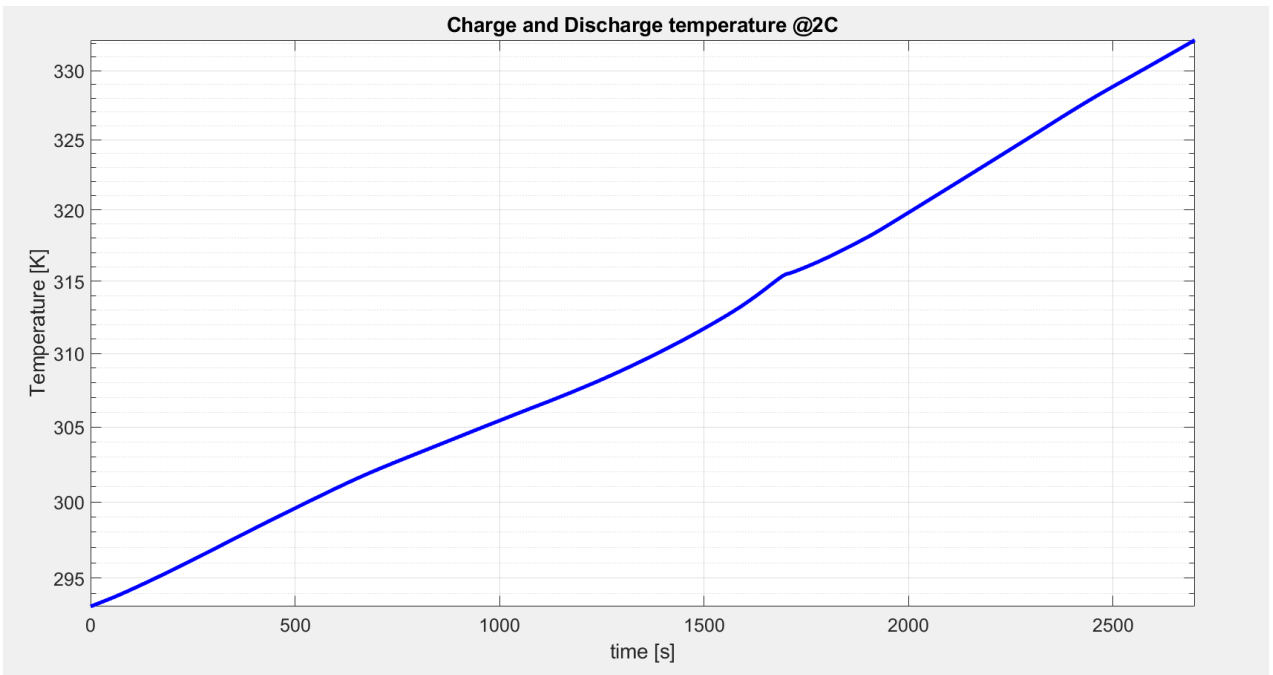


Fig 69-Single cell temperature evolution during discharge and charge cycle @2C.

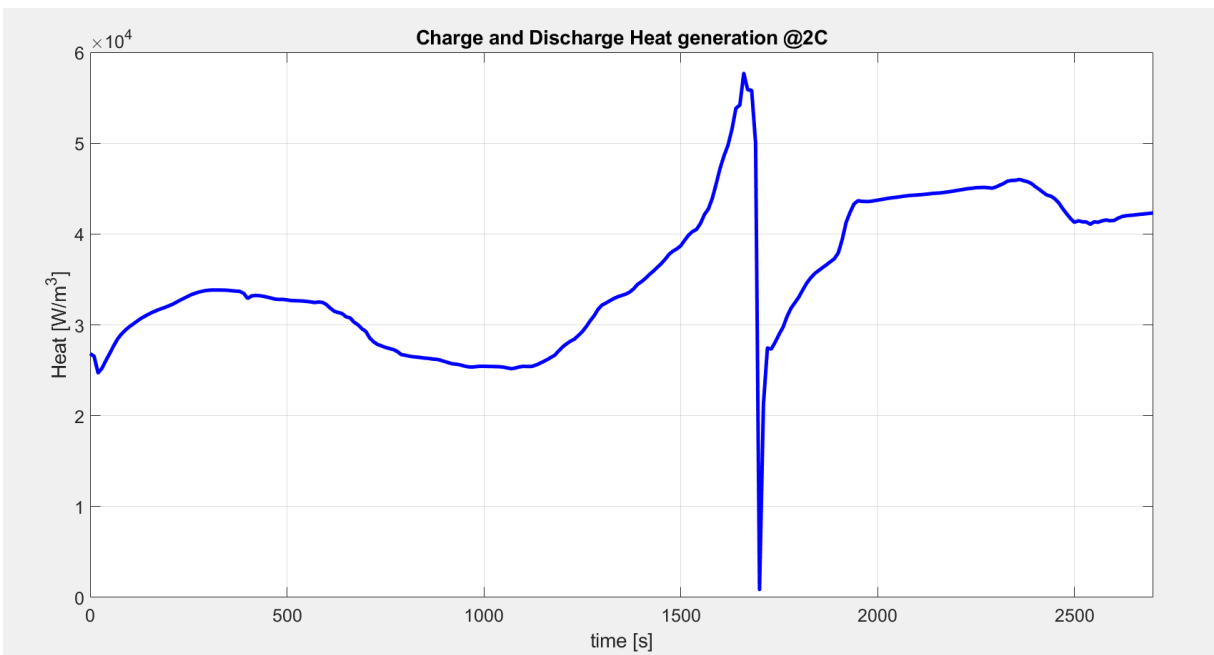


Fig 70-Heat generation during charge and discharge cycle.

By comparison between the heat generated and the useful power produced at 1C rate, the heat generated, and the useful power produced at 2C rate, there is a higher efficiency of the battery system for 1C rate respect to 2C rate. For this reason, it is preferred to choose to work at 1C rate.

Once the single cell heat generation has been defined, it is possible to simulate the heat generation and the temperature evolution of a battery pack module.

To modulate the heat transfer, the computer has to solve a lot of calculation. To be able to make the calculations with the limited computational power, the battery had to be scaled down [43]. The domain of the module of the battery pack has been simplified to reduce the computational cost.

The domain chosen consists of 6 cells with a simplified geometry as the Fig 71 and Fig 72 show.

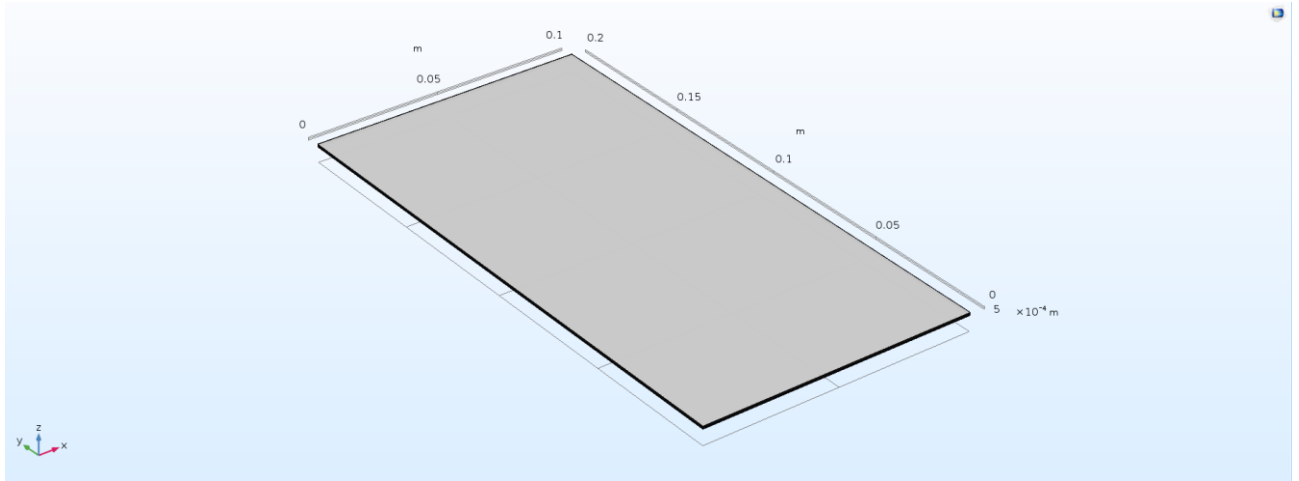


Fig 71- Simplified module geometry.

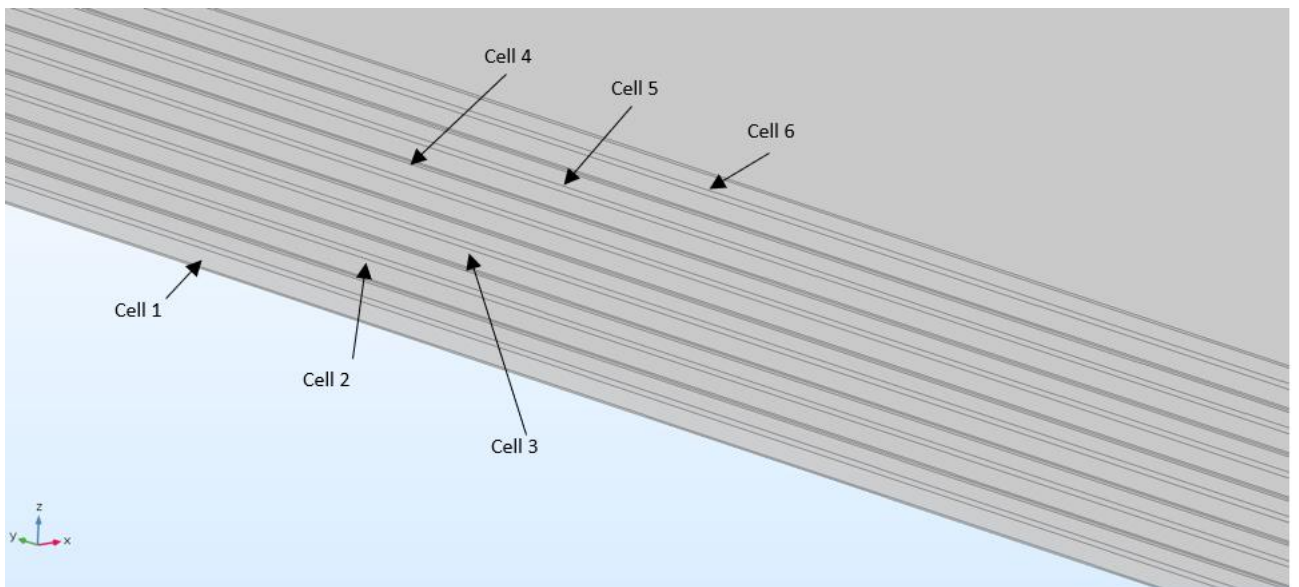


Fig 72- Module domains in detail.

The mesh used in heat transfer calculation is reported below.

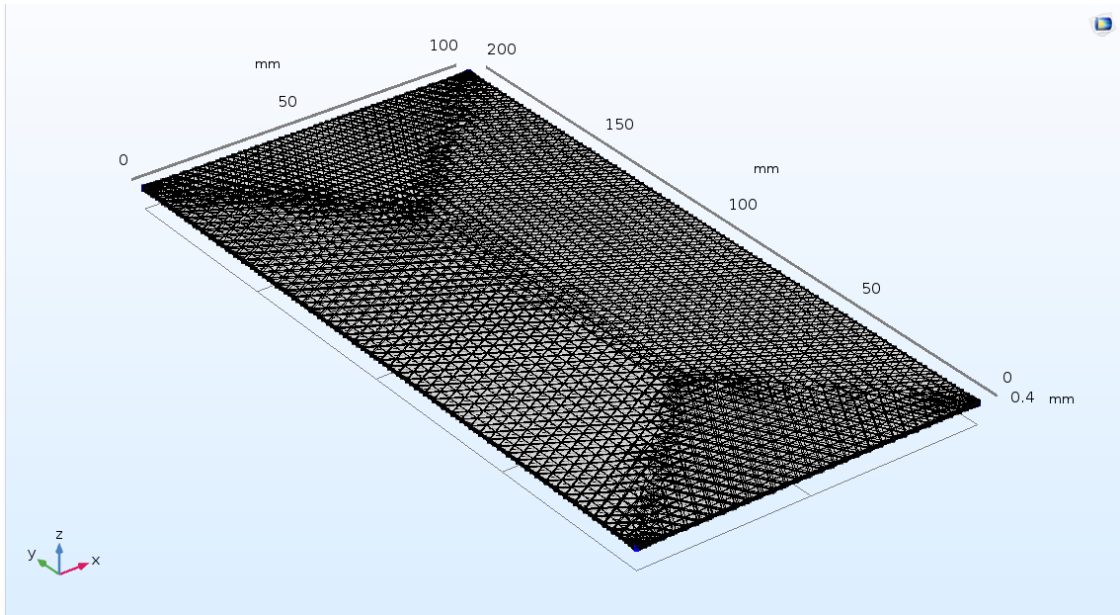


Fig 73- Mesh used in heat transfer calculation.

The heat generated from the single cell study is the input of the battery module model.

Thanks to the function $Q_h(t)$, output of electrochemical and thermal models of a single cell, the electrochemical model in the battery module study is not needed. The heat generated from single cell is set as heat source function in active battery material of each cells of the module.

The adiabatic condition has been imposed to external boundaries.

The Fig 74 shows the temperature evolution during discharge process for the battery module section described above.

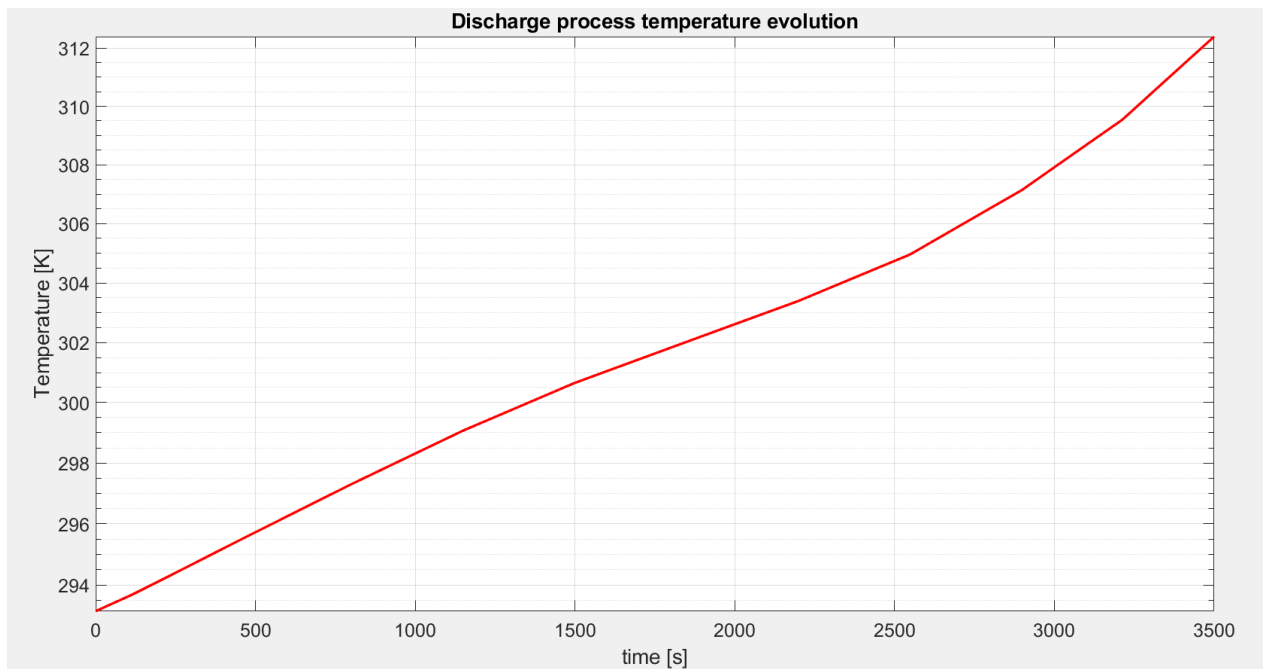


Fig 74-Average temperature evolution during discharge and charge cycle.

The Fig 75 shows the temperature evolution during discharge and charge cycle for the battery module section.

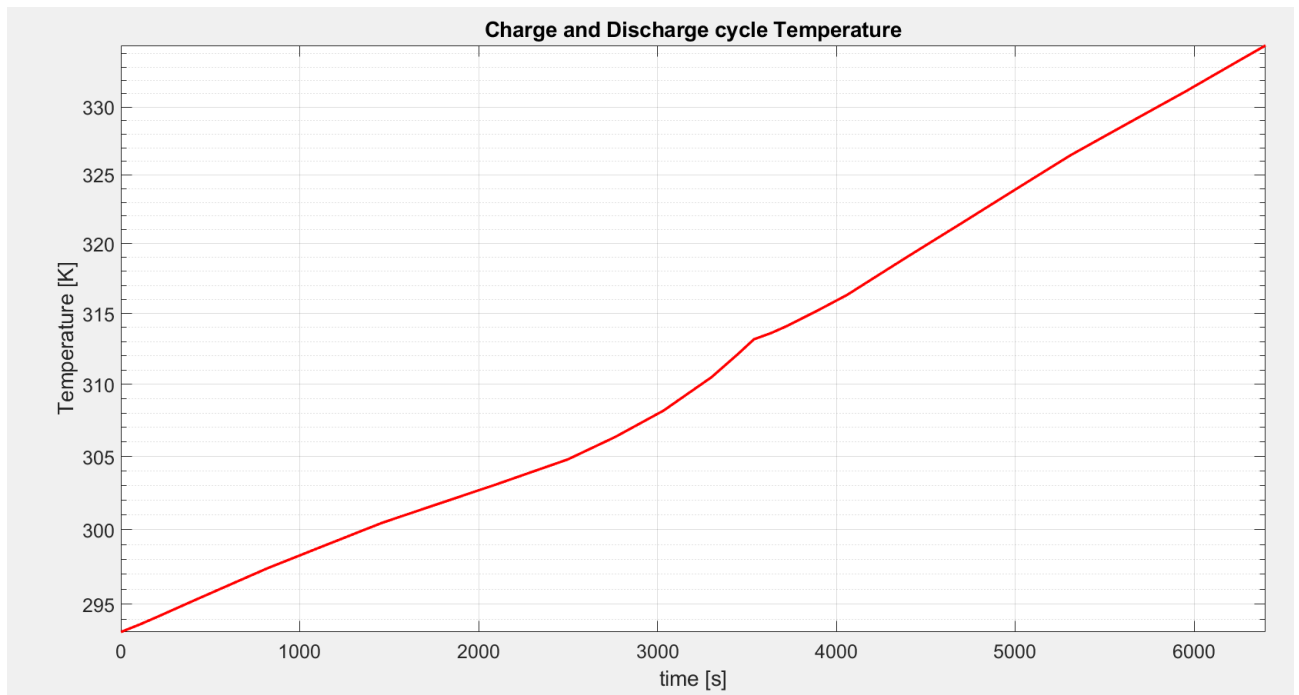


Fig 75- Discharge and charge cycle temperature evolution for the battery module section.

The number of cells increasing means an increase of temperature, it is clear comparing the Fig 64 and Fig 75, that show temperature evolution during discharge and charge cycle of a single cell and temperature evolution during discharge and charge cycle of a battery module section respectively. The ΔT between these two cases is approximately 10K. It is important to remind that the battery module section in the simulation is composed by 6 cells and the hypothesized number of cells in the module is equal to 12 cells in series and 10 cells in parallel. From the results obtained, the behavior of the entire battery module is possible to predict. For these reasons an accurate design of battery thermal management system is needed.

The finally step of this project thesis concerns the design of a cooling system for the battery module. The following study is the base from which an accurate study for the optimization of the battery cooling system begins.

The domain of the battery module section consists in 6 cells and 1 air channels. The 6 cells are divided into two boxes. The domain is shown in Fig 76 and its vertical section is shown in Fig 77.

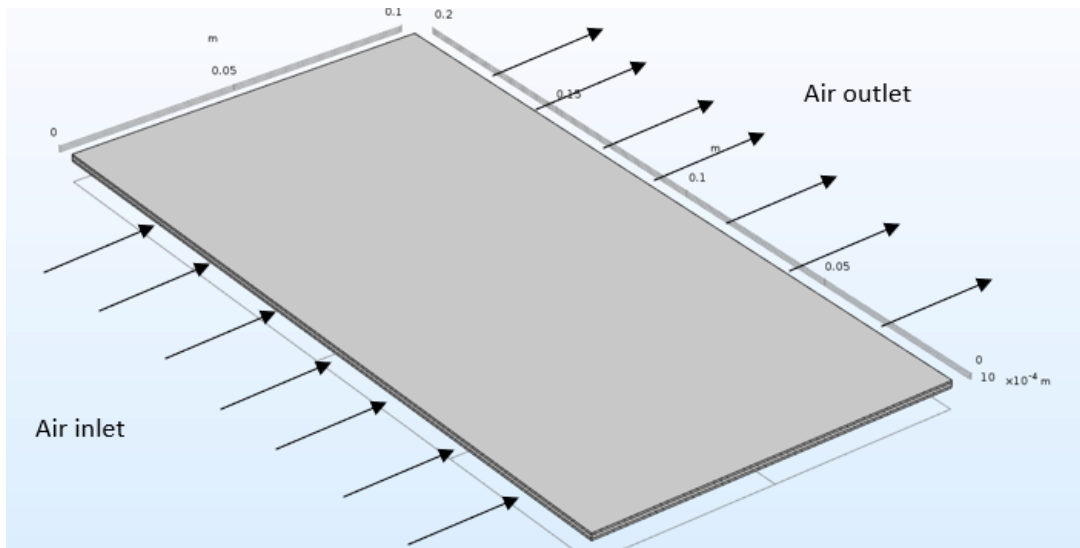


Fig 76-Battery module section domain.

The Fig 77 displayed the battery module section detail.

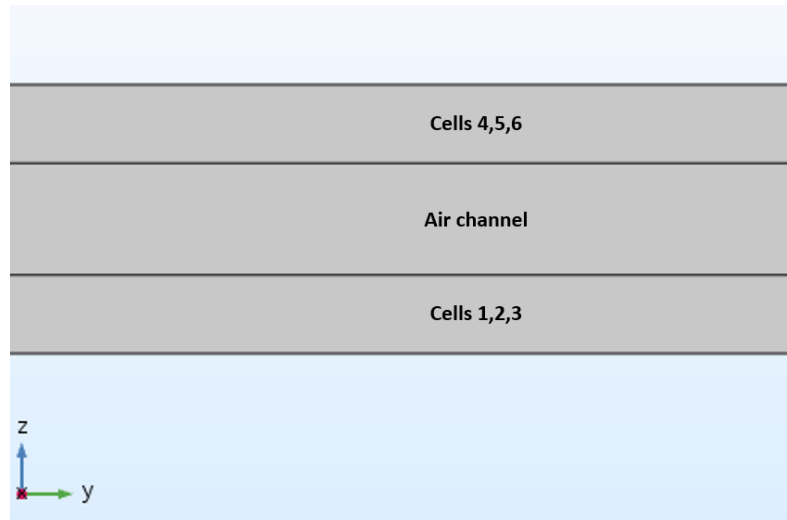


Fig 77-Battery module section detail.

To resolve the heat transfer problem between the electrochemical cells and the refrigerant fluid, a new physics is needed to add to the previous study: the “Laminar flow” physics. The laminar flow is imposed into air channels and no-slip conditions are defined between the cells boxes walls and the air, the air and its channel surface. The following conditions are set to air.

Table 21- Boundary conditions.

Inlet temperature [K]	293.15
Pressure [bar]	1
Velocity [m/s]	0.3

The heat source is located into cells boxes and each box generates a heat flux equal to three times the heat flux produced by a single cell. The temperature distribution in the surface of the cells domain at certain time is shown in Fig 78, Fig 79 and Fig 80.

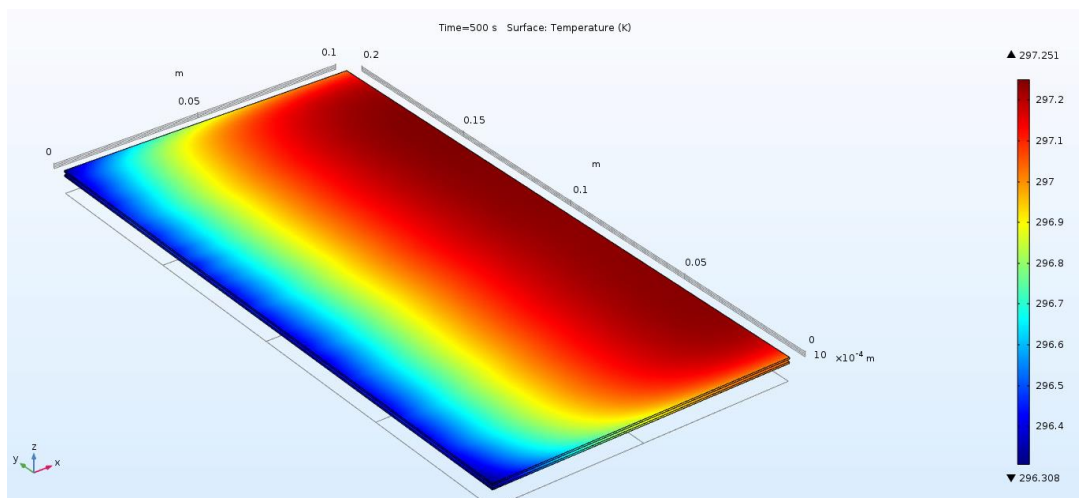


Fig 78- Cells domain temperature distribution @t=500s.

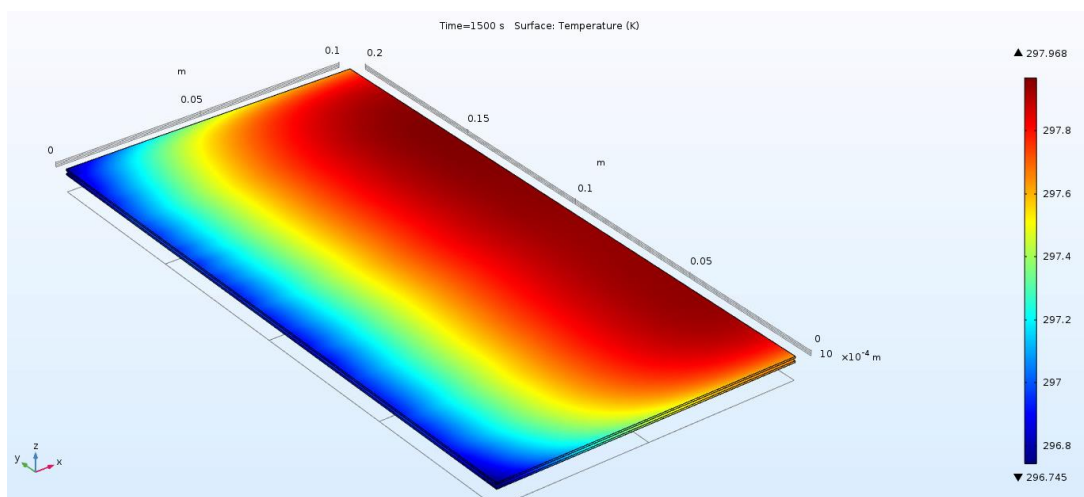


Fig 79- Cells domain temperature distribution @t=1500s.

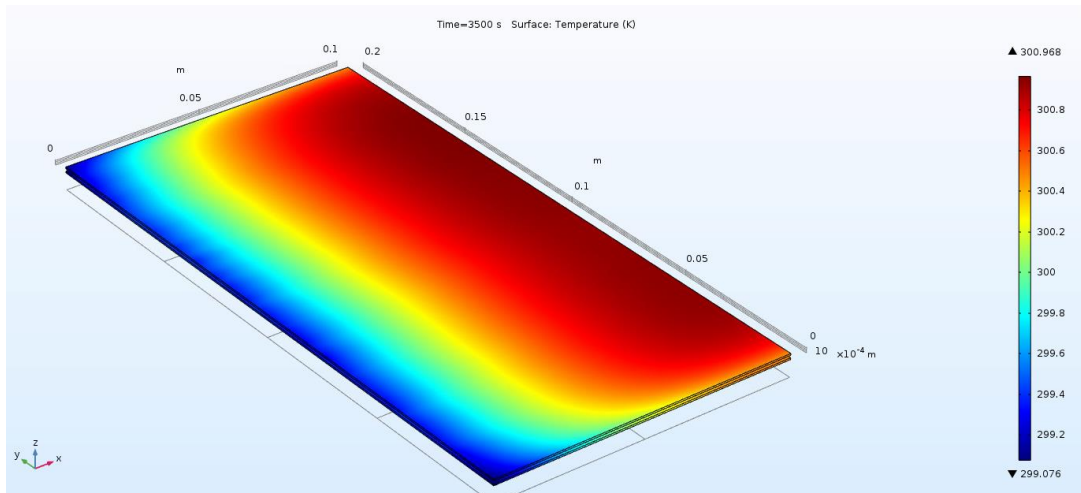


Fig 80- Cells domain temperature distribution @t=3500s.

By comparison between the temperature evolution of the battery module section without cooling system and temperature evolution of same battery module section with cooling system, it is clear that the cooling system is needed to reduce cells temperature, but the cooling system hypothesized is not sufficient to maintain the battery temperature within the right range. These last results are the base for the design of an efficient battery cooling system. This task will be the argument of the project thesis of my colleague Fabio Nasca.

5 Conclusion and future developments

The objective of this project thesis was the thermal characterization of a particular type of a lithium ion battery: NMC-graphite. The final goal was the development of a model able to simulate the correct behavior of this technology in several types of applications, the object of this work was the battery pack installed in a railway regenerative braking system.

As it is shown in the paragraphs “4.2.2” and “4.3.1” , it is possible to assert that the objectives has been obtained. The key to the its achievements was the development of the electrochemical model coupled with the thermal one. Through the calibration of the electrochemical and thermal parameters, an accurate validated model has been created. The validation was based on the comparison between the simulation results and the experimental data. This process was the most hurdles step to overcome but the most important, because this tool defines the accuracy of a computational model and it says how much the model and the real measurements deviate.

Once the model has been validated, it was possible applicate it to the case study of battery pack for railway regenerative braking system. The first step was the simulation of a single cell, to extend the study to battery module section.

The electrochemical and thermal characterization developed for single cell of battery pack at 1C rate and 2C rate for discharge and charge cycle and in adiabatic conditions has shown that the cell temperature increases up to critical values, which can't be tolerated. In particular, if the cell works at 2C rate the heat generated is too high respect to the useful power, in other words the efficiency of the cell decreases. For this reason, to work at 1C rate is more convenient.

To simulate the thermal behavior of the battery module, it was needed reduce the computational costs and a battery module section was chosen as domain. The results described in 4.3.1 have shown what was expected: the cells number increase determines the increase of temperature.

As the paragraph “Battery thermal management system (BTMS)” and the battery module thermal behavior in adiabatic condition explain, the cooling system is needed to maintain the battery temperature within the right range of operation. About that, the last step of this work was the design of a coarse air cooling system: the results are not satisfactory. For this reason, a design improvement of the cooling system is the key of the correct battery operation.

This project thesis can be considered as the base for the future development of an efficient battery cooling system.

APPENDIX

Model validation intermediate steps

0.05C rate

Optimization study varying the quantities shown in Table 22 and fixing the quantities shown in Table 23.

Fig 81- Pre-optimization and optimization study @0.05C.

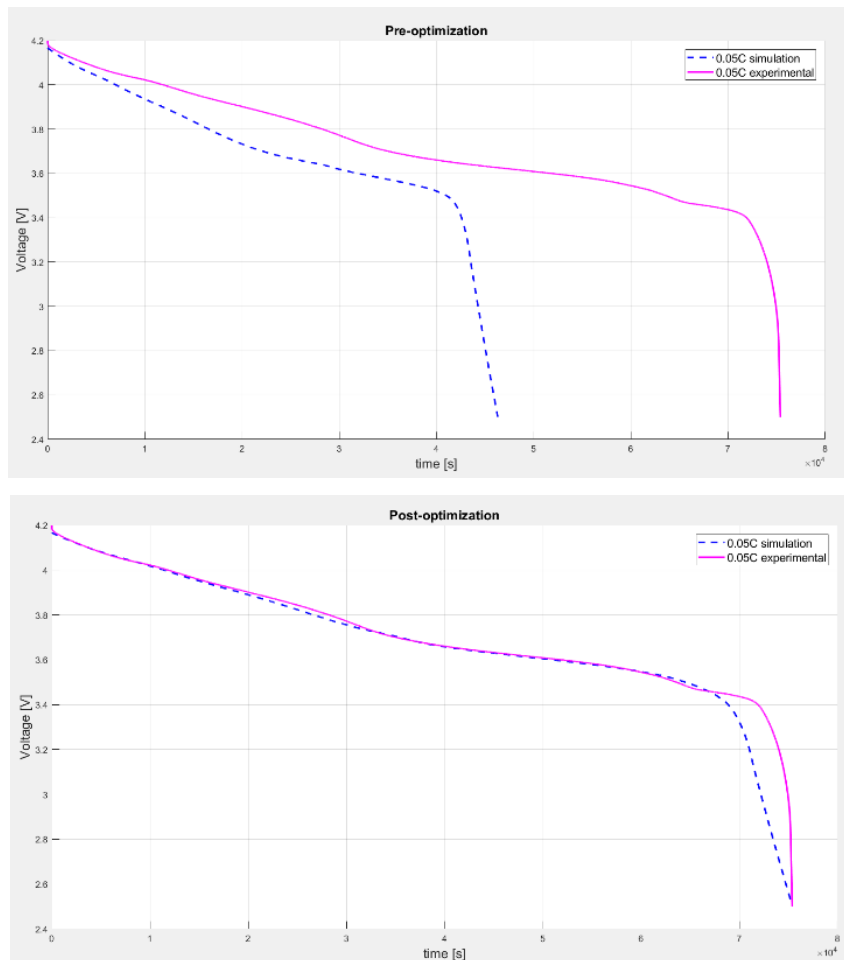


Table 22- Varied quantities for Oprimization study.

	Pre-optimization	Post-optimization
Epsl_neg	0.503	0.711
Eps_pos	0.517	0.633

Table 23- Fixed quantities for optimization study.

Parameter	Value
Ds_neg [m ² /s]	3.9e-14
Ds_pos [m ² /s]	1e-13
K_neg [m/s]	4.4e-10
K_pos [m/s]	4.8e-10
brugg	3.3
R_film [Ωm ²]	0

0.1C rate

Optimization study varying the quantities shown in Table 24 and fixing the quantities shown in Table 25.

Fig 82-Pre-optimization and optimization study @0.1C.

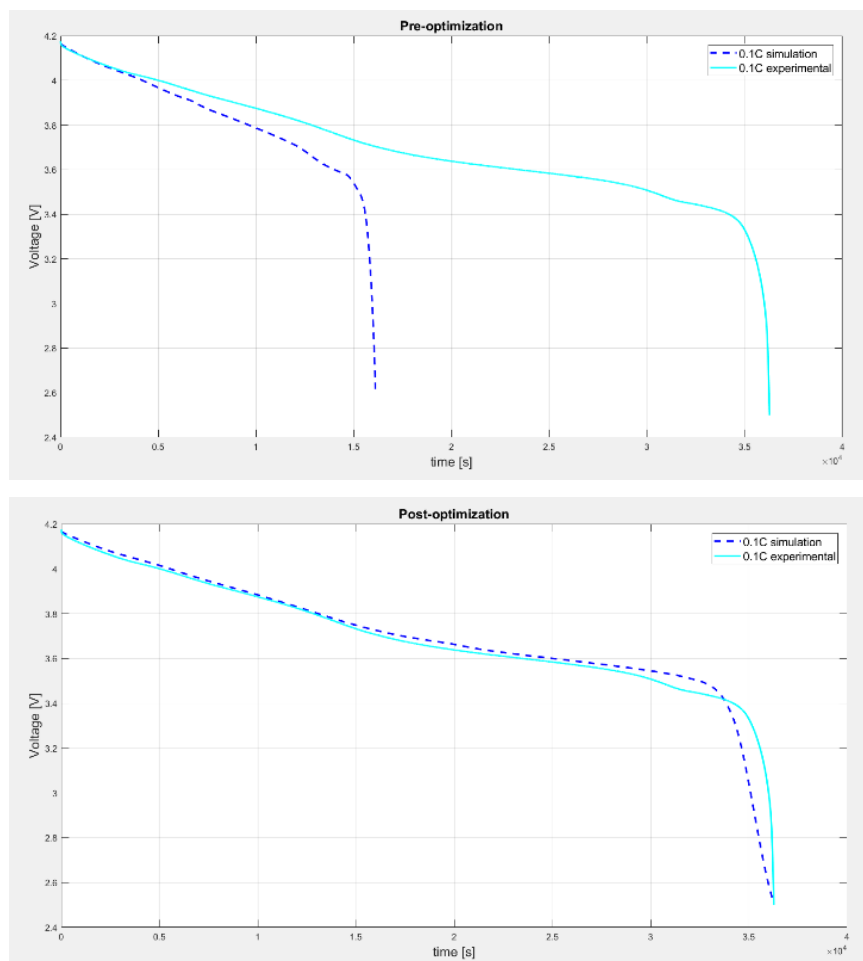


Table 24- Varied quantities for Oprimization study.

	Pre-optimization	Post-optimization
Epsl_neg [-]	0.744	0.639
Eps_pos [-]	0.544	0.690
K_neg [m/s]	6.4e-10	6.09e-10
K_pos [m/s]	6.8e-10	5.33e-10

Table 25- Fixed quantities for optimization study.

Parameter	Value
Ds_neg [m ² /s]	3.9e-14
Ds_pos [m ² /s]	1e-13
brugg	3.3
R_film [Ωm^2]	0

0.2C rate

Optimization study varying the quantities shown in Table 26 and fixing the quantities shown in Table 27.

Fig 83-Pre-optimization and optimization study @0.2C.

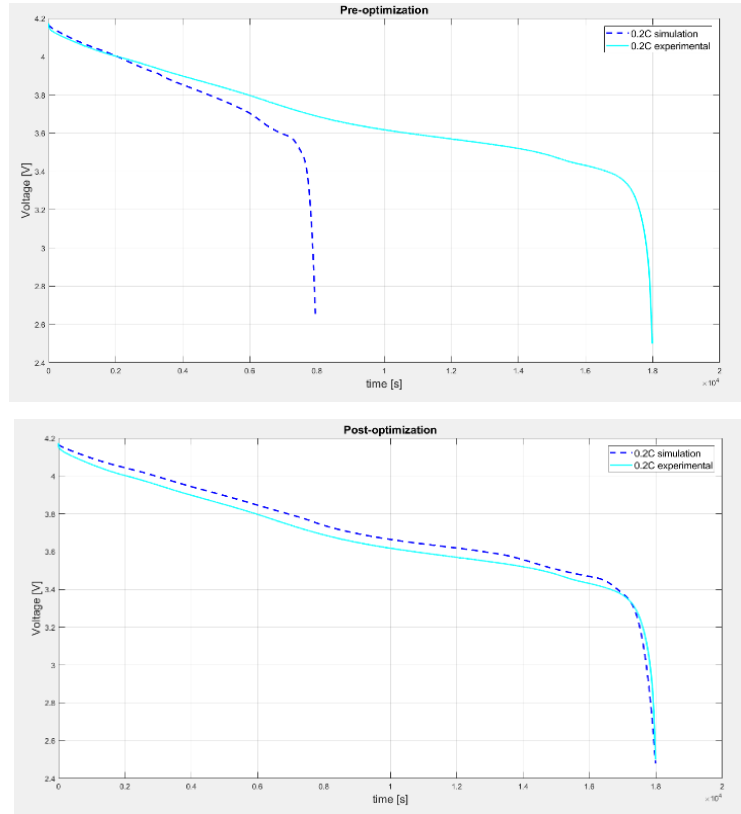


Table 26- Varied quantities for Optimization study.

	Pre-optimization	Post-optimization
Epsl_neg [-]	0.744	0.714
Eps_pos [-]	0.544	0.668
K_neg [m/s]	6.4e-10	4.9e-10
K_pos [m/s]	6.8e-10	4.6e-10

Table 27- Fixed quantities for optimization study.

Parameter	Value
Ds_neg [m ² /s]	3.9e-14
Ds_pos [m ² /s]	1e-13
R_film [Ωm ²]	0

0.5C rate

Optimization study varying the quantities shown in Table 28 and fixing the quantities shown in Table 29.

Fig 84-Pre-optimization and optimization study @0.5C.

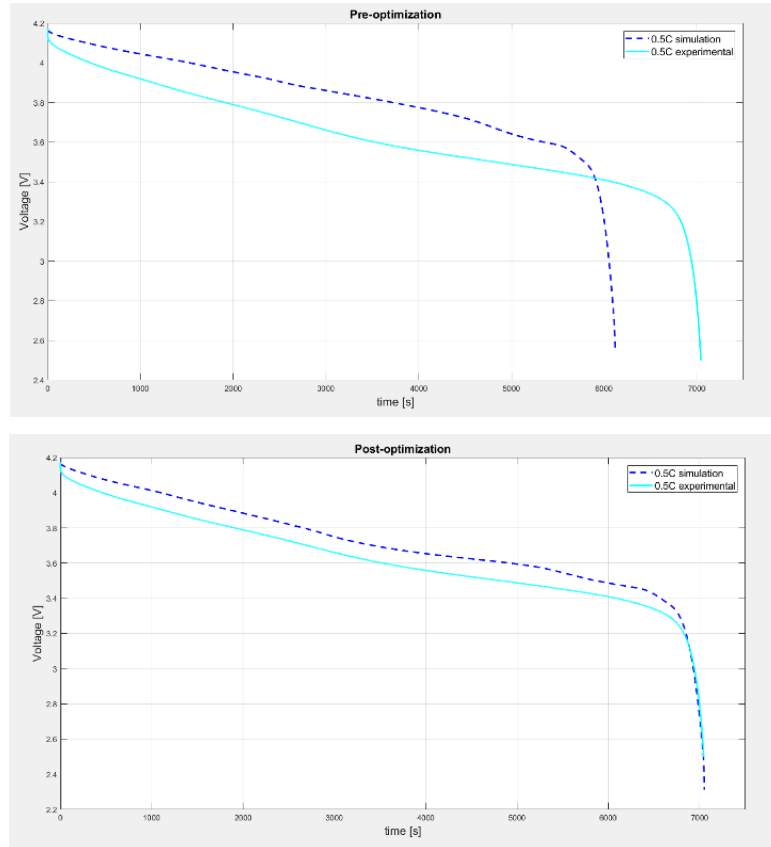


Table 28- Varied quantities for Optimization study.

	Pre-optimization	Post-optimization
Epsl_neg [-]	0.744	0.714
Eps_pos [-]	0.544	0.668
K_neg [m/s]	4.4e-10	5.75e-10
K_pos [m/s]	4.8e-10	5.16e-10

Table 29- Fixed quantities for optimization study

Parameter	Value
Ds_neg [m ² /s]	3.9e-14
Ds_pos [m ² /s]	1e-13
brugg	3.3
R_film [Ωm ²]	0

1C rate

Parametric study varying k_{pos} .

Fig 85-Temperature evolution comparison for different k_{pos} @1C.

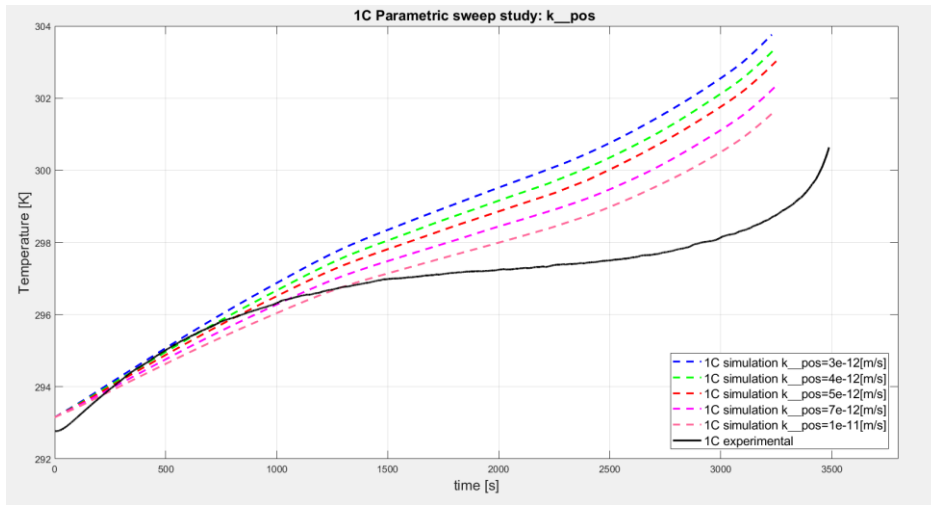
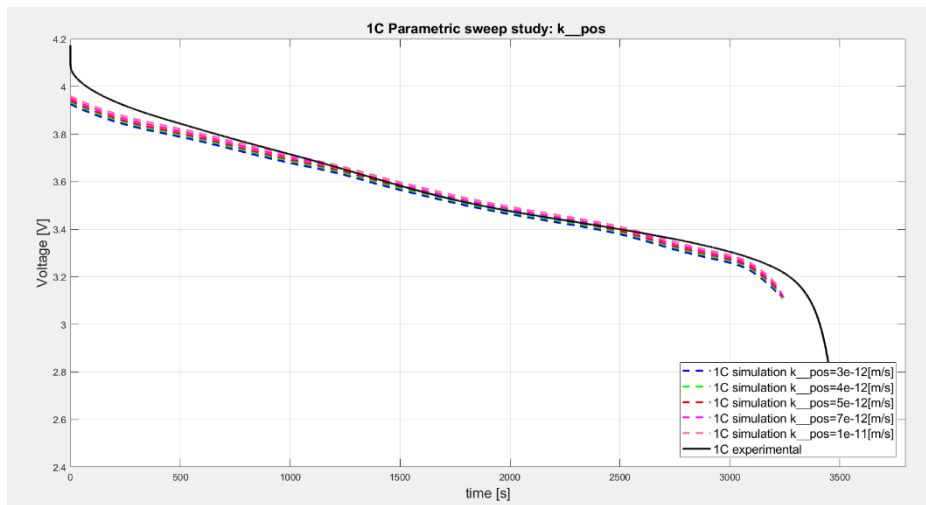


Fig 86- Voltage comparison for different k_{pos} @1C.



Parametric study varying bruggman coefficient.

Fig 87- Temperature evolution comparison for different Bruggeman coefficient @1C.

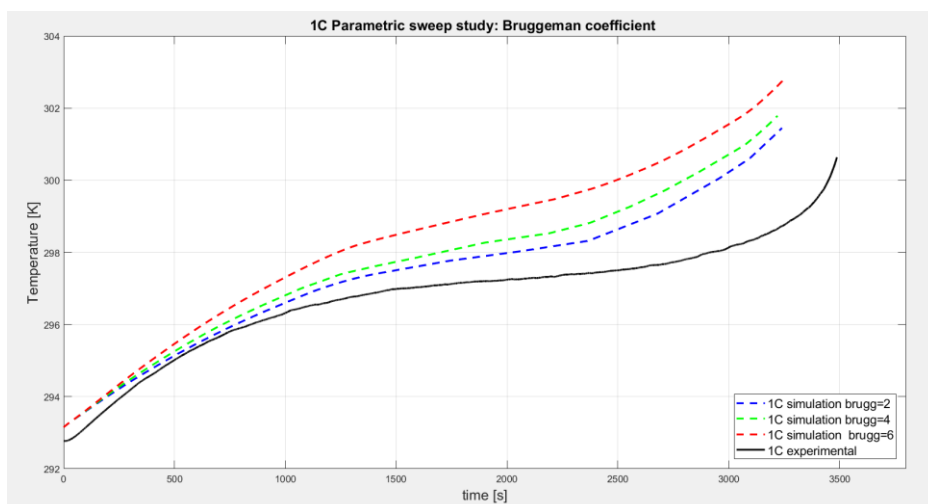
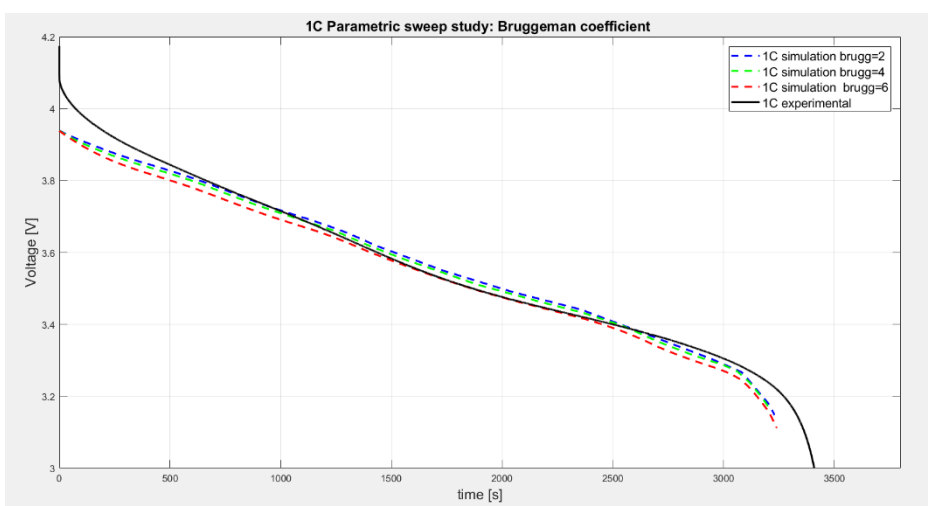


Fig 88- Voltage comparison for different Bruggeman coefficient @1C.



Fixing the follow parameters values.

Table 30-Electrochemical parameters values.

Parameter	Value
Ds_neg [m ² /s]	2e-14
Ds_pos [m ² /s]	3e-9
Epsl_neg	0.711
Epsl_pos	0.633
Epss_neg	1-epsl_neg- 0.026

Epss_pos	1-epsl_pos- 0.073
K_neg [m/s]	5e-12
K_pos [m/s]	4.6e-12
brugg	6
R_film [Ωm^2]	25e-3

Table 31-Materials parameters values.

Parameter	Value
rho_neg [kg/m ³]	1891.99
rho_pos [kg/m ³]	2451.88
Cp_neg [J/kgK]	520.12
Cp_pos [J/kgK]	727.32
h [W/m ² K]	4

2C rate

Parametric study varying k_{pos} .

Fig 89- Temperature evolution comparison for different k_{pos} @2C.

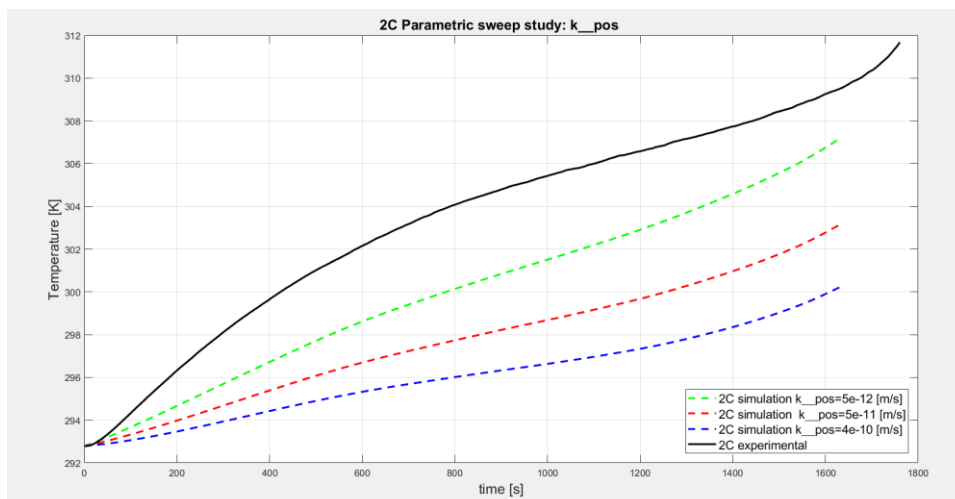
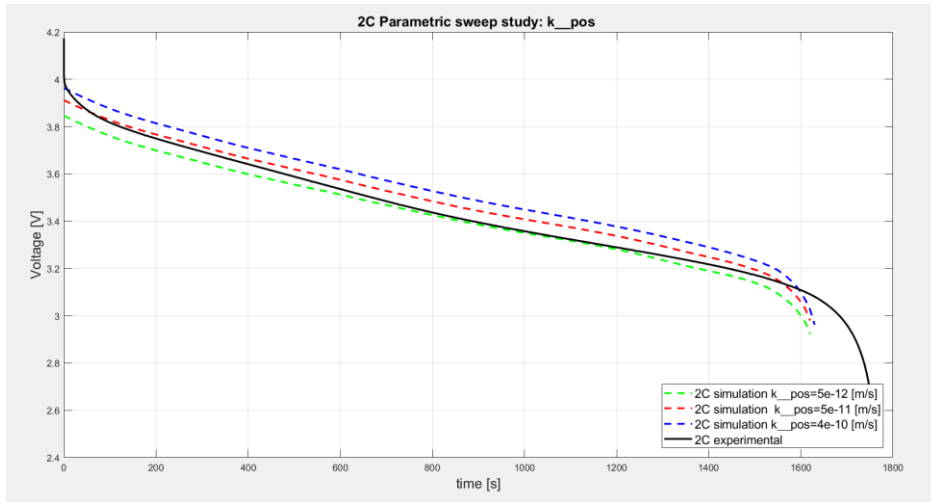


Fig 90- Voltage comparison for different Bruggman coefficient @2C.



Fixing the follow parameters values.

Table 32-Electrochemical parameters values.

Parameter	Value
Ds_neg [m ² /s]	2e-14
Ds_pos [m ² /s]	3e-9
Epsl_neg	0.688
Epsl_pos	0.633
Epss_neg	1-epsl_neg- 0.026
Epss_pos	1-epsl_pos- 0.073
K_neg [m/s]	5e-12
brugg	6
R_film [Ωm ²]	25e-3

Table 33- Materials parameters values.

Parameter	Value
rho_neg [kg/m ³]	1891.99
rho_pos [kg/m ³]	2451.88
Cp_neg [J/kgK]	520.12
Cp_pos [J/kgK]	727.32
h [W/m ² K]	4

Optimization study varying the quantities shown in Table 34 and fixing the quantities shown in Table 35 and Table 36.

Fig 91-Temperature evolution pre-optimization and optimization study @2C.

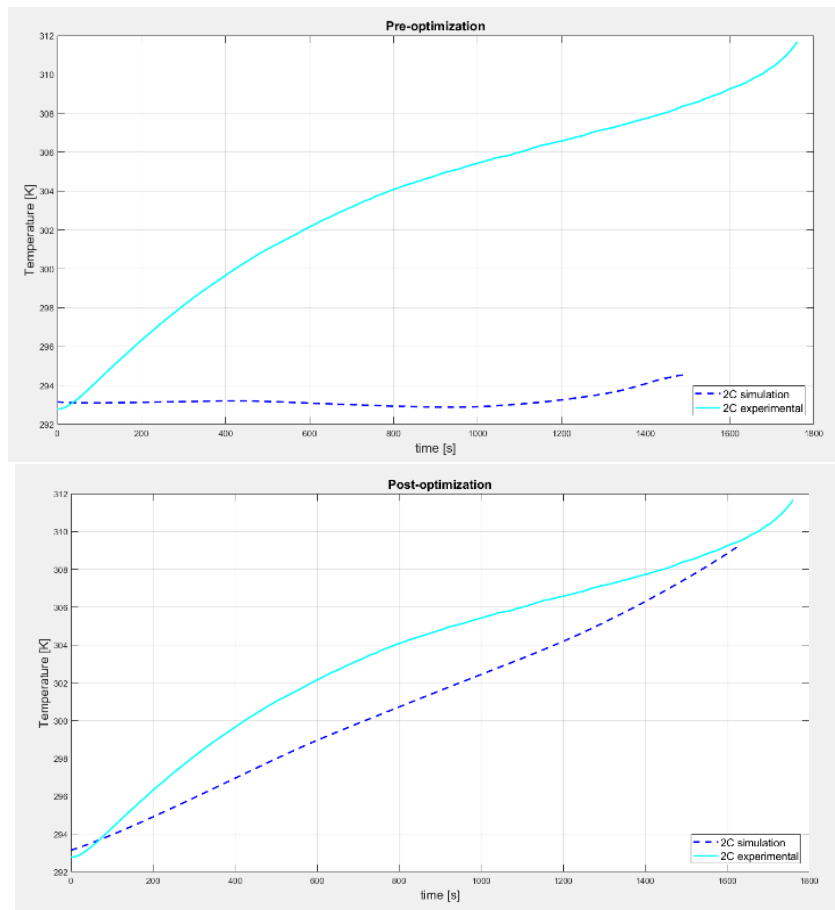


Fig 92-Voltage pre-optimization and optimization @2C.

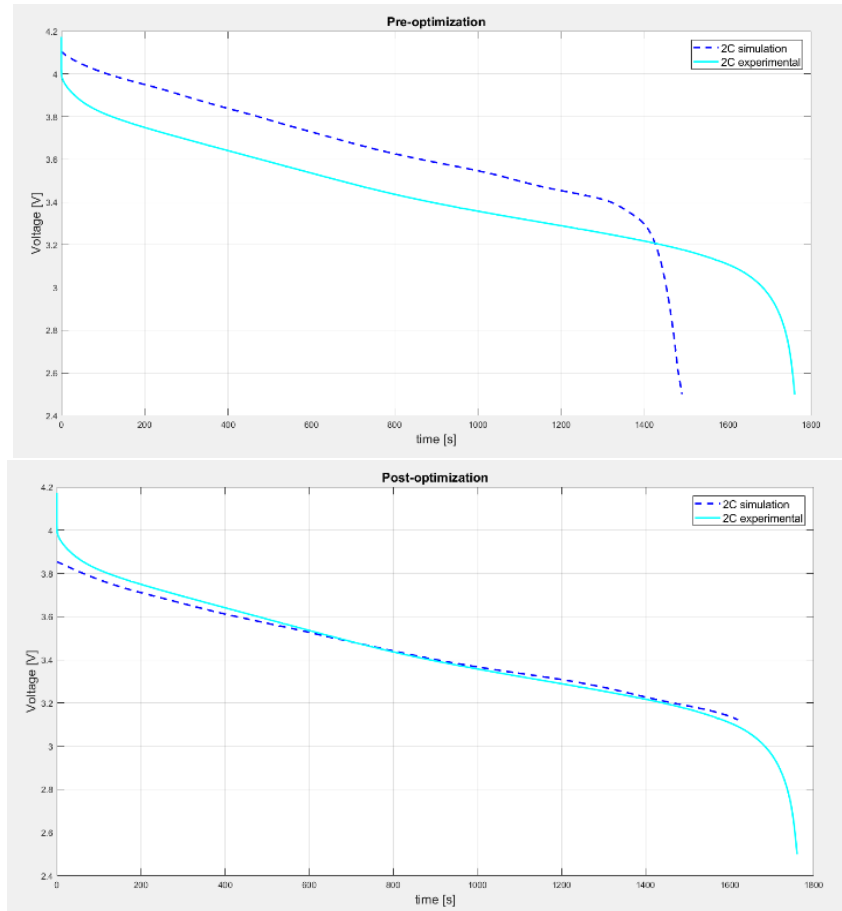


Table 34- Varied quantities for Optimization study.

	Pre-optimization	Post-optimization
Ds_neg [m ² /s]	3.9e-14	2.09e-13
Ds_pos[m ² /s]	1e-13	3.0e-13
K_neg [m/s]	4.9e-10	5.9e-12
K_pos [m/s]	4.64e-10	4.64e-12
R_film [Ωm ²]	10e-3	37e-3

Table 35- Fixed electrochemical parameters for optimization study.

Parameter	Value
Epsl_neg	0.711
Epsl_pos	0.633
Epss_neg	1-epsl_neg-0.026
Epss_pos	1-epsl_pos-0.073
brugg	6

Table 36- Fixed thermal parameters for optimization study.

Parameter	Value
rho_neg [kg/m ³]	2270
rho_pos [kg/m ³]	2328.5
Cp_neg [J/kgK]	520.12
Cp_pos [J/kgK]	727.32
h [W/m ² K]	0

REFERENCES

- [1] "The United Nations Framework Convention on Climate Change," [Online]. Available: <http://unfccc.int>.
- [2] I. E. O. 2016, "Transportation sector energy consumption," 2016.
- [3] NPTEL, "Introduction to Hybrid and Electric Vehicles," [Online]. Available: <https://nptel.ac.in>.
- [4] G. Pistoia, "Electric and Hybrid vehicles".
- [5] M. Granovskii, I. Dincer and M. A. Rosen, "Economic and environmental comparison of conventional, hybrid, electric and hydrogen fuel cell vehicles," *Journal of Power Sources*.
- [6] C. Mi, M. Masrur and D. W. Gao, Hybrid Electric Vehicles.
- [7] S. J. Clegg, "A review of regenerative braking system".
- [8] "auto.howstuffworks," [Online]. Available: <https://auto.howstuffworks.com/auto-parts/brakes/brake-types/regenerative-braking6.htm>.
- [9] G. Boccardo, *Energy saving strategied in diesel railcar*.
- [10] C. D. Rahn and C.-Y. Wang, Battery Systems Engineering.
- [11] "EPECTEC," [Online]. Available: <https://www.epectec.com/batteries/cell-comparison.html>.
- [12] I. Dincer, H. S. Hamut and N. Javani, Thermal managemet of electric vehicle battery systems.
- [13] "Battery University," [Online]. Available: http://batteryuniversity.com/learn/article/lithium_based_batteries.
- [14] H. Liu, Z. Wei, W. He and J. Zhao, "Thermal issues about Li-ion batteries and recent progress in battery thermal management systems: A review".
- [15] D. Linden and T. B. Reddy, Handbook of batteries.
- [16] K. Amine, J. Liu and I. Belharouak, "High-temperature storage and cycling of C-LiFePO₄/graphite Li-ion cells," 2005. [Online]. Available: www.sciencedirect.com.
- [17] A. Senyshyn, M. Mühlbauer, O. Dolotko and H. Ehrenberg, "Low-temperature performance of Li-ion batteries: The behavior of Li-ion batteries: The behavior of lithiated graphite".
- [18] G. NAGASUBRAMANIAN, "Electrical characteristics of 18650 Li-ion cells at low temperatures".
- [19] X. Feng, M. Ouyang, X. Liu, L. Lu, Y. Xia and X. He, "Thermal runaway mechanism of lithium ion battery for electric vehicles: A review".
- [20] G. Xia, L. Cao and G. Bi., "A review on battery thermal management in electric vehicle application," *Journal of Power Sources*, 2017.
- [21] K. E. Thomas, R. M. Darling and J. Newman, "Mathematical modeling of Lithium batteries," 2002.

- [22] J. Jiang and C. Zhang, *Fundamentals and applications of Lithium-ion batteries in electric drive vehicles*, Wiley & Sons Singapore, 2015.
- [23] S. c. u. e. Co., "Sicon Emi," 2015-2018. [Online]. Available: http://www.sicon-emi.com/battery-management-system_p38.html.
- [24] "Battery University," 2018. [Online]. Available: https://batteryuniversity.com/learn/article/how_to_monitor_a_battery.
- [25] M. R. Khan, M. J. Swierczynski and S. K. Kær, "Towards an Ultimate Battery Thermal Management System: A review," Department of Energy Technology, Aalborg University, Pontoppidanstræde 101, Aalborg DK-9220, Denmark;, 2017.
- [26] Q. Wang, B. Jiang and Y. Y. Bo Li, "A critical review of thermal management models and solutions of lithium-ion batteries for the development of pure electric vehicles," *Renewable and Sustainable Energy Reviews*, 2016.
- [27] Z. Rao and S. Wang, "A review of power battery thermal energy management," *Renewable and Sustainable Energy Reviews*, 2011.
- [28] "Advanced engineering service," 2014. [Online]. Available: <https://engineering.mpt.magna.com>.
- [29] K. Murashko, J. J. Pyrhonen and L. I. E. Laurila, "Optimization of the passive thermal control system of a lithium-ion battery with heat pipes embedded in an aluminum plate," *15th European conference on power electronics and applications (EPE)*, 2013.
- [30] M. Thele, O. Bohlen, D. U. Sauer and E. Karden, "Development of a voltage-behavior model for NiMH batteries using an impedance-based modeling concept," *Journal of Power Sources*, pp. 635-643, 2008.
- [31] H. He, R. Xiong and J. Fan, "Evaluation of Lithium-Ion Battery Equivalent Circuit Models for State of Charge Estimation by an Experimental Approach," *Energies*, 2011.
- [32] F. Jin, H. Yongling and W. Guofu, "Comparison Study of Equivalent Circuit Model of Li-Ion Battery for Electrical Vehicles," *Research Journal of Applied Sciences, Engineering and Technology*, pp. 3756-3759, 2013.
- [33] V. Ramadesigan, P. W. C. Northrop, S. D. S. Santhanagopalan, R. D. Braatz and V. R. Subramaniana, "Modeling and Simulation of Lithium-Ion Batteries from a Systems Engineering Perspective," *Journal of The Electrochemical Society*, pp. R31-R45, 2012.
- [34] S. Santhanagopalan, Q. Guo, P. Ramadass and R. E. White, "Review of models for predicting the cycling performance of lithium ion batteries," *Journal of Power Sources*, pp. 620-628, 2006.
- [35] K. A. J. Li, N. Lotfi, R. Landers and J. Park, "A single particle model with chemical/mechanical degradation physics for lithium ion battery State of Health (SOH) estimation," *Applied Energy*, pp. 1178-1190, 2018.
- [36] M. Doyle and T. F. J. Newman, "Modeling of Galvanostatic Charge and Discharge of the Lithium/Polymer/Insertion Cell," University of California, 1992.
- [37] C. Multiphysics, "Comsol Multiphysics," [Online]. Available: www.comsol.it.

- [38] C. Multiphysics, "1D isothermal Lithium-Ion Battery".
- [39] W. Gu and C. Wang, "Thermal-electrochemical coupled modeling of a lithium-ion cell," Department of Mechanical Engineering & Pennsylvania Transportation Institute, University Park, PA 16802, USA.
- [40] Zhao, H. Sun and Kejie, "Electronic Structure and Comparative Properties of $\text{LiNi}_x\text{Mn}_y\text{Co}_z\text{O}_2$ cathode materials," *The journal of physical chemistry*, pp. 6002-6010, 2017.
- [41] C. Multiphysics, "Thermal Modeling of a cylindrical Lithium Ion Battery in 2D".
- [42] B. Rajabloo, M. Désilets and Y. Choquette, "Parameter Estimation of Single Particle Model Using COMSOL Multiphysics® and MATLAB® Optimization Toolbox," Département de génie chimique et de génie biotechnologique, Université de Sherbrooke, QC, Varennes, QC, CANADA.
- [43] A. E. Magnusson, "Modelling of battery cooling for Formula Student application," KTH School of industrial engineering and management, STOCKHOLM, 2016.
- [44] "Wikipedia," [Online]. Available: https://en.wikipedia.org/wiki/Hybrid_electric_vehicle.
- [45] "International Energy Outlook," [Online]. Available: www.eia.gov/forecasts/ieo.
- [46] G. Liu, M. Ouyang, L. Lu, J. Li and X. Han., "Analysis of the heat generation of lithium-ion battery during charging and discharging considering different influencing factors".
- [47] Reimers, L. O. Valøen and Jan, "Transport Properties of LiPF₆ based Li-ion Battery Electrolytes," British Columbia, Canada.
- [48] L. Tao, J. Maa, Y. Chengb, A. Noktehdan, J. Chongf and C. Lu, "A review of stochastic battery models and health management," *Renewable and Sustainable Energy Reviews*, pp. 716-732.
- [49] M. Xu, Z. Zhang, X. Wang, L. Jia and L. Yang, "Two-dimensional electrochemical-thermal coupled modeling of cylindrical LiFePO₄ batteries," *Journal of Power Source*, pp. 233-243, 2014.